BIOACTIVE SCAFFOLDS FOR THERAPEUTIC ANGIOGENESIS ON SKIN INJURIES AND VASCULAR DISEASE MODEL

by
Yu I (Tom), Shen

A dissertation submitted to The Johns Hopkins University in conformity with the requirements for the degree of Doctor of Philosophy

Baltimore, Maryland
March 2015

Abstract

Angiogenesis, defined as the formation of blood vessels from pre-existing vessels, is an important natural process. While angiogenesis does not occur in healthy mammals. it plays a major role in tumor development and wound healing. The tightly controlled process of angiogenesis is dependent on a variety of biochemical and biomechanical cues. Using synthetic bioactive hydrogel systems allows us to investigate this well controlled process. For instance, many have adapted three dimensional (3D) tissue culture models that recapitulate aspects of the tumorogenic *in vivo* microenvironment to study cancer progression *in vitro* and its linkage with angiogenesis. At the same time, a 3D tissue culture bioactive scaffolds can also provide a therapeutic strategy to treat various injuries and diseases.

First we utilized hyaluronic acid hydrogel systems and using mathematical modeling, found that varying viscoelasticity in atmospheric and hypoxic environments affects cancer cell cycles and the expression of autophagy and apoptosis genes. Hypoxic stress enabled greater recovery from apoptosis through autophagy mechanism and induced greater angiogenic leading to extensive endothelial cell (EC) sprouting. Next we used the same hyaluronic acid hydrogel engineer human microvasculature for the treatment of diabetic foot ulcers (DFUs), one of the leading healthcare problems in the US. To this end, we developed an immunodeficient diabetes rodent DFU model. Treatment of DFU with engineered human vascularized hydrogel scaffolds from stem cell derived vascular cells, has shown faster wound healing compared to acellular hydrogel, thus suggestion a potential therapeutic strategy to treat DFU. Finally, we investigated the utilization of dextran

hydrogel system to induce vascularization and healing of third degree burn injuries in a large animal model. We have observed accelerated third degree burn wound healing in porcine by rapid wound closure, improved re-epitheliazation, enhanced extracellular matrix remodeling and greater nerve re-innervation in the hydrogel treated wounds.

Collectively, the results from this thesis showcase the successfully utilization of bioactive hydrogel scaffolds to study various biochemical and biophysical cues that influence angiogenesis. Combing with stem cell technologies, the hydrogel systems can improve wound healing at both diseased and severe skin injuries.

Thesis Advisor:

Prof. Sharon Gerecht, Ph.D.

Thesis Committee:

Prof. Kostas Konstantopoulos, Ph.D.

Prof. Honggang Cui, Ph.D.

Prof. Linzhao Cheng, Ph.D.

Prof. Warren Grayson, Ph.D.

Prof. Denis Wirtz, Ph.D. (internal alternate)

Prof. Hai-Quan Mao, Ph.D. (external alternate)

Acknowledgments

First I would like to thank and express my gratitude to my faculty advisor, Dr. Sharon Gerecht. Without her guidance, support and encouragement throughout the years during graduate studies, I could not have stand here to present my work. I'm fortunate to have her supervision during my intellectual and professional development. She has also resembled how a great researcher a great leader, a great inspirer and most importantly how a contributor to the society to be. There is a Chinese saying "day as a teacher, parent for life." It's a blessing to have her serving as "parent" home away from home and guiding me during this intellectual journey.

I would like to thank Dr. Linzhao Cheng and Dr. Warren Grayson to serve my graduate review board member to evaluate my research progress during the last two years, and Dr. Kostas Konstantopoulos, Dr. Honggan Cui for taking the time from their busy schedule to serve as members of my thesis committee. I would also like to thank Dr. Denis Wirtz and Dr. Hai-Quan Mao to serve as my thesis alternative and all together to witness this very exciting conclusion of my education journey in Hopkins.

It's a fortune to have so many wonderful lab members with whom I have built friendships throughout the past many years. Dr. Guoming Sun, Dr. Abigail Cuddy, Dr. Donny Hanjaya-Putra, Dr. Laura Dickinson, Dr. Hasan Erbil Abaci, Dr. Sravanti Kusuma, Dr. Maureen Wanjare, Dr. Kyungmin Park, Dr. Xin Yi Chan, Ying Wang, Sebastian F. Barretto, and Quinton Smith, Michael Bletchley, Dan Lewis and Greco Song, Matt Davenport, Kim Ellis, Rachael Truitt and many undergraduates in the lab. Lab life with them is not only fun but enjoyable. It's like having many family members away from home

to provide assistance and offer encouragement and support at close proximity. I am also grateful to have mentor many great undergraduate students: Arianne Papa, Jacqueline Burke, Yoni Krupski, Philomena Weng, Katie Herman, Peter Li, who help facilitate the progress of my research through sweat and their precious time away from their school work.

I would also like to thank all the ChemBE and INBT staff where I have been bothering them either asking either money or cookies, as well as helping me resolving various problems in administrative or purchasing tasks. With them, this indeed is the best department in Hopkins.

Lastly, I would like to thank my family. Without their support and encouragement, studying overseas away from home would be impossible. Their unconditional love is always the sources of encouragement and my last resort for support at my roadblock in life. I love them and I miss them but I know it will all worth it at the end. I wish I have made them proud.

Table of Contents

List of Figures & Tables

*靜夜思 (**李白**)*

床 前 明 月 光

疑 是 地 上 霜

舉 頭 望 明 月

低 頭 思 故 鄉

Night Thoughts

I wake, and moonbeams play around my bed,

Glittering like hoar-frost to my wandering eyes;

Up towards the glorious moon I raise my head,

Then lay me down---and thoughts of home arise.

(Tr. Herbert A. Giles)

1 Introduction

1.1 *Biomaterials for Tissue Engineering and Regenerative Medicine*

Tissue engineering (TE) and Regenerative medicine (RM) have the goal of developing a biological substitute that repairs, improves, or maintains the original tissue function. One factor limiting the field is the provision of well-vascularized constructs for nourishment of rapidly proliferating cells. The cell microenvironment consists of the noncellular extracellular matrix (ECM) and the biological molecules which it sequesters, as well as the vascular networks. The ECM provides a living space for cell proliferation and differentiation. Biosignaling molecules sequestered in the ECM serve as messengers to direct cell fate (e.g. growth and differentiation of stem cells and proliferation, differentiation and tube-formation from ECs). Vascular networks provide a means of supporting nutrition (e.g. glucose and O2) and removing waste (e.g. CO2) in the tissue. Because of limitations of oxygen diffusion, cells cannot survive when they are located greater than 150 μm away from the nearest capillary [1]. Without a steady supply of nutrients, cells in the constructs will not survive *in-vivo*. Thus, engineering a vascularized construct is an essential step for the successful regeneration of a tissue of interest.

Several design criteria must be addressed in order to engineer a vascularized construct. The material should: 1. Be biocompatible to the host (i.e. the material must provide a favorable surface for cell attachment and proliferation). 2. Be biodegradable; the resultant degradation product must be non-toxic and easily eliminated from the body

through waste removal systems such as urine. 3. Provide enough mechanical strength in order to withstand surgical implantation and the mechanical stresses imposed by the body itself. 4. Retain a porous structure so that it not only provides sufficient space for cell migration and proliferation, but also allow the encapsulation and delivery of various biosignaling molecules.

1.1.1 **Biocompatible scaffolds for the generation of vascular structures**

Weinberg and Bell were the first to document the design of vascular biomaterials. They formed a vascular conduit initially comprised of smooth muscle cells (SMCs) seeded in a collagen gel [2]. Fibroblasts were later added to the outer rim of the vessel, ECs were added to the interior of the vessel and a polytetrafluoroethylene (Dacron) graft was introduced to provide additional mechanical strength to the newly synthesized vessel [2]. The artificially created vessel possessed differentiated ECs and produced bioactive molecules [2]. Following this discovery, other investigations employed a variety of both natural and synthetic materials to generate vascular conduits both to replace diseased arteries and to expedite the generation of vascular structures for tissue regeneration. The biomaterials utilized to design such vascular constructs are discussed below.

1.1.1.1 Biomaterials inspired by the ECM

The construction of vascular biomaterials depends on the ability of the cell population of interest to deposit a long-term layer of ECM. Living organisms produce a variety of polymers, which can be categorized into three groups: polysaccharides, proteins, and polyesters. Due to the advances in biotechnology, most of these polymers can be obtained from microorganisms. However, these polymers are still mainly obtained from

plants, animals or algae.[3]. Below, we describe the various biomaterials used to mimic the natural environment of ECs.

Collagen, the most abundant protein in the body, belongs to a family consisting of more than 20 genetic splice variants. Collagen gel exhibits shear-thinning behaviors, which means its viscosity decreases as the applied shear increases [4]. Due to collagen's fibrous nature, collagen networks usually require secondary mechanisms to produce scaffolds that can withstand the mechanical stresses induced by encapsulation or TE procedures [5]. Thus, collagen can be cross-linked with a PEG-based polymer. One group found that chondrocytes encapsulated in such a scaffold remained viable three weeks following encapsulation [6]. Another group copolymerized collagen with dextran in order to mimic tertiary embryonic connective tissue, which demonstrated improved tissue growth into the scaffold [7]. Lastly, synthetic vascular structures have been designed by embedding collagen and dermatan sulfate into prosthetic scaffolds, followed by the addition of fibroblasts or SMCs and ECs [8]. This approach yielded patency rates of 80 percent as long as twenty-six weeks following grafting into animal common carotid arteries [9].

Hyaluronanic acid (HA), a linear glycosaminoglycan which is soluble in water, can readily form hydrogels. Hyaluronidase, which exists in cells and serum, degrades it enzymatically. Much of the attention devoted to HA is due to the following HA chemical properties, among others that it can be: 1. obtained in a wide range of molecular weights (by hyaluronidase degradation); 2. enzymatically remodeled by selected cell types, such as chondrocytes; 3. functionalized with reactive group to form hydrogels; and 4. modified to adjust its cell-adhesive properties [10]. It is possible to control the degradation rate and mechanical behavior of photopolymerized HA networks [11]. Moreover, engineers have

additionally developed flat sheets of non-woven HA-based scaffolding as vascular grafts [12]. One group also showed that HA degradation products have proangiogenic activities [13]. Finally, HA-based scaffolds correlate positively with the successful treatment of osteochondral defects [14].

Fibrin is a major component of blood clots and plays an important role in spontaneous tissue repair. It forms a temporary network by polymerization of fibrinogen through the presence of the enzyme thrombin. Clinically, fibrin is used as a glue in surgical procedures. Fibrin can serve as an efficient vehicle for the delivery of growth factors or biomacromolecules [15]. It has also been used to regenerate skin and in the loading and release of growth factors [16]. Alternatively, fibrin scaffolds can serve as provisional reservoirs for the delivery of therapeutic proteins or cells for TE [17].

Alginate, a natural hydrophilic polysaccharide derived from algae, can be cross-linked in a gel with the use of divalent cations, such as $Ca^{2+}$and Mg^{2+}. The shape and strength of the gels in calcium-rich solutions can be altered [18]. Because of its hydrophilic nature, it can promote cellular proliferation with a homogeneous cell distribution within the scaffold. One author of this chapter was part of a group that effectively employed capillary action to pull human embryonic stem cells (hESCs) into an alginate scaffold [19]. Additional applications include injectable cell delivery vehicles [20] and alginate hydrogels used for cartilage TE [21]. Alginate gels can also serve as delivery vessels for proangiogenic growth factors necessary for the treatment of ischemia.

Chitin can be found in animal shells and exoskeletons of insects. It is insoluble in most common solvents but can be chemically modified into soluble derivatives, such as chitosan [22]. The derivatives are enzymatically degradable by lysozyme, which is present

in blood serum. The properties of porous chitosan matrices can be varied by altering the chitosan concentration, freezing rate, and molecular weight. It is also utilized for the controlled release of pharmacological agents and as an effective nonviral vector for gene delivery [23]. It can also be engineered into sponge-like scaffolds in bone formation and cartilage TE [24].

Dextran, a bacteria-derived polysaccharide, has been used as a potential biomaterial for TE. It is soluble in both water and organic solvents. Its chemical structure consists of a large number of hydroxyl groups, which are available for chemical modification. Such modifications are necessary since dextran is naturally resistant to cell adhesion and is used as a biomaterial surface coating to limit cell adhesion. Functional group modifications can also alter its chemical and physical properties [25]. As a result, researchers have observed different vasculature responses. Lastly, by incorporating a cell adhesion peptide, one group showed that dextran, modified with Arg-Gly-Asp (RGD) peptides, promoted EC adhesion and spreading [26].

Natural polymers are found in the living organism and are appealing for the design of biomimetic scaffolds, since they are inherently biocompatible and can be enzymatically degraded. For example, native, tissue-derived ECM may be harvested from small intestinal submucosa (SIS), umbilical veins, cadaveral arteries [27] and even xeno-geneic materials such as porcine aortas, common carotid arteries, iliac arteries and bovine ureters. The use of such natural materials is highly desirable since native ECM possesses the appropriate spatiotemporal features [28], and acts as a natural reservoir for proangiogenic molecules, [29, 30] which together efficiently direct angiogenesis. However, some major drawbacks

associated with the use of natural matrices are their susceptibility to enzymatic digestion, their propensity for thrombus formation, and their decreased mechanical strength.

1.1.1.2 Biomaterials from synthetic sources

Due to present limitations in the application of natural ECM for the fabrication of vascular constructs, other strategies are being developed and investigated. One strategy uses biodegradable (biomimetic) scaffolds to direct the synthesis of vascular structures. Interestingly, when compared to naturally derived polymers, synthetic materials have captured more attention in the recent years. Investigators have increasingly relied on scaffolds made of artificial materials to take advantage of the versatility and functionality that they provide [31]. Most synthetic polymers have the advantage that they are degraded via chemical hydrolysis and are insensitive to enzymatic processes, which limits variation among batches.

The most frequently utilized biodegradable scaffold is *polyglycolic acid (PGA),* since it is not only pliable and thus can be formed into a multitude of shapes, but it is also highly porous, allowing the diffusion of oxygen and nutrients necessary to facilitate angiogenesis.[143] PGA, which consists of monomers linked by ester bonds, can easily be degraded to glycolic acid by water through hydrolysis, both *in-vitro* and *in-vivo.* In addition, it is hydrophilic in nature, resulting in its tendency to lose mechanical strength rapidly over a period of weeks and becoming fully absorbed within a few months [32]. Its controlled rate of degradation allows cells to deposit ECM and, in so doing, permits them to establish themselves within their own microenvironment [33].

Polylactic acid (PLA) is structurally similar to PGA; however, PLA and PGA have different chemical, physical, and mechanical properties. Due to its chiral structure, PLA

can exist in two forms, PLLA or PDLLA. The former is more widely used since L-lactic acid occurs naturally; however, it is more hydrophobic compared to PGA. As a result, its degradation half-time (i.e., from months to a year) is much longer than PGA [34]. Some studies have indicated that neither PGA nor PLA may actively provoke an immune response since they pack peptide bonds [35]. The mechanical and degradation profile of the scaffold can be controlled by creating a copolymer of PGA and PLA (PLGA). However, PLGA's characteristic property is not always a linear correlation with the pure polymer. For example, PLGA containing equal ratios of PGA and PLA degrades faster than a pure PGA scaffold [32]. The hybrid scaffold was developed to differentiate hESCs since it facilitates cellular adhesion, proliferation, and viability [36].

Polyethylene glycol (PEG) is a hydrophilic polymer the native structure of which does not permit cellular adhesion. It does, however, contain one hydroxyl group at each end which can be chemically modified so as to facilitate cellular attachment. The reactive group on the PEG polymer can be cross-linked by UV irradiation to form a hydrogel that mimics tissue ECM. Additionally, the chemically modified hydrogel can incorporate bioactive molecules in order to direct cell fate. For example, *in-vivo* studies demonstrated that a VEGF-conjugated hydrogel prompted the local release of VEGF, which, in turn, promoted EC survival, growth, and concomitant vessel formation [37]. Using PEG polymers has the advantage that they can be easily cleared by the kidneys [38]. Due to their high hydration content, PEG gels can also act as a barrier to macromolecules involved in immune responses [39]. For instance, One group found that PEG gels provided a biocompatible scaffold in which chondrocytes could readily proliferate and secret ECM

[40]. Another group also reported that ECs cultured in a modified PEG hydrogel organized into stable, intricate networks of capillary like structures (CLSs) [41].

1.1.2 **Biomaterials modification**

It's important to consider cell-matrix interactions in natural ECM. In order to truly mimic the natural ECM, the aforementioned biomaterials require additional surface modifications. Modifying their surfaces with bioactive molecules is a simple way to make biomimetic materials. Earlier studies using two naturally occurring ECM components, fibronectin and laminin, to coat biomaterials, yielded improved cell adhesion and proliferation [42]. With recent advances in synthetic biology, active peptide chains on the long ECM proteins have been identified; however, laboratories can produce short peptide chains in larger quantities and more efficiently. In addition, short peptide chains are more stable during the modification process than the original long-chain protein. Moreover, the modified materials can be used in TE and can also serve as an artificial ECM, therefore providing suitable receptor-binding domains for cell attachment [43]. The biological cue that initiates the cell-signaling cascade as a result of cell-to-matrix interactions can be used to promote viability, to direct cell fate, and to guide 3D tissue formation. One of the most commonly used peptide sequences for the modification of scaffolds is RGD, the active binding site sequence on fibronectin (Table 1-1**)**. For example, to ensure covalent binding of the peptides to the surface, the surface amine reactive moieties were chemically reacted with the carboxyl functional groups presented within the bioactive peptide. A bifunctional cross-linker was used to immobilize the peptide to the surface [44]. Utilizing an RGD-modified scaffold containing sphingosine-1-phosphate, one group noted that EC migration

speeds were enhanced, thus potentially lessening the time required for ECs to organize into patent blood vessels [45].

Table 1-1. ECM Sequences and Associated Functions

Origin	Synthetic sequence	Function
Fibronectin	RGD	Cell adhesion
	KQAGDV	Smooth muscle cell adhesion[46]
	REDV	Endothelial cell adhesion [47]
Laminin	IKVAV	Neurite extension[48]
Laminin B1	YIGSR	Cell adhesion[48]
Laminin B2	RNIAEIIKDI	Neurite extension[49]
Cell adhesion molecules	KHIFSDDSSE	Astrocyte adhesion[50]
Elastin	VPGIG	Enhance elastic modulus[51]
Heparin binding domain	KRSR	Osteoblast adhesion[52]
	AGPL	Collagenase mediated degradation[53]

1.1.2.1 Biochemical cue incorporation

Surface modifications provide control over cell behavior; however, these modifications are limited because they are applicable for 2D structures rather than tissue-specific 3D structures. Bulk modifications are preferable in TE and RM applications. Several cell binding peptides have been introduced in 3D scaffolds through chemical[54], photochemical, [55], and ionic cross-linking [56]. For example, one group synthesized alginate-based hydrogels covalently coupled with RGD. The peptide-modified hydrogel promoted soft tissue augmentation *in-vivo* [57]. Also, another group demonstrated that hydrogels, fabricated with integrin binding sites and protease cleavage sites, not only promoted CLS formation but also recruited MSCs to mechanically stabilize the newly formed CLSs [41].

1.1.2.2 Biophysical cue incorporation

The mechanical properties of biomaterial scaffolds are also important. For example, in living skin substitutes used clinically to treat burns, the tension generated by fibroblasts in the collagen scaffolds is essential for the production of constructs with adequate biomechanical integrity. The ability to modify such scaffolds via extrinsic mechanisms is highly desirable, as recent studies have indicated that stem-cell differentiation may be modulated by varying the stiffness of the scaffold [58]. For instance, researchers demonstrated that, following the application of cyclic tension, SMCs seeded in scaffolds could be effectively utilized to produce bypass grafts *in vitro* [59]. Aside from vascular engineering, scientists have also demonstrated that the growth of fasciculated axons can be sustained via application of continuous mechanical tension [60]. In addition to the

application of mechanical tension, the physical properties of scaffolds may also be modified so as to facilitate cellular retention and proliferation. For instance, one group found that they could alter the local physical properties of scaffolds via exposure to a light source [61]. This study showed that the scaffold degraded following its exposure to light which, in turn, decreased its mechanical strength [61]. As a result of light-induced degradation, the scaffold-encapsulated MSCs exhibited enhanced cell spreading, a pre-requisite for cellular survival and proliferation. A vascular engineering group found that vessel diameter was increased and vessel density decreased when EPCs were cultured on a stiff, more concentrated collagen gel [62].

1.1.2.3 Drug release strategies

While scaffold architecture is important for promoting cellular attachment, proliferation and differentiation, the therapeutic efficacy of the cellular source is limited if the mitogens necessary for cellular proliferation are not present. Generally, the local injection of growth factors is not effective, because these biomacromolecules rapidly diffuse away from the injection site [63]. Thus, the local concentration of the injected growth factors cannot effectively facilitate the proliferation of the cells encapsulated in the scaffold. In order to overcome this limitation, scaffolds should be designed so that the biomacromolecules are sequestered in the scaffold, but are also released in a steady state fashion to promote prolonged cell proliferation. Considering that most biosignaling molecules have a short life span and are unstable *in-vivo*, the scaffold should be designed to serve as a protective barrier against protease and/or immune degradation. In this way, the scaffold must act as a protective agent for the biosignaling molecules, preventing their

degradation by the harsh physiologic surroundings. When the scaffold does degrade, whether through hydrolysis or enzymatic degradation, biosignaling molecules may be released, which may recruit surrounding cells, such as ECs, to contribute to the delivery of oxygen and nutrients to the rapidly proliferating cells.

1.2 *Blood vessels and vascular therapy*

1.2.1 **Angiogenesis and vascular system**

The vascular system — the sole means for delivery of nutrients, water, oxygen, and proteins to tissues and for removal of wastes and other by-products — is essential for the proper functioning of tissue. During embryogenesis, blood vessels are optimally constructed, so that new formation of blood vessels (neovascularization) is rarely needed for adults in normal physiological condition. Neovascularization is commonly divided in two subcategories (Figure 1-1): vasculogenesis and angiogenesis. Angiogenesis is the formation of new blood vessels from pre-existing vessels, whereas vasculogenesis occurs in the absence of pre-existing vessels. Both occur in adult neovascularization, such as in the process of wound healing or during women's ovarian cycle. But abnormal blood vessel formation can also occur during such pathologies as inflammation or tumors: chronic inflammation will induce angiogenesis in attempts at healing, while tumors will induce angiogenesis to provide nutrients for malignant cells' metabolic demands.

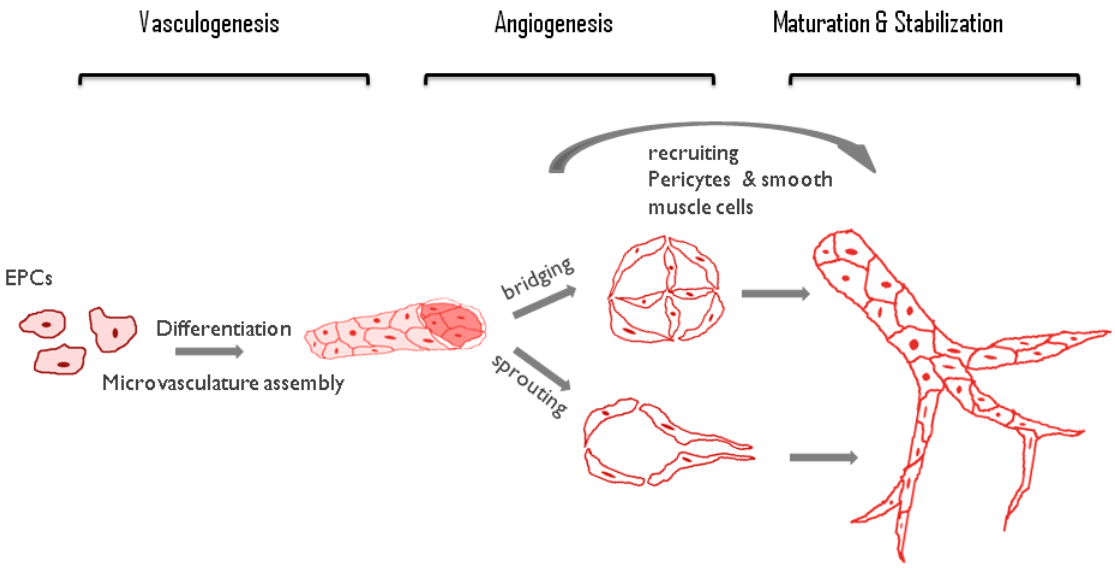

Figure 1-1. Schematic of neovascularization process, which begins with EPCs.

1.2.2 Stem Cells for regenerative medicine

Stem cells (SCs) are defined as clonogenic populations of cells capable of self-renewal into additional stem cells and of differentiation into the various cell lineages [64]. Not all stem cells are alike, differing in their degree of plasticity. For example, totipotent stem cells (from fertilized embryos) can give rise to a functional organism; pluripotent stem cells (from the inner cell mass of the embryo) can produce all tissue types; and multipotent stem cells (from adult tissue stem cells) can generate a limited range of cells within a given tissue (e.g., blood and lymphoid cells in the hematopoietic system). As our understanding of these stem cell populations (briefly explored below) continues to grow, scientists are harnessing the seemingly unlimited potential of these once ambiguous cells for a wide array of therapeutic modalities.

1.2.2.1 Endothelial progenitor cells (EPCs).

There are studies have shown that EPCs, first derived from peripheral blood and from bone marrow, are the major factor in neovascularization: during postnatal vasculogenesis, EPCs circulate from bone marrow, incorporate into sites of neovascularization, and differentiate into ECs to form blood vessels [65]. Following these studies, EPCs were isolated from various sources: umbilical cord blood, the liver, tissue-residing cells, or vascular walls themselves. Despite the proliferative potential of adult EPCs and other progenitor cells, several reports have indicated that a decline in the proliferation and differentiation abilities of these cells is associated with aging and chronic diseases[66].

1.2.2.2 Induced pluripotent stem cells (hiPSCs).

The field of stem cell technology was revolutionized when the discovery was announced that a patient's terminally differentiated cells (somatic cells) could be re-programmed to produce any cell type of interest [67]. Reportedly, such cells not only offer the advantage of supplying unlimited numbers of cells for patient needs, but perhaps more importantly, pose no threat to immune-mediated graft rejection since the cells are derived directly from the patient. Such cells have been termed induced pluripotent stem cells (iPS), adult somatic cells which have been re-programmed to assume an ESC-like phenotype via introduction of either of two transcription factor sets: Oct4, Nanog, Sox2, Lin28 or Oct4, c-Myc, Sox2, Klf4 [68]. The breakthrough discovery that terminally differentiated adult cells could be induced to de-differentiate into pluripotent stem cells intensified research into the use of such cells for the treatment of a wide array of diseases. Using animal models, iPS cells have been demonstrated to regenerate cardiac tissue and restore

contractile function after experimentally-induced ischemia [69]. For instance, researchers discovered that iPS cell lines could be guided to form vascular structures through the use of methodology previously validated to direct the differentiation of hESCs into vascular cells [70]. It also reported that the iPS-derived vascular cells expressed EC-specific markers and organized into capillary-like structures (CLS) when cultured on Matrigel, an extracellular matrix (ECM)- rich material known to support the formation of CLS. Interestingly, a fraction of the vascular lineage-differentiated iPS cells were further differentiated into perivascular-like cells (e.g., SMCs) as evidenced by their expression of SMC specific markers α-smooth muscle actin (α-SMA) and calponin [70].

Stem cell-based therapy can be an approach to enhancing neovascularization. Biomaterial scaffolds are widely used to provide a three-dimensional (3-D) microenvironment for culturing vascular SCs *in vitro* and as their carrier for transplantation. The aim is to maximize angiogenic potential in the scaffold to mimic the microenvironment in nature. Modifications of the scaffold are necessary to ensure favorable biocompatibility with seeded cells and surrounding tissues.

1.3 *Merging Biomaterials science and stem cell technology for vascular regenerative medicine*

1.3.1 **Vascularized constructs.**

There are two methods of vascularize a construct: extrinsic and intrinsic. In the extrinsic method, vascularization of the engineered scaffold is promoted by materials

design, cell sources, and culture environment. The scaffold is prevascularized *ex vivo* and is transplanted *in vivo* to encourage integration with the local vasculature. Prevascularization is mostly achieved by modifying the scaffold with extracellular matrix (ECM) proteins and peptides organized to guide angiogenesis. The intrinsic method utilizes several vectors (SCs or angiogenic factors) to direct local microvasculature to infiltrate the scaffold *in vivo*.

While the cellular environment plays a key role in directing stem cell fate, the ubiquitous availability of oxygen and nutrients to drive sustained cellular proliferation and tissue growth is essential. Indeed, without the availability of oxygen and nutrients carried by red blood cells circulating within patent blood vessels, all attempts to regenerate a tissue of interest will be futile. Thus, researchers have focused designing biomaterials which facilitate the formation of blood vessels both *in-vivo* and *ex-vivo*. Appreciating the cellular components that comprise blood vessels must precede understanding what cell populations produce blood vessels and which biomaterials favor their growth. While variations exist depending on the type of vessel (i.e., artery, capillary or vein), all blood vessels have the same general structure: the tunica intima, the innermost layer of the blood vessel, is composed of endothelial cells (ECs) which line the lumen of the vessel; the tunica media, the middle layer of the blood vessel, comprises mural cells (pericytes and smooth muscle cells [SMCs]) which provide the vessel with its contractile and mechanical properties; and the tunica adventitia, the outermost layer of the blood vessel, comprises a variety of connective tissues and fibroblasts which provide the vessel with structural stability. Along these lines, biomaterials must be designed so as to favor the migration, proliferation, and tube-like formation of vascular ECs. In order to design such a scaffold, these materials

must not only provide favorable attachment sites for ECs but must additionally possess pores of an appropriate size, quantity, and distribution to allow both the 3D migration and tube formation from ECs and the subsequent diffusion of oxygen and nutrients necessary to facilitate tissue regeneration [71, 72].

It is also well known now that cells inside the human body are in a 3D microenvironment. A scaffold can serve as a structural template for cell adhesion, proliferation, and differentiation or as a delivery vehicle for bioactive molecules during tissue assembly. A variety of both natural and synthetic materials have been developed to optimize the interactions with SCs. These materials are often constructed into porous, fibrous hydrogel scaffolds. A porous structure can provide the structural void into which cells can migrate, whereas a fibrous scaffold mimics the structure of the ECM. Hydrogels, which are water-swollen polymers, may be fabricated from natural ECM components or from synthetic materials to mimic the microenvironment. Vasculogenesis from hESCs has been demonstrated in alginate, dextran, and hyaluronic acid hydrogels [73-75], while ECs derived from hESCs have generated functional vascular networks within a synthetic porous scaffold [76]. One study has demonstrated that EPCs are able to form tube-like structures; it compared the formation and functions of tissue-engineered blood vessels generated by peripheral-blood- and umbilical-cord-blood-derived EPCs in a model of *in vivo* vasculogenesis. The study found that adult peripheral blood EPCs formed blood vessels that were unstable and that regressed within three weeks. In contrast, umbilical cord blood EPCs formed normal functioning blood vessels that lasted for more than four weeks [77].

1.3.2 **Delivery of angiogenic factors.**

One intrinsic method for enhancing neovascularization of an engineered scaffold utilizes biochemical signaling pathways. Studies have shown that to improve the ability of host vessels to infiltrate the scaffold and damaged tissues, many growth factors such as vascular endothelial growth factor (VEGF), platelet-derived growth factor, transforming growth factor-beta, and basic fibroblast growth factor promote angiogenesis and vasculogenesis in either cell culture or animal models[78]. Incorporating angiogenic factors into scaffolds has proven to have positive effects on vascularization. For example, VEGF is one of the most extensively studied and crucial angiogenic factors. Upon implantation of a VEGF-hyaluronic acid hydrogel into mice to study its *in vivo* effects, researchers observed an increase in microvessel density and growth, demonstrating that ECs are able to migrate through the hydrogel and that the VEGF contributed a strong angiogenic effect [79]. EPCs from umbilical cord blood, cultured on a VEGF-fibrin hydrogel, were observed to maturate and differentiate towards ECs [80], while collagen gel modified with VEGF has been shown to enhance capillary formation and tissue in growth [81].

Overall, a great deal of effort has been expended to develop scaffolds which mimic the natural environment in which stem cell populations reside. However, additional work is required in order to obtain clinically successful implants. Therefore, the future of TE and RM requires focusing on design techniques that improve stem cell retention, survival, proliferation, and differentiation. This endeavor will involve many interdisciplinary fields, including medicine, biology, engineering and material science. In addition, such factors as oxygen diffusion, hypoxia, and cell-cell interactions must also be considered when

designing a biomimetic scaffold. Continued improvements in biomaterial design and greater understanding of stem cell biology hold the promise of allowing the successful treatment of many diseases. To reach this goal, TE and RM must cooperate to create functional biological substitutes which repair, improve, and maintain the original tissue function.

1.4 *Thesis Overview*

Tissue engineering and regenerative medicine have been playing a pivotal role in recent biomedical field advancement. Combining improved biomaterials designs and stem cell technology enable researchers testing novel approaches for their clinical relevance. The overall hypothesis of this thesis is that synthetic bioactive hydrogel can be exploited for translational approach to study vascular disease and to elicit translational angiogenesis therapy to treat injuries. This thesis can be divided into three specific aims:

Specific Aim 1: Using *in vitro* 3D bioactive hydrogel to study cancer angiogenesis.

There is a growing trend for *in vitro* platforms to model basic biological sequences in disease model, here we utilized 3D hydrogel scaffold to resemble the microenvironmental effects on cancer cell fate and its angiogenic potential. The study for this specific aim will be presented in Chapter 3.

Specific Aim 2: Investigate *in vivo* diabetic disease model for therapeutic wound healing.

For regenerative medicine purpose, we further expand the vascularized bioactive constructs with combination of stem cell vascular technology and translated to a disease

injury model to investigate potential therapeutic strategy. The study for this specific aim will be presented in Chapter 4.

Specific Aim 3: Utilizing bioactive hydrogel scaffold to treat *in vivo* porcine burn injury.

Severe deep tissue injuries also pose opportunities for new therapeutic strategy. Here we utilize our bioactive hydrogel platforms to investigate the burn wound healing in larger animal as an approach for future regenerated medicine application in human. The study for this specific aim will be presented in Chapter 5.

Parts of the current chapter is reproduced by permission of World Scientific Company.

2 *Overview of Experimental Methods*

2.1 *Macromer synthesis*

Acrylated HA macromer synthesis was conducted as previously reported [82-84]. In brief, AHA was synthesized in two steps: (1) the tetrabutyl-ammonium salt of HA (HA-TBA) was formed by reacting sodium hyaluronate (90 kDa, LifeCore Biomedical) with the ion exchange resin Dowex-100 (Sigma) and neutralizing with 0.2M TBA-OF (Sigma); (2) acrylic acid (3 eq) and HA-TBA (1 eq) were coupled in the presence of dimethylaminopyridine (DMAP; 0.15 eq) and di-tert-butyl dicarbonate (3 eq) in DMSO, followed by dialysis and lyophilization. ^{1}H NMR spectra were used to confirm the modification of the AHA. The cell-adhesive peptide GCGYGRGDSPG (RGDS, molecular weight [MW]: 1025.1 Da) and MMP-sensitive peptide crosslinker GCRDGPQGWGQDRCG (MMP, MW: 1754 Da) were purchased (Genscript, > 95% purity per manufacturer HPLC analysis.)

The dextran hydrogel macromere was synthesized and characterized as previously [85-87]. Briefly, allyl isocyanate (AI) was incorporated into dextran by dissolving pre-dried dextran (e.g. 2g) in anhydrous DMSO (20mL) at room temperature under nitrogen gas. Reaction catalyst DBTDL was added (0.210mL), and AI (0.240 mL) was added to the solution dropwise. After the reaction, the solution was precipitated in cold excess isopropanol and filtered. Next the remaining hydroxyl groups in Dex-AI were substituted with ethylamine groups. For this step, pre-dried Dex-AI (e.g. 2g) was first dissolved in

DMSO (30ml) under nitrogen gas. Meanwhile, BEAHB (3.75g) was dissolved in DMSO (10ml) in a separate chamber. Catalyst TEA (11.2mL) was added to the Dex-AI DMSO solution, and the dissolved BEAHB in DMSO was added to the solution dropwise. After the reaction, TEA salt was filtered and the resulting solution was precipitated in cold excess isopropanol and filtered. The resulting Dex-AE was then dialysized against distilled water for 3 days and lyophilized for additional 3 days. The purified polymer was stored in vacuum until further use. For characterization NMR of the polymer for degree of substitution for thiol group (AI) and aminated group (AE) was performed. For crosslinking, polyethylglycol diacrylate (PEGDA) was synthesized as previously established and dialysized against distilled water for 3 days and lyophilized for additional 3 days. The purified polymer was stored in 4°C until further use.

2.2 *Cell cultures*

HT1080 cells (ATCC, Manassas, Virginia) were cultured according to the manufacturer's instructions in Dulbecco's Modified Eagle's medium (DMEM, GIBCO) supplemented with 10 % fetal bovine serum (FBS GIBCO). For cell encapsulation and cell cycle studies, HT1080 cells were synchronized under serum-free media for three days with daily media change. Human umbilical cord blood ECFCs were provided by Dr. Merv C. Yoder, Indiana University School of Medicine, and expanded and used for experiments between passages 6 and 9, as previously described [82, 88]. ECFCs were cultured in flasks precoated with type I collagen (Roche Diagnostics, Basel, Switzerland), in endothelial growth medium (EGM, PromoCell, Heidelberg, Germany) supplemented with 1 ng/ml

$VEGF_{165}$ (Pierce, Rockford, IL). All cell cultures were incubated in a humidified incubator at 37 °C in an atmosphere containing 5 % CO_2. Both HT1080 cells and ECFCs were passaged every four to five days with 0.05 % trypsin (Invitrogen, Carlsbad, CA), and media were changed every other day.

Early vascular cells (EVCs) expansion and differentiation from BC1 and type 1 diabetes (T1D) human induced pluripotent stem cell (hiPSC) lines were followed our establsihed protocols [89, 90]. Briefly, undifferentiated hiPSC (BC1 and T1D) were maintained on inactived mouse embryonic fibroblast feeder layers in growth medium with 80 percent ES-EMEM/F12 (Global Stem), 20 percent serum replacement (Invitrogen), and 10ng/ml basic fibroblast growth factor (bFGF). For differentiation, hiPSCs were collected through digestion with EDTA (Promega), single cells were seeded and plated onto collagen IV (Trevigen)-coated with concentration of 5 X 10^4 cell/cm^2 supplemented with 10μM ROCK inhibitor Y-27632 (Stemcell Technologies). Cells were cultured for 6 days in a differentiation medium composed of alpha-MEM (Invitrogen), 10% FBS (HyClone), and 0.1 mM β-mercaptoethanol (β-ME), with the medium changed daily. Differentiated cells were collected through digestion with TrypLE (Invitrogen) on day 6 and seeded at a concentration of 2 X 10^4 cells/cm^2 on collagen type IV-coated plates in endothelial cell growth media (ECGM) (PromoCell) supplemented with 2% FBS, 50 ng/mL VEGF with 10 μM SB431542 (Tocris) for 6 d. The medium was changed every other day. ECFC (Lonza) were cultured under manufactured protocols. Briefly, cells were seeded and expanded in endothelial growth media EGM-2 (Lonza) and cells with passages 6 through 8 were used for experiments as previously described [89, 91].

2.3 *In vitro cellular scaffolds*

2.3.1 **Hydrogel formation**

For hydrogel formation, AHA macromer was dissolved in triethanolamine-buffered saline (TEOA buffer: 0.2 M TEOA) at 3 % w/w. The cell adhesive peptides (RGDS, GenScript) were dissolved in TEOA buffer and added to the AHA solution to reach a final peptide concentration of 3.8 mM and allowed to react for one hour with gentle shaking. For crosslinking, MMP crosslinker (MMP, GenScript) dissolved in TEOA buffer was added to reach a final concentration of 2.57 mM (soft) 5.15 mM (medium), or 10.3mM (stiff). Hydrogels were allowed to swell for three hours prior to mechanical testing.

For hydrogel preparation Dex-AE and PEGDA were dissolved at the weight ratio of 80:20 into phosphate-buffered saline containing 0.1% (w/w) Irgacure® 2959. The mixture was pipetted into a sterile mold made by polydimethylsiloxane and photocrosslinked (10mW/cm^2 of UV light for 10 minutes). Hydrogels were swelled against PBS for swelling ratio and crosslink density characterization. *In vitro* cell toxicity was carried using WST assay (Sigma) as well as pilot *in vivo* burn mice tests [87] were done to confirm AE hydrogel therapeutic properties.

2.3.2 **Cell encapsulation**

We engineered human vascular networks within the AHA hydrogels similar to our previous studies [82, 91]. AHA macromer was dissolved in triethanolamine buffered saline (TEOA buffer: 0.2M TEOA) at 3 wt%. Cell adhesive peptides (RGDS, GenScript) were dissolved in TEOA buffer and added to the AHA solution to the final peptide concentration

of 4.8mM along with Recombinant human $VEGF_{165}$ (Pierce), bFGF (Invitrogen), Ang-1 (R&D Systems), TNF-alpha (R&D Systems), and stromal cell-derived factor-1 (SDF-1; R&D Systems) were also added into the AHA-RGDs mixture at 50 ng/ml. The mixture was allowed to react for 1 hour with gentle shaking. For crosslinking, MMP cross linker (MMP, GenScript) dissolved in TEOA buffer was added to a final concentration of 5.15 mM. Preconditioned ECFCs and EVCs were encapsulated in AHA hydrogels at a density of 5 X 10^6 cells/ml by suspending the cells in the AHA-RGD solution as described above prior to the addition of the MMP crosslinker. A 50ul volume of the final mixture was pipette into sterile molds (5 mm diameter, 2 mm height) and allowed to react for 10 minutes at room temperature in laminar flow hood.

Preconditioned HT1080 cells were encapsulated in AHA hydrogels with densities of 1, 5, and 10 x 10^6 cells/ml by suspending the cells in HA-RGD solution, prior to addition of the MMP crosslinker. We pipetted 50 µl of the final mixture into sterile molds and allowed it to react for ten minutes at room temperature in a laminar flow hood. The constructs were then cultured in HT1080 growth media in the conditions described throughout this paper.

2.4 *Animal use*

2.4.1 **Rodent**

The standard protocol for STZ induced diabetes mellitus provided by Animal Models of Diabetic Complications Consortium was followed [92-94]. Nude mice at about 2-2.5 months of age (about 20-25 g body weight) were randomly assigned to a diabetic or a non-diabetic group. Animals in the diabetic group were induced by 5 intraperitoneal

injection of STZ at a dose of 50 mg/kg body weight (STZ is freshly dissolved in citrate buffer, pH 4.5). Prior to injection, mice were fasted for 4 to 6 hours. The weight and blood glucose of each mouse were checked daily for up to 2 weeks after the STZ injection. Successful STZ-induced diabetic mellitus nude mice were confirmed by two consecutive blood glucose levels readings which were higher than 300 mg/dl over a 48 hour period. Blood glucose was measured using an Accuchek blood glucose meter (Roche) by obtaining 20-25µl of blood from the tail vein puncture (30 gauge needle).

DFU animal model was constructed by incorporating varies protocols from the literatures [92, 95-98]. After diabetic mellitus was confirmed, diabetic induced nude mice were anesthetized with isoflurane (Thermo Fisher). A depilatory was applied (Nair), prior to wound creation, to ensure better dressing adherence. Next, 2 x 6mm diameter punch wounds were made, using a biopsy punch (Integra), taking care to remove full-thickness skin on each side of the posterior dorsum. Vascularized constructs, which were generated *in vitro*, were then transplanted into one side of the animal (one per wound). The time point was logged as day 0 post-wounding. Betadine was applied around the periphery of the wound to enhance dressing adherence. The other wound on the other side is left no vascularized constructs treatment. Both wounds were then covered with Tegaderm dressing (3M). 6 to 8 constructs were implanted for each group at each time point. At each time point of interests, as described below, human specific fluorescein- conjugated *Ulex europaeus I* (*UEA-I*) *Lectin* (1:10; Vector Laborato) and mouse-specific rhodamine-conjugated *Isolectin Griffonia simplicifolia* (*GS*)-IB_4 (1:10; Invitrogen) were injected through the tail veins of the mice [82, 89, 91]. After 30 minutes, the mice were euthanized, and the constructs were harvested and fixed in 3.7% formaldehyde (Sigma). The tissue was

processed for immunohistochemistry or histology. The Johns Hopkins University Institutional Animal Care and Use Committee approved all animal protocols.

2.4.2 **Procine**

Surgical procedures were approved by the Institutional Animal Care and Use Committee at Thomas D. Morris, Inc. prior to the experiments. All pigs were fasted for at least 12 hours prior to any surgical procedure. Anasthesia was induced by an intramuscular injection of Telazol cocktail reconstituted with ketamine and xylazine. Then, the pig was endotracheally intubated and ventilated mechanically to aid breathing and to provide up to 1.5% of isoflurane (depending on the painfulness of the procedure) to maintain anasthesia. In addition, blood pressure, heart rate, body temperature, and blood oxygen level was monitored. Bair Hugger® was placed under the pig and set to 43°C to maintain a normal body temperature.

Circular biopsy punches were used for partial or complete excision for full-thickness wound down to the necrotic adipose layer. Wounds were at least 3cm apart from one another to minimize hindered wound healing process due to proximity. After the excision procedure, wounds were cleaned with sterile gauze to temporarily stop bleeding. Half of the wounds were treated with dextran hydrogel and the other half were left untreated. Hydrogels were crosslinked in molds that matched the size of the excised wounds. Treated and untreated wounds were first sealed with Tegaderm® (3M). The peripheries of the wound site was applied with compound benzoin tincture (Medical Chemical, Corp) to enhance the Tegaderm® adherence to the skin. An additional layer of Vetrap® (3M) was applied to the torso and elastic body suit (VetMedCare) were worn over the body in order to minimize the disturbance of the healing wounds. To protect the newly

forming epidermis from traumatization during bandage change, a non-adhesive Curity® dressing (Covidian) was placed under the Tegaderm®. After wound closure, only an elastic body suit was worn over the wounds. For retreatment, re-debridement was made and a new half the thickness hydrogel was placed on top for retreatment. Secondary excision was made on control group as well for the retreatment group. Dressings were changed three times a week until wound closure was complete. Before the dress change, the pig was put under anesthesia with an intramuscular injection of Telazol cocktail reconstituted with ketamine and xylazine. The pig did not receive isoflurane because the procedure was quick. Before reapplying dressings, the wound area was scrubbed with 4% chlorhexidine and ethanol. The area was wiped with dry gauze and new dressings were applied.

To evaluate healing, skin specimens were biopsied at each time point as complete horizontal cross-sections of approximately 5cm in thickness with a sterile blade. Analgesics were administered before wound creating and biopsy procedures, and transdermal fentanyl patch was applied for 9 days post-operation. Blood tests were performed regularly to monitor the pig's health throughout the study.

2.5 *Healing analysis*

2.5.1 **Bloodflow and Planetary Measurement**

During the study, the blood flow profiles inside the wounds were monitored noninvasively using moorFLPI speckle contrast imager (Moor Instruments, Inc.). The measurements were normalized by the blood flow measurements of the adjacent healthy skin area. Wound gap area was measure photometrically by tracing the opened wound edge using Image J. Photometric analysis of wound closure rate was done along with blood flow

measurement.

2.5.2 **Histology**

Following fixation of the explants, the samples were dehydrated in serial ethanol (70%–100%), embedded in paraffin, serially sectioned at 5 μm, and stained with either H&E, Masson trichrome, and Verhoeff-van Gieson's stain or immunohistochemistry for CD31 (1:50 Abcam), cytokeratin 14 (1:50 Abcam), MAC387 (1:50 Abcam), SMA (1:100 Dako), Dapi (1:1000), PGP9.5 (1:500 AbD Serotec) and matching Alexaflour secondary (1:500 Lifetech) or immunoperoxidase stains for anti-mouse alpha-smooth muscle actin (alpha-SMA) (Abcam), or anti-human CD31 (Dako). Double staining was performed using the same anti-human CD31 and anti-mouse alpha-SMA followed by conjugation with anti-mouse Alexa Fluor 488 (Life Technologies) or anti-rabbit Alexa Fluor 564 (Life Technologies) and counter stain with Dapi. Histological images were taken with an upright light microscope (Nikon Accuscope 3000) and a camera (Nikon DS-F12). Full specimens images were scanned and tiled together using automated motor controlled Nikon T1 and tiled together with corresponded software (Nikon Nis-Element). Fluorescent images were taken with confocal (Zeiss LSM780). The area and number of vessels inside the wounds were quantified using ImageJ software (National Institutes of Health) with histology sample of each wound stained with CD31. The vessels were imaged at the edges, middle, and top portions of each wound, and the positively stained areas were selected using the software's threshold function. The selected areas were then quantified using "Analyze Particles" plugin of ImageJ. "Microvessels" with areas less than 78μm^2 were excluded to filter out noise.

Histologically analysis for the maturation of the re-epithelialization is quantified by

rete ridge formation density as previously described [99]. Collagen fiber deposition was quantified from Masson trichrome images by calculating the percentage of collagen fiber presented in the wound. Briefly, using ImageJ, we quantified the percentage of stained collagen fibers in the given area in each group. Elastin fibers were quantified from Verhoeff-van Gieson's stain across the dermis area adjacent to the epidermis similarly to the collagen. Nerve innervation analysis was performed on a 25μm paraffin sections on gelatin coated slides. Samples were incubated in primary antibody overnight and 1 hour in secondary antibody. Slides were then analyzed in confocal using serial z-stack imaging. Final images were maximum intensity projected through z axis for the final images.

2.6 ***Gene Expression***

Two-step RT-PCR was performed for *VEGF*, *ANG-1*, *MMP-1*, *GLUT*-1, *BNIP3*, *BNIP3L*, *18S*, *GAPDH*, and *beta-actin*, and samples were examined in triplicate, analyzed, and graphed. Briefly, RNA was extracted using TRIzol (GIBCO) according to the manufacturer's instructions. To extract porcine RNA, a small specimen was collected from each wound at different time points and snap-frozen in liquid nitrogen. The specimen was crushed with pestle and mortar, and the powdered sample was put in 1mL of Trizol reagent and stored in -80°C until further use. Total RNA was quantified by nanodrop spectrophotometer. Gene expression assays were performed on an Applied Biosystems StepOne Real-Time PCR system according to the manufacturer's instructions. The relative expression of genes was normalized to the indigenous control genes. The comparative CT method was used to calculate amplification differences on targeted genes. The values for

experiments (n=3) were averaged and graphed. Wound healing and ECM RT-PCR array sets (Qiagen) were used to compare the expression profile inside the treated and non-treated wounds at different time points. For each primer, the comparative computerized method provided by the manufacturer was used to calculate the amplification differences between different samples.

3 *Hylauronic acid hydrogel stiffness and oxygen tension affect cancer cell fate and endothelial sprouting*

Three-dimensional (3D) tissue culture models may recapitulate aspects of the tumorigenic microenvironment *in vivo*, enabling the study of cancer progression *in vitro*. Both hypoxia and matrix stiffness are known to regulate tumor growth. Using a modular culture system employing an acrylated hyaluronic acid (AHA) hydrogel, three hydrogel matrices with distinctive degrees of viscoelasticity — soft (78±16 Pa), medium (309± 57 Pa), and stiff (596± 73 Pa) — were generated using the same concentration of adhesion ligands. Oxygen levels within the hydrogel in atmospheric (21 %), hypoxic (5 %), and severely hypoxic (1 %) conditions were assessed with a mathematical model. HT1080 fibrosarcoma cells, encapsulated within the AHA hydrogels in high densities, generated nonuniform oxygen distributions, while lower cell densities resulted in more uniform oxygen distributions in the atmospheric and hypoxic environments. When we examined how varying viscoelasticity in atmospheric and hypoxic environments affects cell cycles and the expression of *BNIP3* and *BNIP3L* (autophagy and apoptosis genes), and *GLUT-1* (a glucose transport gene), we observed that HT1080 cells in 3D hydrogel adapted better to hypoxic conditions than those in a Petri dish, with no obvious correlation to matrix viscoelasticity, by recovering rapidly from possible autophagy/apoptotic events and

alternating metabolism mechanisms. Further, we examined how HT1080 cells cultured in varying viscoelasticity and oxygen tension conditions affected endothelial sprouting and invasion. We observed that increased matrix stiffness reduced endothelial sprouting and invasion in atmospheric conditions; however, we observed increased endothelial sprouting and invasion under hypoxia at all levels of matrix stiffness with the upregulation of vascular endothelial growth factor (*VEGF*) and angiopoeitin-1 (*ANG-1*). Overall, HT1080 cells encapsulated in the AHA hydrogels under hypoxic stress recovered better from apoptosis and demonstrated greater angiogenic induction. Thus, we propose that oxygen tension more profoundly influences cell fate and the angiogenic potential of 3D cultured HT1080 fibrosarcoma cells than does the matrix stiffness.

3.1 *Introduction*

Three-dimensional (3D) cell culture models recapitulate aspects of the *in vivo* extracellular matrix (ECM) microenvironment, allowing the study of tumor development and progression under pathologically relevant culture conditions [100-104]. Specifically, hydrogels are structurally and mechanically similar to the native ECM of many tissues and have been utilized as matrices to study cellular responses to a range of microenvironmental signals [105-107]. Hydrogels composed of natural matrices have inherently limited tunability for independently studying effects of several physiochemical properties on cellular responses, since changes in features such as mechanics and adhesion are coupled [9–11].

In contrast, engineered hydrogels that mimic various cues of the tumor microenvironment and ECM-cell interactions can be used to study the independent and codependent effects of specific cues in the microenvironment on cancer cell responses [104, 108]. For example, highly porous scaffolds fabricated from synthetic poly(lactide-co-glycolide) have been used to generate an *in vitro* human tumor model that exhibits microenvironmental conditions representative of tumors *in vivo* [109]. More recently, Gill et al. utilized a synthetic polymer-based scaffold composed primarily of polyethylene glycol, which offers biospecific cell adhesion and cell-mediated proteolytic degradation with independently adjustable matrix stiffness. They demonstrated that altering both matrix stiffness and the concentration of cell-adhesive ligand significantly influenced epithelial morphogenesis of a metastatic cell line (344SQ) [110]. ECM rigidity has been show to alter tumor cell proliferation and migration [111, 112] and resistance to chemotherapeutics [112]. Similarly, ECs have been found to change their behavior and morphology depending on substrate stiffness [113, 114]. Hence, engineering the mechanical stiffness of hydrogel, while decoupling it from other key properties such as cell adhesion, may elucidate how the tumor's physical environment contributes to its growth and angiogenesis.

Along with the adhesive and mechanical properties of the microenvironment, hypoxia is an important determinant of cell behavior. Hypoxia occurs when the partial pressure of O_2 falls below 5 %, inducing myriad cellular and systemic adaptations [115, 116]. In fact, during tumor growth, cells inevitably experience depletion of nutrients, including oxygen due to extensive growth [117]. Cellular responses to hypoxia are primarily regulated by hypoxia-inducible factors that accumulate under hypoxic conditions and activate numerous pathways that regulate a variety of cellular activities [118-122],

such as promoting tumor growth and angiogenesis during embryonic development [117, 123, 124].

3.2 *Materials and Methods*

3.2.1 **Cell cultures**

HT1080 cells (ATCC, Manassas, Virginia) were cultured according to the manufacturer's instructions in Dulbecco's Modified Eagle's medium (DMEM, GIBCO) supplemented with 10 % fetal bovine serum (FBS GIBCO). For cell encapsulation and cell cycle studies, HT1080 cells were synchronized under serum-free media for three days with daily media change. Human umbilical cord blood ECFCs were provided by Dr. Merv C. Yoder, Indiana University School of Medicine, and expanded and used for experiments between passages 6 and 9, as previously described [82, 88]. ECFCs were cultured in flasks precoated with type I collagen (Roche Diagnostics, Basel, Switzerland), in endothelial growth medium (EGM, PromoCell, Heidelberg, Germany) supplemented with 1 ng/ml $VEGF_{165}$ (Pierce, Rockford, IL). All cell cultures were incubated in a humidified incubator at 37 °C in an atmosphere containing 5 % CO_2. Both HT1080 cells and ECFCs were passaged every four to five days with 0.05 % trypsin (Invitrogen, Carlsbad, CA), and media were changed every other day.

3.2.2 **Macromer synthesis**

AHA macromer synthesis was performed as reported previously [125]. Briefly, we synthesized AHA in two steps: (1) the tetrabutyl-ammonium salt of HA (HA-TBA) was formed by reacting sodium hyaluronate (90 kDa; LifeCore Biomedical, Chaska, MN) with the ion exchange resin Dowex-100 (Sigma) and neutralizing with 0.2 M TBA-OF (Sigma);

(2) acrylic acid (3 [eq]) and HA-TBA (1 eq) were coupled in the presence of dimethylaminopyridine (DMAP; 0.15 eq) and di-tert-butyl dicarbonate (3 eq) in DMSO, followed by dialysis and lyophilization. We used ^{1}H NMR spectra to confirm the modification of the AHA. The cell-adhesive peptide GCGYGRGDSPG (RGDS, molecular weight [MW]: 1025.1 Da) and MMP-sensitive peptide crosslinker GCRDGPQGWGQDRCG (MMP, MW: 1754 Da) were purchased (Genscript; greater than 95 % purity, per manufacturer's HPLC analysis).

3.2.3 *In vitro* cellular scaffolds

3.2.3.1 Hydrogel formation

For hydrogel formation, AHA macromer was dissolved in triethanolamine-buffered saline (TEOA buffer: 0.2 M TEOA) at 3 % w/w. The cell adhesive peptides (RGDS, GenScript) were dissolved in TEOA buffer and added to the AHA solution to reach a final peptide concentration of 3.8 mM and allowed to react for one hour with gentle shaking. For crosslinking, MMP crosslinker (MMP, GenScript) dissolved in TEOA buffer was added to reach a final concentration of 2.57 mM (soft) 5.15 mM (medium), or 10.3mM (stiff). Hydrogels were allowed to swell for three hours prior to mechanical testing. The elastic modulus (G') was measured using a constant strain rheometer with steel cone plate geometry (25 mm in diameter; RFS3; TA Instruments). The strain was maintained at 20 % during the time sweeps by adjusting the stress amplitude at a frequency of 10 Hz. Three samples were tested for each gel. The tests occurred in a humidified chamber at a constant temperature (25 °C) at 30-second intervals. We then calculated Young's elastic modulus using $E = 2G'(1 + \nu)$. Assuming the hydrogel is incompressible, the Poisson ratios (v)

approach 0.5, and the relationship becomes $E=3G'$. The same approach was used to measure the constructs along the culture period.

3.2.3.2 Cell encapsulation

Preconditioned HT1080 cells were encapsulated in HA hydrogels with densities of 1, 5, and 10 x 10^6 cells/ml by suspending the cells in HA-RGD solution, as above, prior to addition of the MMP crosslinker. We pipetted 50 µl of the final mixture into sterile molds and allowed it to react for ten minutes at room temperature in a laminar flow hood. The constructs were then cultured in HT1080 growth media in the conditions described throughout this paper.

3.2.4 *In vitro* hypoxia construct

3.2.4.1 Oxygen modeling

Oxygen tension profiles were modeled within the gels following a previously established method for collagen gels [126]. Briefly, to estimate DO gradients in 3D AHA gels, we first determined the V_{max} and K_m parameters of HT1080 cells in 3D AHA 3 % w/w gel. We attached oxygen sensor patches (Presens, Regensburg, Germany) to the bottoms of the 96-well plates. Cells were then seeded at 2 million cells/ml with 50 µl of media in the well. Next, we sealed the well completely, to provide a closed system for oxygen measurement, and allowed them to reach anoxia. Using DO level data measured continuously, we estimated V_{max} and K_m using the RSS method to find the best fit between analytical and numerical data. We then used the Michaelis-Menten parameters determined

for the given conditions to estimate the DO gradients throughout the gel depth, using the commercial software package Comsol Multiphysics (Comsol, Los Angeles, CA).

3.2.4.2 Hypoxia experiments

AHA constructs were modeled within culture media, allowing oxygen permeability in all directions. Hypoxia (5 % O_2) experiments were conducted as described previously [127]. Briefly, cells were cultured in a hermetically sealed, humidified modular incubator chamber (Billups-Rothenberg, Del Mar, CA, USA), which was flushed with an appropriate gas mixture (a 5 % O_2/5 % CO_2/N_2 balance) three times every 30 minutes at the beginning of each experiment. Placing a plastic Petri dish containing 10 ml of sterile water on the chamber bottom maintained humidity during experiments.

3.2.5 **Flow cytometry and cell cycle analysis**

Flow cytometry was performed for cell cycle analysis and proliferation. Briefly, encapsulated HT1080 cells were exposed to hypoxia at 5 % O_2 tension for up to three days. Gels were harvested at desired time points and digested with hyaluronidase (Sigma) for ten minutes and then 0.25 % trypsin for five minutes to dissociate the cell from the hydrogel. The samples were then centrifuged to separate gels and cells. Next, we fixed the cell pellets in ice-cold 70 % ethanol overnight at 4 °C. Triton X-100 (0.1 %) and RNase A (100 μg/ml; Qiagen, Valencia, CA) were added to obtain a final concentration of 10^6 cells/ml, and cells were incubated in the solution for two hours at 37 °C before being stained with 50 μg/ml propidium iodide (Sigma Aldrich, St. Louis, MO) for 15 minutes at 37 °C. For proliferation, constructs were fixed with ethanol, harvested using hyaluronidase, stained

with anti-human Ki67 (Life Technology) for 30 minutes, and washed with PBS. To avoid clumping, we strained the cells through a 40 μm cell strainer. Cell cycles were analyzed with the BD FACSCalibur flow cytometer (Becton Dickinson, NJ), reading the signals detected by FL2. Data were analyzed using FlowJo software, version 7.5, to determine the frequencies of each cell cycle phase.

3.2.6 **Real-time quantitative RT-PCR**

Two-step RT-PCR was performed for *VEGF*, *ANG-1*, *MMP-1*, *GLUT*-1, *BNIP3*, *BNIP3L*, *18S*, *GAPDH*, and *beta-actin*, and samples were examined in triplicate, analyzed, and graphed. Briefly, RNA was extracted using TRIzol (GIBCO) according to the manufacturer's instructions. Total RNA was quantified by nanodrop spectrophotometer. Gene expression assays were performed on an Applied Biosystems StepOne Real-Time PCR system according to the manufacturer's instructions. The relative expression of genes was normalized to the indigenous control genes. The comparative CT method was used to calculate amplification differences on targeted genes. The values for experiments (n=3) were averaged and graphed.

3.2.7 **2D sprouting assay**

2D sprouting assays to assess the sprouting potential were based on previously established methods using collagen or fibrin gels [88, 128]. AHA hydrogels were prepared as described above, with or without the encapsulation of HT1080 cells or with the addition of sphingosine-1-phosphate (S1P, Avanti Polar Lipids) and stromal cell-derived factor-1

(SDF-1, R&D Systems) at a concentration of 125 μM. ECFCs were seeded on top of the AHA hydrogels and cultured for an additional 24 hours to allow invasion into the gels. Samples were then fixed and processed for fluorescence staining and further image analysis (see below).

3.2.8 **Fluorescence staining**

Following sprouting assay, ECFC-HT1080 constructs were fixed using formalin for 30 minutes and washed with PBS. For staining, the constructs were permeabilized with a solution of 0.1 % Triton-X for 15 minutes, washed with PBS, stained with fluorescein-conjugated UEA-I lectin for two hours, rinsed, and then stained with DAPI for 15 minutes. The labeled samples were examined using a side view perpendicular to the sprouting direction by either fluorescence microscopy (Olympus BX60; Olympus, Center Valley, PA) or confocal microscopy (LSM 510 Meta; Carl Zeiss). To analyze the sprouting length of ECFCs, measurement tools in Image J (NIH) were used and normalized to the medium gel without encapsulated cancer cells under atmospheric conditions while keeping all other formulations the same; this served as a positive control and reference point across different sets of experiments.

3.2.9 **Graphs and statistics**

All experiments and assays were performed on at least triplicate samples with triplicate readings. Graphs were plotted with standard deviation (SD). Significance levels

were determined using unpaired two-tailed t-tests or two-way ANOVA where appropriate (GraphPad Prism 4.02). Significance levels were determined using post-tests with *P<.05, **P<.01 and ***P<.001.

3.3 *Results and Discussion*

3.3.1 **Hyaluronic hydrogel viscoelasticity during culture**

Hyaluronic acid (HA), a glycosaminoglycan abundantly present in the ECM, holds potential as an important component of matrices for the study of cancers and angiogenic responses, since it may facilitate cancer progression, invasion, migration, and angiogenesis [129]. Previously, we engineered a modular culture system using an acrylated HA (AHA) hydrogel to generate a functional human microvascular network [82] and to induce endothelial cell (EC) sprouting and angiogenesis [88]. This same AHA hydrogel system may be useful for studying how hypoxia and stiffness cues in the tumor microenvironment affect cancer cell fate (Figure 3-1**A**). The AHA macromers contain acrylate groups that react with thiols in a Michael-type addition reaction, such that crosslinking can occur with a dithiol and chemical modification can occur with a monothiol. Specifically, we crosslinked AHA with an enzymatically degradable peptide (with a sequence susceptible to matrix metalloproteinases [MMPs] -1 and -2) that contained two cysteines and incorporated adhesion through a peptide (i.e., RGD) that contained one cysteine, where the cysteines provided thiol groups to react with acrylates. This system enables us to alter the hydrogel's crosslinking density by changing the amount of MMP crosslinker added while maintaining the overall backbone and adhesion site concentration (Figure 3-1**B**). With this

approach, we generated three hydrogel matrices with distinctive levels of viscoelasticity: soft (78±16Pa); medium (309± 57Pa) and stiff (596± 73Pa; Figure 3-1**C**).

We first examined cancer cell encapsulation in the AHA hydrogels with defined viscoelasticity. For our studies, we chose a fibrosarcoma-derived cell line, HT1080, which tends to be highly angiogenic, mobile, and metastatic, making it a good candidate for the soft tissue viscoelasticity range [130-132]. We noticed that, after 24 hours of encapsulation, HT1080 cells in both medium and stiff hydrogels began to spread, but they started to form aggregates in the softest hydrogels (data not shown). Within 72 hours, most of the HT1080 cells encapsulated in stiff and medium hydrogels had spread, while most of those in the soft hydrogels aggregated into clumps and spread only occasionally (Figure 3-2**A**). Examining the viscoelasticity, we first noticed that after cell encapsulation, the stiffness of the hydrogels slightly altered to soft (66±13Pa); medium (361± 65Pa) and stiff (485± 63Pa) constructs; we also found that all constructs types, but not hydrogels alone, became softer along the culture period, reaching 14±10Pa; 77±49Pa; and 96±71Pa in the soft, medium, and stiff hydrogels, respectively. (Figure 3-2**B**). Indeed, due to the cell clusters, constructs made of soft gels became unstable and difficult to maintain, with many clusters falling off the AHA hydrogels. Thus, the studies were limited to the first three days of encapsulation of HT1080 cells.

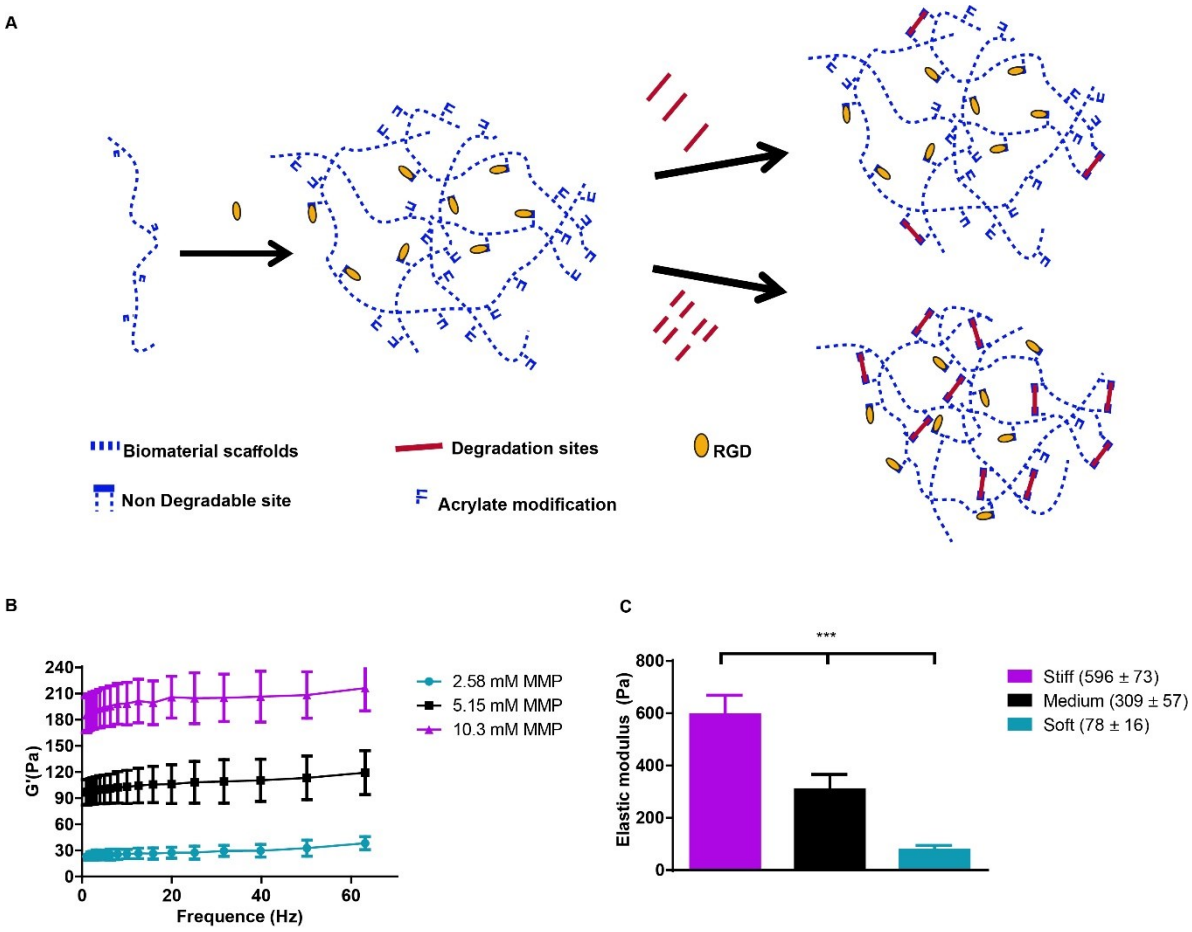

Figure 3-1. Acrylated HA hydrogels.
(A) Schematic representation of AHA hydrogels, which are formed by reacting AHA macromers with RGD-containing peptides and MMP-sensitive crosslinkers, where the crosslinker concentration controls viscoelasticity. (B) Rheology frequency sweeps of AHA hydrogel with varying MMP crosslinker concentrations, showing that the modulus depends on crosslinker concentration. (C) Elastic modulus following polymerization and swelling: soft (78±16 Pa); medium (309± 57 Pa), and stiff (596± 73 Pa).

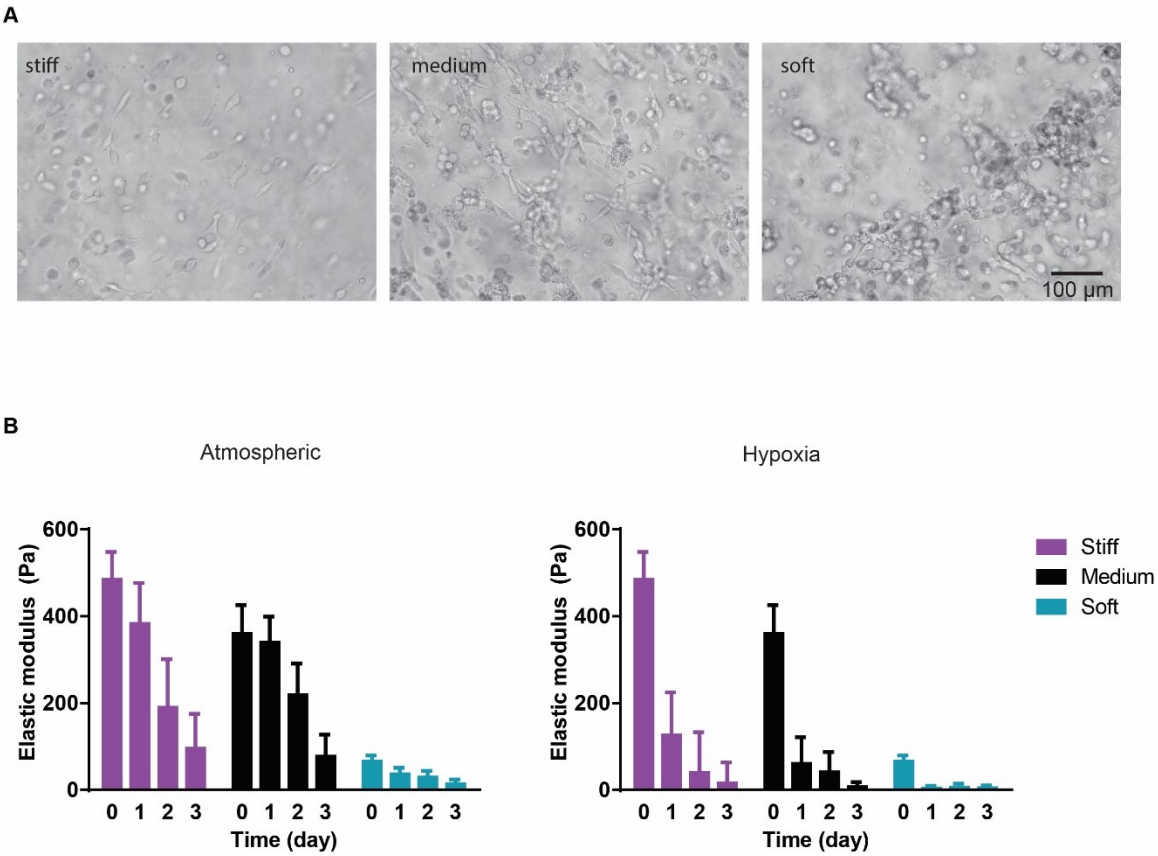

Figure 3-2. HT1080 cells encapsulated in AHA hydrogels with defined stiffnesses. (A) Light microscopy images of three-day culture of HT1080 cells in stiff, medium, and soft AHA hydrogels. (B) Viscoelasticity measurements of the different HT1080 construct types (left) or hydrogels alone (right) along the three-day culture period.

3.3.2 Oxygen tension gradient in hydrogel scaffold

We next determined the oxygen tension and gradients throughout the hydrogel matrices. Our previous studies showed that dissolved oxygen (DO) levels decrease during 2D culture of various human cell types [133] and that these decreases become even more dramatic in 3D hydrogel cultures, which require higher cell-seeding concentrations [126]. Indeed, in a 3D hydrogel culture system, the availability of DO to the cells depends on both oxygen diffusion from the air to the culture media and the oxygen consumption of the encapsulated cells. The oxygen consumption rate of cells depends on their spatial density

and oxygen uptake rate, which is assumed to follow Michaelis-Menten kinetics. Therefore, we first determined the V_{max} and K_m parameters of HT1080 fibrosarcoma cells. We measured DO levels in culture media of HT1080 cells until they reached steady state. We plotted the oxygen consumption rate of the HT1080 cells (experimental data) and the theoretical Michaelis-Menten equation (numerical model) using the initial V_{max} and K_m values. We then calibrated the graphs while varying the V_{max} and K_m parameters to obtain the best fit to the experimental values according to the residual sum of squares (RSS) method (Figure 3-3**A**). We determined that the V_{max} and K_m values of HT1080 cells were 83.19 x 10^{-18} mol/s and 66 μM, respectively. Mathematical modeling then projected [134, 135] equilibrium oxygen tension distributions at different boundary conditions (1, 5, and 21 %) with different cell encapsulation densities (1, 5, and 10 x 10^6 cells/ml; Figure 3-3**B**). We found that, during the initial culture period, DO gradients were generated throughout the thickness of the hydrogel. Specifically, cells at the center regions of the hydrogel experienced lower oxygen tensions than either those in the experimental setup (i.e., air gas) or those at the edge of the hydrogel. In atmospheric conditions, HT1080 cells encapsulated at 10 x 10^6 cells/ml % experienced around 13 % O_2 at the center, compared to 17 % O_2 at the edge after 30 minutes of gel formation (Figure 3-3**C**). At 5 % O_2, while encapsulation densities of 5 x 10^6 cells/ml or 10 x 10^6 cells/ml led to oxygen levels below 2 % at the center of the hydrogel, at the 1 x 10^6 cells/ml encapsulation density, cells experienced a relatively uniform distribution of 5 % oxygen tension throughout the hydrogel (Figure 3-3**D**). At 1 % O_2, encapsulation of 5 x 10^6 cells/ml or 10 x 10^6 cells/ml resulted in anoxic conditions at the center of the hydrogel, while encapsulation of 1 x 10^6 cells/ml yielded oxygen levels below 0.4 % at the center (Figure 3-3**E**). Based on this analysis, we decided

that using 1 x 10^6 cells/ml in a 5 % setup would allow us to study the responses of HT1080 cells to varying stiffnesses in conditions that support uniform DO levels throughout the hydrogel. This setting also mimics the initial circulating cancer cell attachment environment, which is marked by low cell density and moderate hypoxia [136].

A

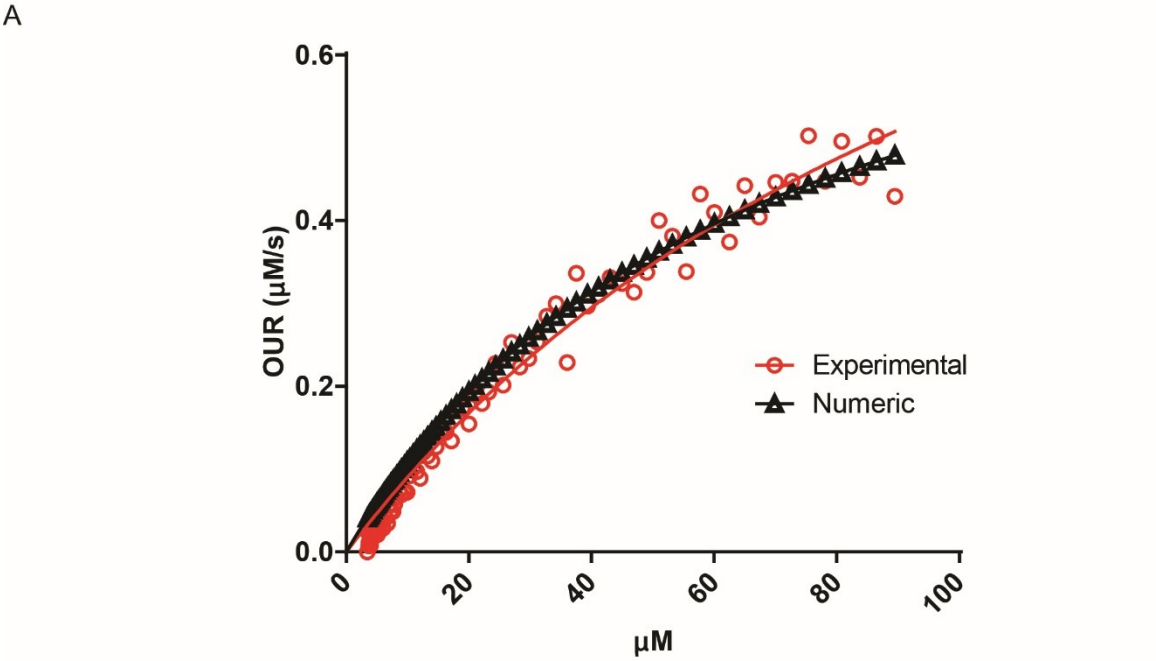

B

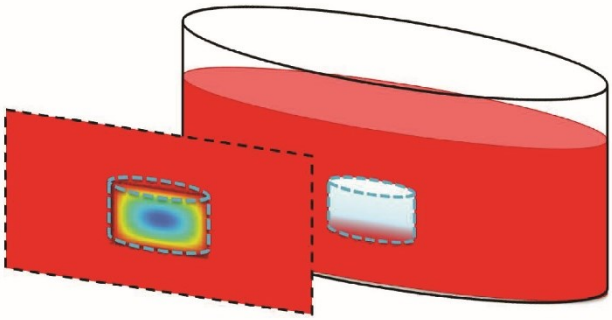

C

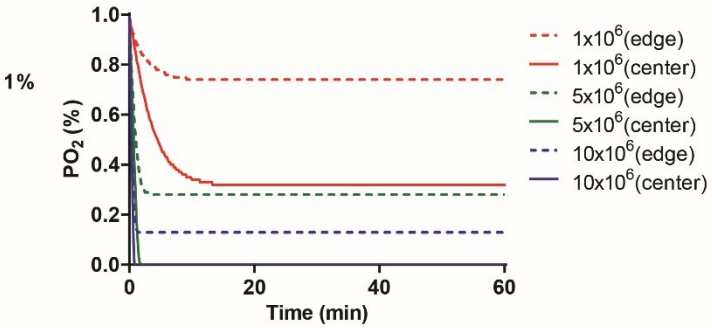
1%
PO2 (%)
1.0
0.8
0.6
0.4
0.2
0.0
0
20
40
60
Time (min)
1x10^6(edge)
1x10^6(center)
5x10^6(edge)
5x10^6(center)
10x10^6(edge)
10x10^6(center)

D

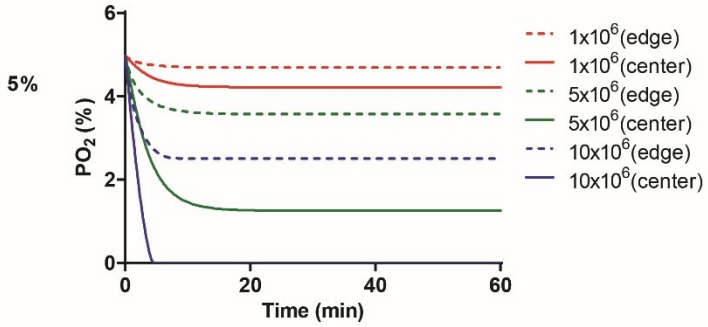
5%
PO2 (%)
6
4
2
0
0
20
40
60
Time (min)
1x10^6(edge)
1x10^6(center)
5x10^6(edge)
5x10^6(center)
10x10^6(edge)
10x10^6(center)

E

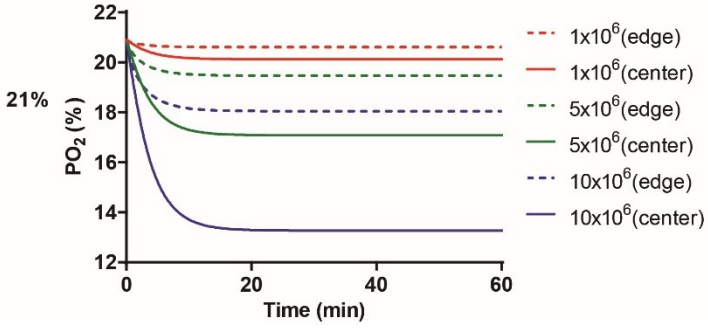
21%
PO2 (%)
22
20
18
16
14
12
0
20
40
60
Time (min)
1x10^6(edge)
1x10^6(center)
5x10^6(edge)
5x10^6(center)
10x10^6(edge)
10x10^6(center)

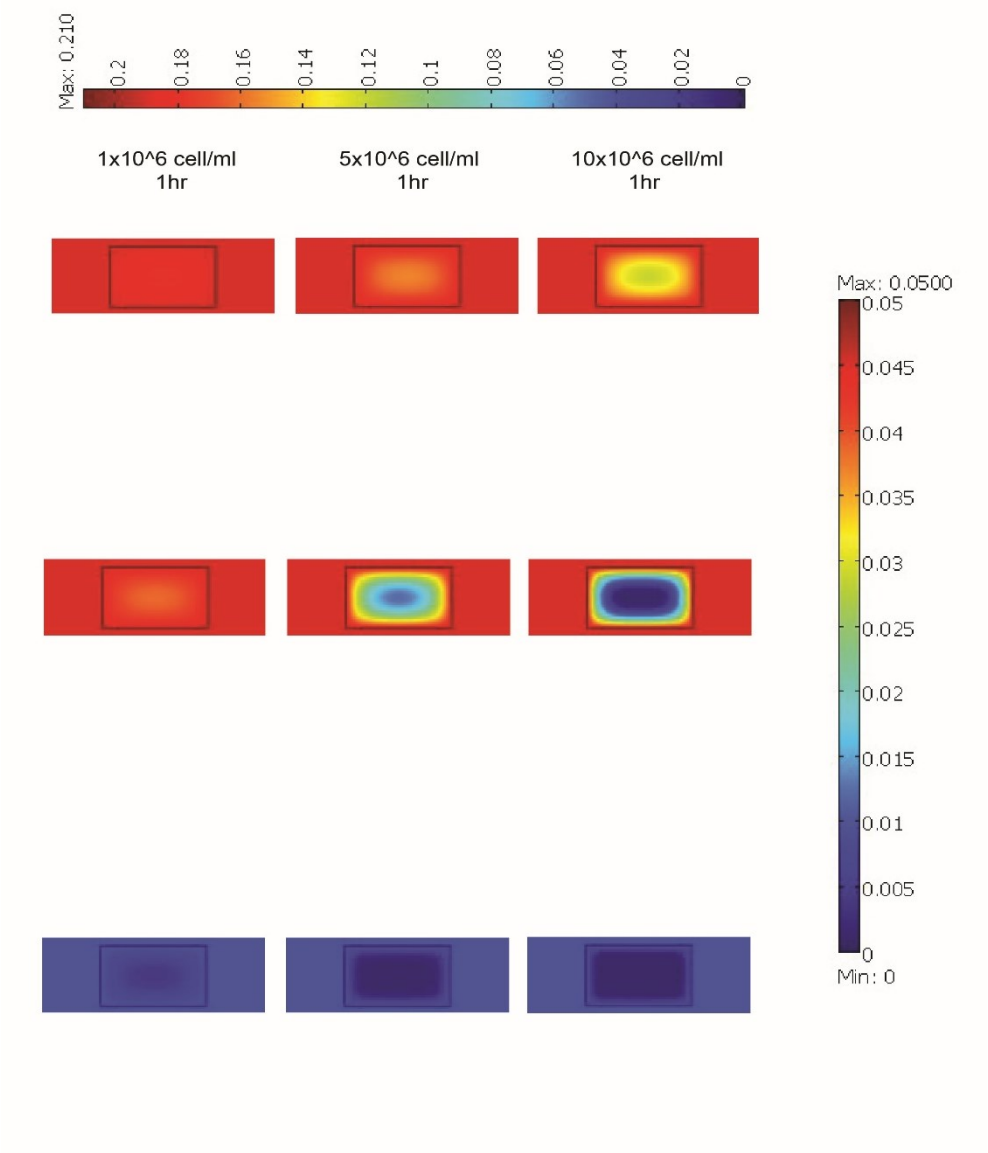

Figure 3-3. Predicting DO levels in AHA hydrogels.
(A) Oxygen consumption rate of HT1080 cells following Michaelis-Menten kinetics. Plots were calibrated according to the residual sum of squares method to find the best fit between theoretical and experimental values. Vmax and Km values of HT1080 cells were 83.19 x 10-18 mol/s and 66 µM, respectively. (B) Schematic of the 3D HT1080-AHA construct in culture comprises three individual layers: (i) AHA gel containing HT1080 cells (middle layer), (ii) growth medium (surrounding layer), and (iii) air (top layer). Model prediction of DO levels within the hydrogels at (C) 21 %, (D) 5 %, and (E) 1 % O2, with HT1080 cells encapsulated at concentrations ranging from 1 to 10 x 106 cells/ml during the first hours (left panel: lines show DO levels at the center of the hydrogel; broken lines, the DO levels at the edge of the hydrogel), and DO gradient profile throughout the hydrogels' depth after an hour (right panel).

3.3.3 **Cancer cell fate at various microenvironment parameter**

Many cancer cells are shed into circulation every day. However, very few of them survive and become metastatic [137]. Rate-limiting steps at the metastatic site pose challenges to circulating cancer cells in their interaction with their microenvironment [136], where they can meet several fates (death, dormancy, or survival) modulated by the microenvironment. For example, some cancer cells stay quiescent or dormant and only later become triggered into a proliferative state for angiogenic purposes [138]. Other tumor cells enter the apoptotic/necrotic pathway. To determine the effect of hypoxia on HT1080 cell fates at different matrix stiffnesses, cells were cultured in serum-free media to synchronize their G_0 stages before encapsulation. After encapsulation, AHA-HT1080 constructs were cultured under atmospheric and hypoxic condition for three days. We could not observe morphological differences between 3D HT1080 cells cultured under atmospheric and hypoxic conditions (data not shown). To examine cell growth, we stained the cells with Ki67 proliferation marker. While we detected overall reduced proliferation in the 3D AHA hydrogel compared to Petri dish control, we could not detect a significant difference in proliferating cells between hypoxic and atmospheric conditions in any of the cultures examined (Figure 3-4**A**). Daily cell cycle analysis further revealed no significant differences in population percentage at the S phase or G_2 phase (Figure 3-5), suggesting that, over the 72 hours, HT1080 cells divide at a similar rate in all conditions examined. We noticed that, 24 hours following encapsulation, HT1080 cells experienced apoptosis (indicated by the sub-G_1 population) and that, under hypoxia, they recover better, resulting in significantly lower percentages of apoptotic cells after 48 hours (Figure 3-4**B–C**). Matrix stiffness seemed to affect recovery from cell apoptosis minimally. After 24 hours under

hypoxic conditions, HT1080 cells encapsulated in matrix with medium stiffness experienced high levels of apoptotic events compared to cell encapsulated in soft or stiff matrices. We therefore examined the upregulation of the autophagy gene of the BCL-2 family, BCL-2/adenovirus E1B 19 kDa-interacting protein 3 (*BNIP3*) [139], and the proapoptotic gene Bnip3-like protein X (*BNIP3L*), also of the BCL-2 family, in HT1080 cells encapsulated in medium AHA hydrogels. While we could not detect differences in the expression of *BNIP3L (*data not shown*)*, upregulation in the expression of *BNIP3* was detected 24 hours following encapsulation and was downregulated after 48 hours of culture (Figure 3-4**Di**). The same expression pattern could also be detected for glucose transport (*GLUT-1)* in hypoxic HT1080 cells (Figure 3-4**Dii**). When HT1080 cells were cultured in a Petri dish, hypoxia upregulated the expression of GLUT-1 and BNIP3 after 24 hours, which further increased after 48 hours, suggesting a rapid response and adaptation to the oxygen conditions within the 3D AHA culture microenvironment (Figure 3-4**D**). These results suggest the adaptation of HT1080 cells under hypoxic conditions, rapidly recovering from possible autophagy events and alternating metabolism mechanisms. This also suggests that HT1080 cells, when cultured in AHA hydrogel under atmospheric conditions, experience apoptosis induced by a different mechanism than those examined here. Overall, these results suggest that hypoxia and, to a lesser extent, hydrogel stiffness affected cell fate throughout the three-day study.

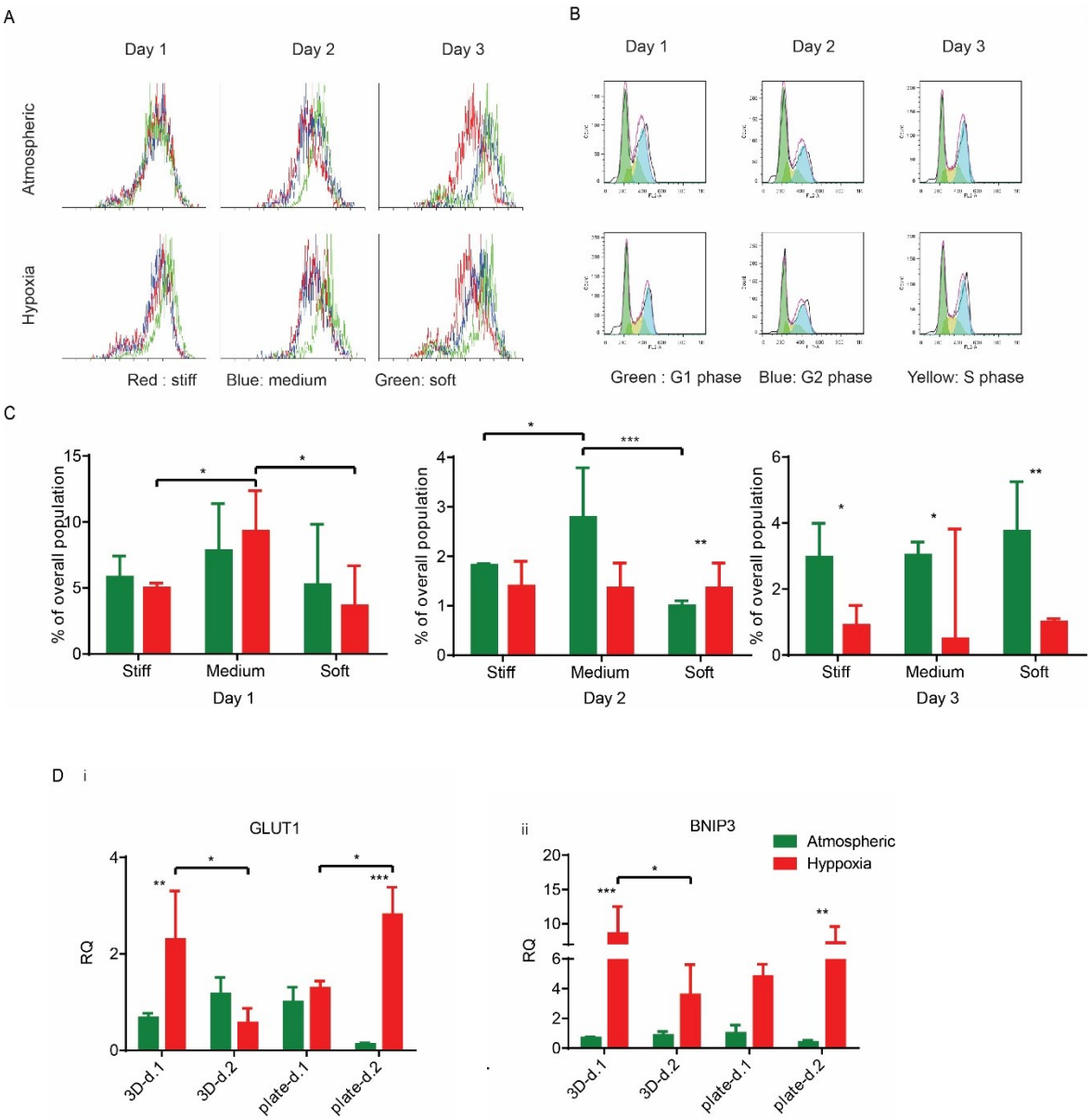

Figure 3-4. . HT1080 cell fate in AHA hydrogels with varying stiffnesses in atmospheric and hypoxic conditions.
(A) Proliferation of HT1080 cells encapsulated in stiff hydrogels over the three-day experiment in atmospheric and hypoxic conditions. (B) Representative cell cycle flow analysis of HT1080 cells encapsulated in stiff hydrogels over the three-day experiment in atmospheric and hypoxic conditions. (C) Quantification of the percentage of apoptotic cells (sub-G1) in the various conditions. (Di, ii) Quantitative RT-PCR for BNIP3 and GLUT-1 expression in HT1080 cells encapsulated in hydrogels of medium stiffness (3D) and in Petri dishes (plates) in atmospheric and hypoxic conditions. Significance levels (n=3) were set at: *p<0.05, **p<0.01, and ***p<0.001.

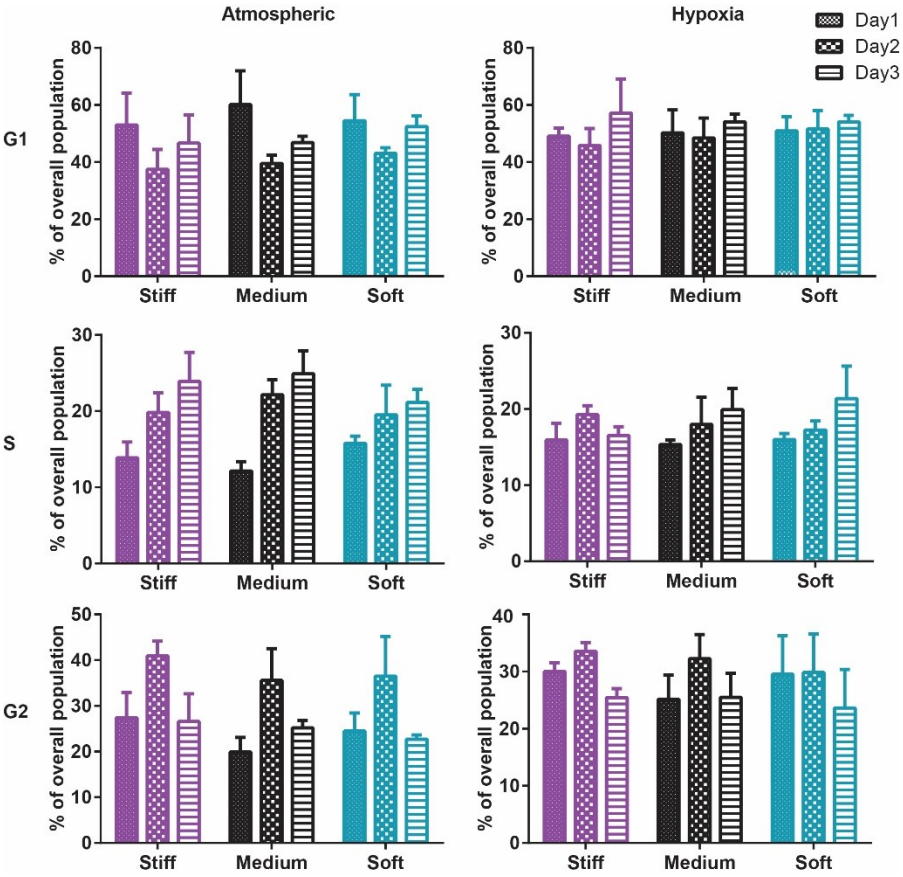

Figure 3-5. Cell cycle.
Flow analysis of cell cycle phases (G1, S, G2) in HT1080 cells encapsulated in hydrogels over the three-day experiment in atmospheric and hypoxic conditions.

3.3.4 **Angiogenic potential at different stiffness and oxygen tension.**

Finally, we sought to examine the ability of 3D encapsulated HT1080 cells to induce endothelial sprouting under hypoxia at different matrix stiffnesses. Davis and colleagues developed an *in vitro* angiogenesis assay using collagen gels [140, 141]. They showed that, in response to sphingosine-1-phosphate (S1P) and stromal cell-derived factor-1 (SDF-1α), a confluent monolayer of ECs invaded and sprouted into the collagen gels underneath in a way that mimicked the appearance of tip cells from preexisting blood vessels [141]. We previously adapted this approach and showed that AHA hydrogels could serve as an *in vitro* angiogenesis assay and, as such, provide opportunities to elucidate the

role of matrix remodeling during angiogenesis in synthetic biomaterials [142]. In this earlier study, we found that endothelial colony-forming cells (ECFCs) cultured on top of the medium AHA matrix loaded with SDF1-α and S1P sprouted and invaded the hydrogel in atmospheric conditions. These results suggest that, with the necessary adhesion and degradation properties, low viscoelasticity, and cytokine stimuli, ECs can sprout and invade such AHA hydrogels. In the current study, we modified this approach and encapsulated HT1080 cells with SDF-1α and S1P for 24 hours in atmospheric or hypoxic conditions, following which we seeded a monolayer of ECFCs and analyzed their sprouting and invasion into the AHA hydrogels after a further 24 hours in atmospheric conditions (Figure 3-6**A**). AHA hydrogel encapsulating only SDF-1α and S1P served as controls. It should be noted that HT1080 cells encapsulated without the addition of SDF-1α and S1P induced little to no EC sprouting and invasion. We observed similar EC sprouting and invasion into soft-matrix-encapsulated HT1080 cells in atmospheric and hypoxic conditions. While EC sprouting was observed in HT1080 constructs with medium viscoelasticity cultured in atmospheric conditions, a significant increase in sprouting length was observed in hypoxic conditions. Finally, HT1080 cells encapsulated in stiff hydrogels underwent EC sprouting and invasion in hypoxic but not in atmospheric conditions (Figure 3-6**B–C**). Overall, we found that, in atmospheric conditions, softer matrices promoted EC sprouting and invasion, corresponding to similar cellular events during vasculogenesis [82, 88, 142-146]. In hypoxia, while the lowest angiogenic response occurred in the stiff matrix, soft and medium hydrogels had similarly higher responses. Gene expression analysis of HT1080 cells after 24 hours in 3D culture revealed the upregulated expression of MMP-1 in hypoxic HT1080 cells within stiff hydrogels, suggesting that the cells may alter the

viscoelastic properties of these hydrogels under hypoxic conditions, enabling EC sprouting and invasion (Figure 3-7**A**). Indeed, when we examined HT1080 construct viscoelasticity, we found that after 24 hours in hypoxic conditions, all constructs became significantly softer; stiff constructs reached 127±98Pa; medium constructs reached 61±60Pa; and soft constructs reached 4±4Pa (Figure 3-7**B**). Gene expression analysis of the angiogenic factors vascular endothelial growth factor (*VEGF*) and angiopoeitin-1 (*ANG-1*) showed that hypoxia upregulated secretion of these angiogenic factors by the HT1080 cells more than atmospheric conditions (Figure 3-7**C–D)** also, we observed a greater upregulation of these factors in cells cultured in a 3D than in a 2D environment. These factors most likely contribute to the angiogenic state of the ECFCs.

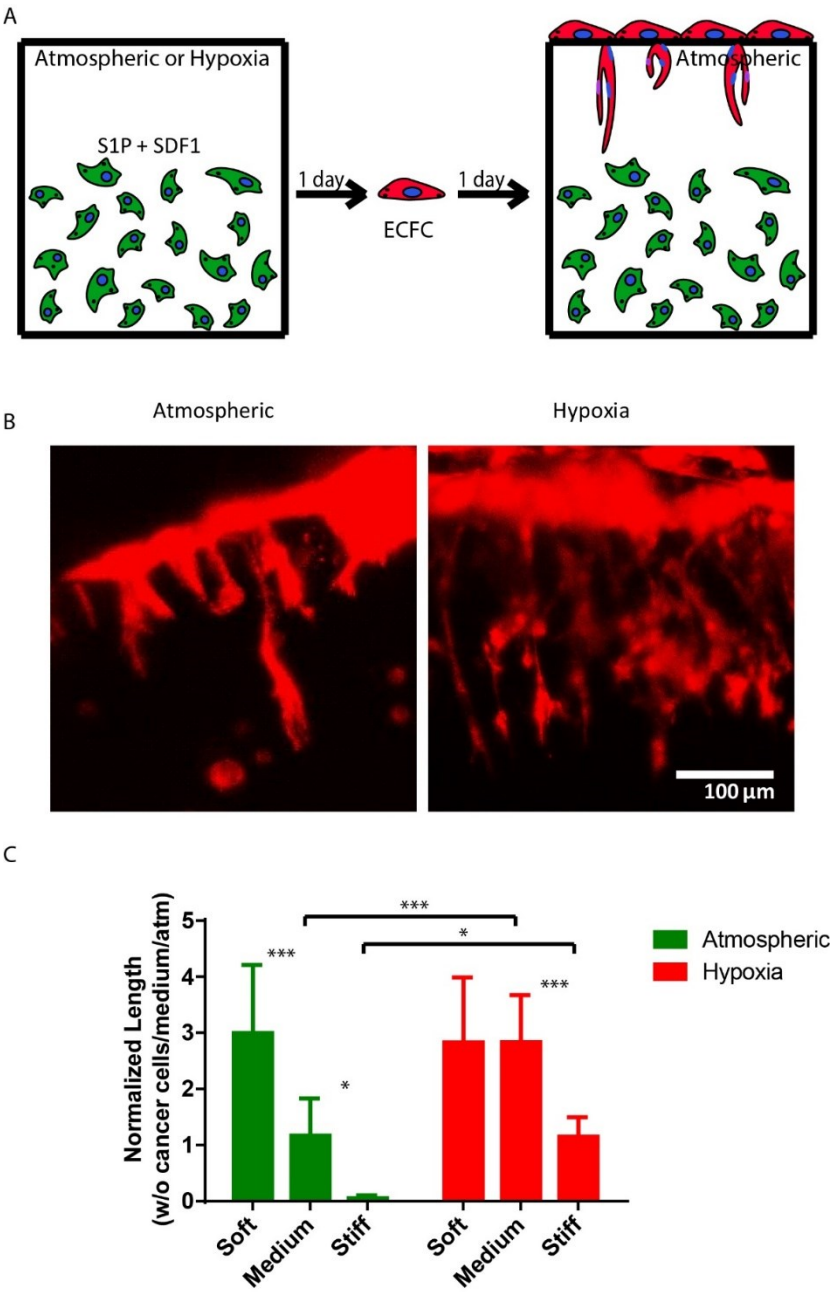

Figure 3-6. Effect of AHA-HT1080 on ECFC sprouting and invasion.
(A) Schematic of study strategy for examining the angiogenic potential of AHA-HT1080 constructs: HT1080 cells, SDF1-α and S1P were encapsulated in AHA hydrogels of different stiffnesses and cultured for 24 hours in hypoxic or atmospheric conditions, followed by seeding of ECFCs as a monolayer on top of the hydrogels and culturing for an additional 24 hours. (B) Lectin stain (in red) and side-view imaging of endothelial sprouting in medium hydrogel in atmospheric and hypoxic conditions. (C) Quantification of sprouting length of ECFCs in the different stiffness and oxygen tension conditions. Significance levels (n=3) were set at: *p<0.05, **p<0.01, and ***p<0.001.

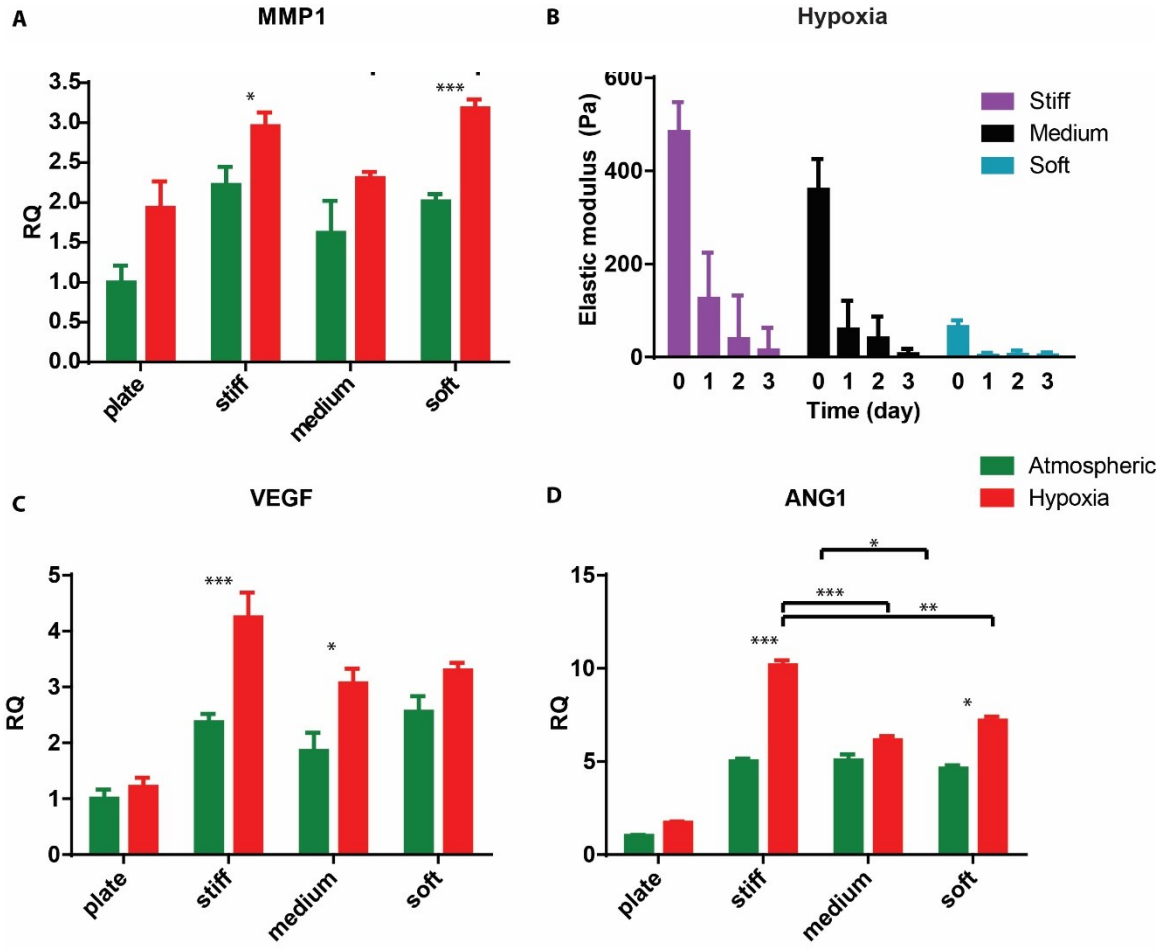

Figure 3-7. Angiogenic gene expression.
(A) Quantitative RT-PCR for the expression of MMP-1 in HT1080 cells cultured in Petri dishes (plates) or encapsulated in the different hydrogels for 24 hours. (B) Viscoelasticity measurements of the different construct types along the three-day hypoxic culture period. (C-D) Quantitative RT-PCR for the expression of VEGF, and ANG-1 in HT1080 cells cultured in Petri dishes (plates) or encapsulated in the different hydrogels for 24 hours. Significance levels (n=3) were set at: *p<0.05, **p<0.01, and ***p<0.001.

3.4 *Conclusions*

Overall, our results imply that oxygen tension influences 3D cultured HT1080 cells more profoundly than matrix stiffness. Encapsulated in the AHA hydrogels under hypoxic stress, HT1080 cells recovered from apoptosis better and demonstrated greater angiogenic

induction. While it seems surprising that matrix stiffness plays a minimal role in determining cell fate and triggering the angiogenic capability of HT1080 cells, it is possible that conducting experiments over longer time periods or examining a wider viscoelasticity range would activate signaling pathways that are dependent on stiffness mechanism in 3D constructs. In the study of EC sprouting, it is worth noting that, without the addition SDF-1α and S1P, we observed little or no sprouting, suggesting that other cell types in the tumor microenvironment secrete these two (or similar) growth factors. Candidates include stromal cells or leukocytes, which are recruited toward malignant cell sites and produce S1P or SDF-1 [136, 147].

Utilizing AHA hydrogels, we generated a well-defined 3D culture system to study the effects of matrix viscoelasticity and oxygen tension on cancer cell behavior. We found that encapsulation of 5 to 10 x 10^6 cells/ml generated DO gradients throughout the hydrogel matrix in atmospheric (21 %), hypoxic (5 %), and severely hypoxic (1 %) conditions. Encapsulation of low cell concentrations (1 x 10^6 cells/ml) maintained a uniform DO distribution under atmospheric and hypoxic conditions. We demonstrated that, using our 3D AHA hydrogel culture system, encapsulated HT1080 cells recovered more rapidly from apoptosis under hypoxic conditions than under atmospheric conditions without obvious correlation to the matrix's stiffness. We found that angiogenic induction correlated highly to decreases in matrix stiffness under atmospheric conditions, while hypoxia upregulated angiogenic responses in the stiffer hydrogels. Overall, we suggest that hypoxic pathways activation of HT1080 cells encapsulated in the 3D AHA hydrogel enables better cell survival and supports EC sprouting. Other potential uses for this system including

comparing the responses of different cancer cell lines at different stages of tumorigenesis, supporting the basic study of tumor biology, and selectively impeding cancerous processes.

Current chapter is reproduce[148] by permission of Royal Society of Chemistry.

4 *Engineered human vascularized hyaluronic acid hydrogels to treat diabetic food ulcer wounds.*

Diabetic foot ulcers (DFUs) are a severe healthcare problem that poses a high risk in most diabetes patients. Current treatments are often lengthy and insufficient to prevent further complications. New therapeutic strategies aim to enhance blood vessel growth in diabetic patients. At the same time, stem cell therapy is emerging as a promising approach, especially for patient-specific treatment. Here, we propose to combine both angiogenesis and stem cell therapy, which could serve as a novel therapeutic modality by promoting neovascularization and wound healing in patients. We first developed an immunodeficient diabetes mellitus rodent DFU model using streptozotocin (STZ). We then successfully engineered vascularized constructs by encapsulating various vascular cell sources (ECFCs, iPSC derived EVCs from a healthy patient, BC1 or a diabetic patient, T1D) in HA hydrogels. We tracked and analyzed the closure of the wounds with multiple assessments such as photometric measurements, blood flow profiles, histology, and a macroscopic wound healing rate model. We found that all vascularized constructs enhanced and expedited wound closures when compared to non-treated wounds. We also observed the best wound healing mechanics for the ECFC vascularized construct treatment followed by both the BC1 and T1D derived EVC vascularized construct treatment. Here we have

showcased a potential therapeutic strategy using a stem cell derived vascularized scaffold to treat diabetic foot ulcers.

4.1 *Introduction*

In humans, wound healing is a continuum of processes, which consists of several overlapping stages. These stages include inflammation, cell proliferation, migration, angiogenesis, re-epithelialization, and reconstruction of the extracellular matrix [149]. In diabetic patients, constant hyperglycemia can cause dysfunction at several stages throughout the wound healing process. For example, inflammation is prolonged and intensified due to the intrinsic high glucose environment, as the ability of macrophages to removed necrotic cells is diminished [150]. Hyperglycemia also induces alterations in cellular and molecular processes, such as growth factor, chemokine, and cytokine expression [151]. Abnormal granulation tissue formation has also been linked to impaired diabetic cutaneous wound healing [152]. Additionally, perpetual high glucose levels in the blood prevent proper blood flow to the extremities, which causes a lack of oxygen and nutrient supply, thereby limiting angiogenesis and altering the permeability of the vasculature [92]. Further, peripheral nerve damage, especially distal symmetrical polyneuropathy (DSP), is most commonly seen in this patient group [153, 154]. Neuropathy causes a lack of feeling in the extremities, leading patients to suffer from injury unawareness and repeated trauma [5]. Thus, patients often suffer from an impaired wound healing process and exhibit non-healing wounds, which consequently can lead to ulcers, especially in the lower extremities.

The current standard of treatment for these recurring wounds includes improving blood glucose control and pain management [92]. However, in many cases this is not adequate, as non-healing diabetic ulcers have become a leading cause of non-traumatic amputation in the U.S [155]. The economic and health care burden as well as the decreased quality of life for the diabetic mellitus patients suggests a clear need to investigate alternative treatments for diabetic ulcers.

Tissue engineering approaches pose possible solutions for treatment of impaired wound healing. For these applications, the construct materials need to be biocompatible. Additionally, it would be beneficial to vascularize the constructs. It is widely accepted that timely vascularization, is needed for successful regeneration of injured tissues, since vascularization supplies necessary oxygen and nutrients to support the renewal and differentiation of new tissue [156]. Previously, our group, along with many others, has utilized bioactive natural matrices to study the pre-vascularization potential of various human stem cells [77, 156-162]. Specifically, our group has demonstrated successful integration of engineered microvascular constructs consisting of endothelial colony forming cells (ECFCs; [82, 91]) or induced pluripotent stem cell (iPSC)-derived early vascular cells (EVCs) [89] in hyaluronic acid (HA) hydrogels, with the host circulation [89]. In recent studies, we have derived EVCs from type 1 diabetic patient (T1D) iPSCs and demonstrated their functionality and ability to form networks in HA hydrogels [90].

In this study, we hypothesized that our *in vitro* vascularized constructs would survive implantation into diabetic wounds and integrate with the diabetic host to reestablish blood flow and improve the wound healing of diabetic ulcers.

4.2 *Materials and Methods*

4.2.1 **Differentiation Protocol and Cell Culture**

EVC expansion and differentiation from BC1 and T1D human induced pluripotent stem cell (hiPSC) lines followed our established protocols [89, 90]. Briefly, undifferentiated hiPSC (BC1 and T1D) were maintained on inactived mouse embryonic fibroblast feeder layers in growth medium with 80 percent ES-EMEM/F12 (Global Stem), 20 percent serum replacement (Invitrogen), and 10ng/ml basic fibroblast growth factor (bFGF). For differentiation, hiPSCs were collected through digestion with EDTA (Promega), single cells were seeded and plated onto collagen IV (Trevigen)-coated cell culture plates with a concentration of 5 X 10^4 cell/cm^2 supplemented with 10μM ROCK inhibitor Y-27632 (Stemcell Technologies). Cells were cultured for 6 days in a differentiation medium composed of alpha-MEM (Invitrogen), 10% FBS (HyClone), and 0.1 mM β-mercaptoethanol (β-ME), with the medium changed daily. Differentiated cells were collected through digestion with TrypLE (Invitrogen) on day 6 and seeded at a concentration of 2 X 10^4 cells/cm^2 on collagen type IV-coated plates in endothelial cell growth media (ECGM) (PromoCell) supplemented with 2% FBS, 50 ng/mL VEGF with 10 μM SB431542 (Tocris) for 6 days. The medium was changed every other day. ECFCs (Lonza) were cultured under the manufacturer'ss protocol. Briefly, cells were seeded and expanded in endothelial growth media EGM-2 (Lonza) and cells with passages 6 through 8 were used for experiments, as previously described [89, 91].

4.2.2 **Synthesis of Acrylated Hyaluronic Acid (AHA) Hydrogels Macromer**

AHA macromer synthesis was conducted as previously reported [82-84]. In brief,

AHA was synthesized in two steps: (1) the tetrabutyl-ammonium salt of HA (HA-TBA) was formed by reacting sodium hyaluronate (90 kDa, LifeCore Biomedical) with the ion exchange resin Dowex-100 (Sigma) and neutralized with 0.2M TBA-OF (Sigma); (2) acrylic acid (3 eq) and HA-TBA (1 eq) were coupled in the presence of dimethylaminopyridine (DMAP; 0.15 eq) and di-tert-butyl dicarbonate (3 eq) in DMSO, followed by dialysis and lyophilization. ^{1}H NMR spectra were used to confirm the modification of the AHA. The cell-adhesive peptide GCGYGRGDSPG (RGDS, molecular weight [MW]: 1025.1 Da) and MMP-sensitive peptide crosslinker GCRDGPQGWGQDRCG (MMP, MW: 1754 Da) were purchased (Genscript, > 95% purity per manufacturer HPLC analysis.)

4.2.3 **Generation of Human Vascular Constructs from ECFCs and EVCs**

We engineered human vascular networks within the AHA hydrogels similar to our previous studies [82, 91]. AHA macromer was dissolved in triethanolamine buffered saline (TEOA buffer: 0.2M TEOA) at 3 wt%. Cell adhesive peptides (RGDS, GenScript) were dissolved in TEOA buffer and added to the AHA solution to the final peptide concentration of 4.8mM Recombinant human $VEGF_{165}$ (Pierce), bFGF (Invitrogen), Ang-1 (R&D Systems), TNF-alpha (R&D Systems), and stromal cell-derived factor-1 (SDF-1; R&D Systems) were also added into the AHA-RGD mixture at 50 ng/ml. The mixture was allowed to react for 1 hour with gentle shaking. For crosslinking, an MMP cross linker (MMP, GenScript) dissolved in TEOA buffer was added to a final concentration of 5.15 mM. Preconditioned ECFCs and EVCs were encapsulated in AHA hydrogels at a density of 5 X 10^6 cells/ml by suspending the cells in the AHA-RGD solution as described above prior to the addition of the MMP crosslinker. A 50 µl volume of the final mixture was

pipetted into sterile molds (5 mm diameter, 2 mm height) and allowed to react for 10 minutes at room temperature in a laminar flow hood. The constructs were then cultured in ECFC culture media in the conditions described throughout the study.

4.2.4 **Streptozotocin (STZ) Induced Diabetes Mellitus Nude Mice**

The standard protocol for STZ induced diabetes mellitus provided by Animal Models of Diabetic Complications Consortium was followed [92-94]. Nude mice at about 2-2.5 months of age (about 20-25 g body weight) were randomly assigned to a diabetic or a non-diabetic group. Animals in the diabetic group were induced by 5 intraperitoneal injections of STZ at a dose of 50 mg/kg body weight (STZ is freshly dissolved in citrate buffer, pH 4.5). Prior to injection, mice were fasted for 4 to 6 hours. The weight and blood glucose of each mouse were checked daily for up to 2 weeks after the STZ injection. Successful STZ-induced diabetic mellitus nude mice were confirmed by two consecutive blood glucose levels readings higher than 300 mg/dl over a 48 hour period. Blood glucose was measured using an Accuchek blood glucose meter (Roche) by obtaining 20-25µl of blood from a tail vein puncture (30 gauge needle).

4.2.5 **Diabetic Foot Ulcer (DFU) Animal Model and Vascularized Construct Transplantation**

DFU animal model was constructed by incorporating various protocols from the literature [92, 95-98]. After diabetic mellitus was confirmed, diabetic induced nude mice were anesthetized with isoflurane (Thermo Fisher). A depilatory was applied (Nair), prior to wound creation, to ensure better dressing adherence. Next, 2 x 6mm diameter punch wounds were made, using a biopsy punch (Integra), taking care to remove full-thickness

skin on each side of the posterior dorsum. Vascularized constructs, which were generated *in vitro*, were then transplanted into one side of the animal (one per wound). The time point was logged as day 0 post-wound. Betadine was applied around the periphery of the wound to enhance dressing adherence. The wound on the opposing side was left with no vascularized construct treatment. Both wounds were then covered with Tegaderm dressing (3M). 6 to 8 constructs were implanted for each group at each time point. At each time point of interest, as described below, human specific fluorescein- conjugated *Ulex europaeus I* (*UEA-I*) *Lectin* (1:10; Vector Laborato) and mouse-specific rhodamine-conjugated *Isolectin Griffonia simplicifolia* (*GS*)-IB_4 (1:10; Invitrogen) were injected through the tail veins of the mice [82, 89, 91]. After 30 minutes, the mice were euthanized, and the constructs were harvested and fixed in 3.7% formaldehyde (Sigma). The tissue was processed for immunohistochemistry or histology. The Johns Hopkins University Institutional Animal Care and Use Committee approved all animal protocols.

4.2.6 **Bloodflow and Planetary Measurement**

During the study, the blood flow profiles inside the wounds were monitored noninvasively using moorFLPI speckle contrast imager (Moor Instruments, Inc.). The measurements were normalized by the blood flow measurements of the adjacent healthy skin area. Photometric analysis of wound closure rate was done along with blood flow measurement.

4.2.7 **Immunohistochemistry and Histology Analysis**

Following fixation of the explants, the samples were dehydrated in serial ethanol (70%–100%), embedded in paraffin, serially sectioned at 5 μm, and treated with

hematoxylin and eosin (H&E) stain or immunoperoxidase stains for anti-mouse alpha-smooth muscle actin (alpha-SMA) (Abcam), or anti-human CD31 (Dako). Double staining was performed using the same anti-human CD31 and anti-mouse alpha-SMA followed by conjugation with anti-mouse Alexa Fluor 488 (Life Technologies) or anti-rabbit Alexa Fluor 564 (Life Technologies) and counter stain with Dapi. Histological images were taken with an upright light microscope (Nikon Accuscope 3000) and a camera (Nikon DS-F12).

4.2.8 **Statistical Analysis and Regression fit**

Statistical analysis was performed using GraphPad Prism 6.01 (GraphPad Software Inc.), A non-linear regression fit, One Way ANOVA with Tukey's posttest, or Two Way ANOVA with Bonferroni's posttest were used where appropriate. Analysis consisted of t-tests, in which significance levels were set at *$p<0.05$, **$p<0.01$, ***$p<0.001$, and ****$p<0.0001$. Unless otherwise indicated, all graphical data are reported ±SD.

4.3 ***Results***

4.3.1 **Immunodeficient Diabetes Mellitus Rodent DFU Model**

We have previously reported that AHA hydrogels can be engineered to support functional human microvascular networks with either ECFCs or EVCs [82, 89]. We have also reported that AHA *in vitro* formulated microvasculature can be delivered to the site of deep burn injury models. Here, we sought to investigate the treatment applications of our *in vitro* microvasculature in diabetic wound healing. The STZ-induced diabetic mouse model is one of the most extensively used models in diabetic wound repair and provides a deep understanding of diabetic wound healing [97, 98, 163-166]. Since we are delivering a human cellular network, we first established a robust immunodeficient diabetic mellitus

rodent model in order to further investigate our microvasculature's therapeutic potential.

We followed standard protocol suggested by Animal Models of Diabetic Complications Consortium for inducing a diabetic animal using streptozotocin (STZ; [92-94]). We tested both a single large STZ dose (150 mg/kg body weight) and multiple low STZ doses (50 mg/kg body weight). Both methods successfully induced diabetic nude mice, however, the single large dosage had a higher mortality rate after 14 days from the time of the first injection (data not shown). The higher dosage would have limited the length of the study, thus we opted for multiple low dose induction protocol (Figure 4-1**A**). Animals received daily STZ injection for 5 days. Their blood glucose levels rose around one week following their first injection (Figure 4-1**Bi**). At the same time, their body weight dropped about 15~20% (Figure 4-1**Bii**), correspondingly. We also noticed variation of drug tolerances in different batches of animals. However, more than 80% of all animals receiving STZ were successfully induced (not shown).

We next aimed to mimic diabetic foot ulcer wounds in order to test the therapeutic potential of the engineered human vascular constructs. Following successful diabetic mellitus (confirmed by 2 consecutive readings separated by 48 hours), we removed 2 X 6mm full thickness skin biopsy punches at the dorsum region of the animals. One served as a treatment group and the other served as a paired non-treatment control. Human vascular network constructs were generated during the induction period. Constructs were placed into the wounds and layered with Tegaderm to enable their placement and to maintain a moist and sterile environment during would healing (Figure 4-1**C**). This setup also enabled us to observe and monitor skin closure as well as blood flow measurement during wound healing.

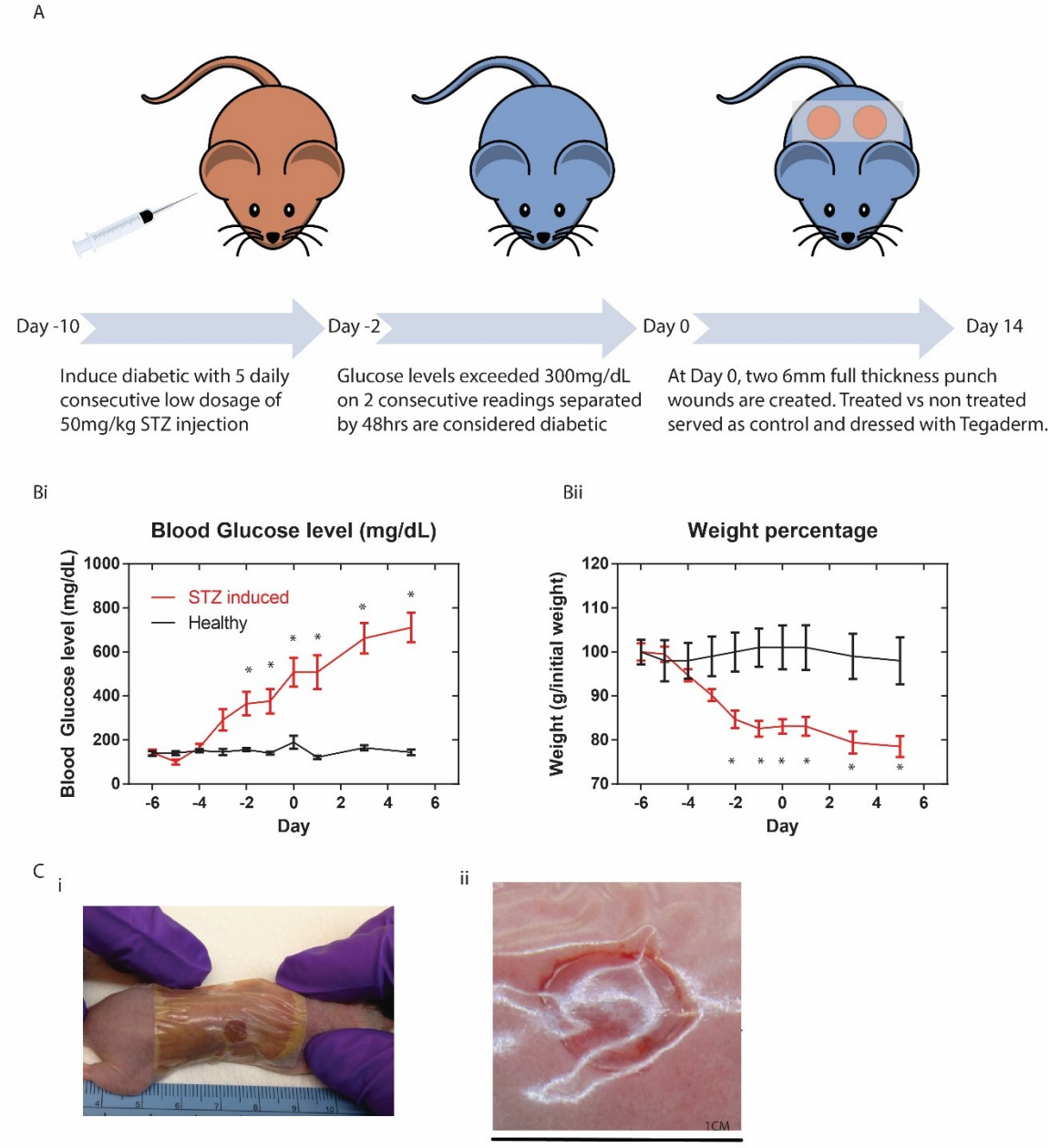

Figure 4-1. Diabetic immunodeficient mouse model
(A) Schematic drawing of our DFU immunodeficient diabetic mellitus animal model. (B) Blood glucose measurements (i) and corresponding weight of the animals (ii) during the experimental period. 300 mg/dL is considered diabetic (C) (i) Wound creation after bandage using betadine and tegaderm and (ii) planetary measurement of the wound (shown at day 0). Scale bar is 1cm.

4.3.2 *In* vitro Microvascular Networks from Varies Cell Sources

We recently developed a robust and controlled method to differentiate hiPSCs, sourced from healthy and Type 1 diabetic patients (T1D), into a bicellular vasculogenic population of both endothelial cells (ECs) and pericytes [89, 90]. Together with our already established adult progenitor cell source (ECFC), we established 4 different test groups (Figure 4-2**A**). Groups ECFC, EVC- BC1 and EVC-T1D were of constructs generated with corresponding vasculogenic cell sources [82]. The acellular construct group, Group AHA, were treated with AHA hydrogels encapsulated with growth factors. All constructs were cultured under the same conditions *in vitro* for 72 hours. In the cellular constructs, we observed vacuole formation on day 1, marked with red arrows, followed by capillary like microvasculature (multicellular network structures longer than 100μm) formation on day 3 for all three cellular treatment groups (Figure 4-2**B**).

4.3.3 Macroscopic Wound Closure and Bloodflow Profile

We closely followed the progress of wound closure for all groups at various time points. Complete wound closure occurred within 2 weeks following treatment. By week 2, wounds treated with acellular constructs were mostly closed while some of the no-treatment (NT) wounds were not fully closed. When treated with acellular constructs, wounds healed about 2 to 3 days faster than wounds that received NT (Figure 4-3**A**). During the 2 week period, all treatments accelerated wound closure significantly when compared to NT control. Planetary photos of day 7 following treatment found that the largest open wounds remained in the NT wounds, followed by wounds treated with the acellular constructs. The difference in wound size between wounds treated with EVC-BC1 and EVC-T1D constructs was indistinguishable. The smallest open wounds were found in

wounds treated with ECFCs (**Fig 3Bi**). Correspondingly, when treated with microvasculature constructs, EVC-BC1 and EVC-T1D constructs induced wound closure at a similar rate, while wounds treated with microvascular constructs composed of ECFCs closed at the fastest rate among all treatment groups (Figure 4-3**B**).

We further preformed blood flow measurements along the treatment period. Measurements on day 3 were neglected since the machine was reading the muscle layer underneath the wound bed. On day 5, we observed significantly higher blood flow in all 3 groups that received the microvessel construct treatment (Figure 4-3**C**). Both NT wounds and wounds treated with acellular constructs had lower blood flow readings compared to wounds treated with the cellular constructs. Interestingly, on day 7, we observed a delayed increased bloodflow in wounds treated with acellular constructs. Notably, wounds treated with cellular constructs (ECFC, EVC- BC1/T1D) all had higher blood flow readings when compared with wounds treated with acellular constructs and NT.

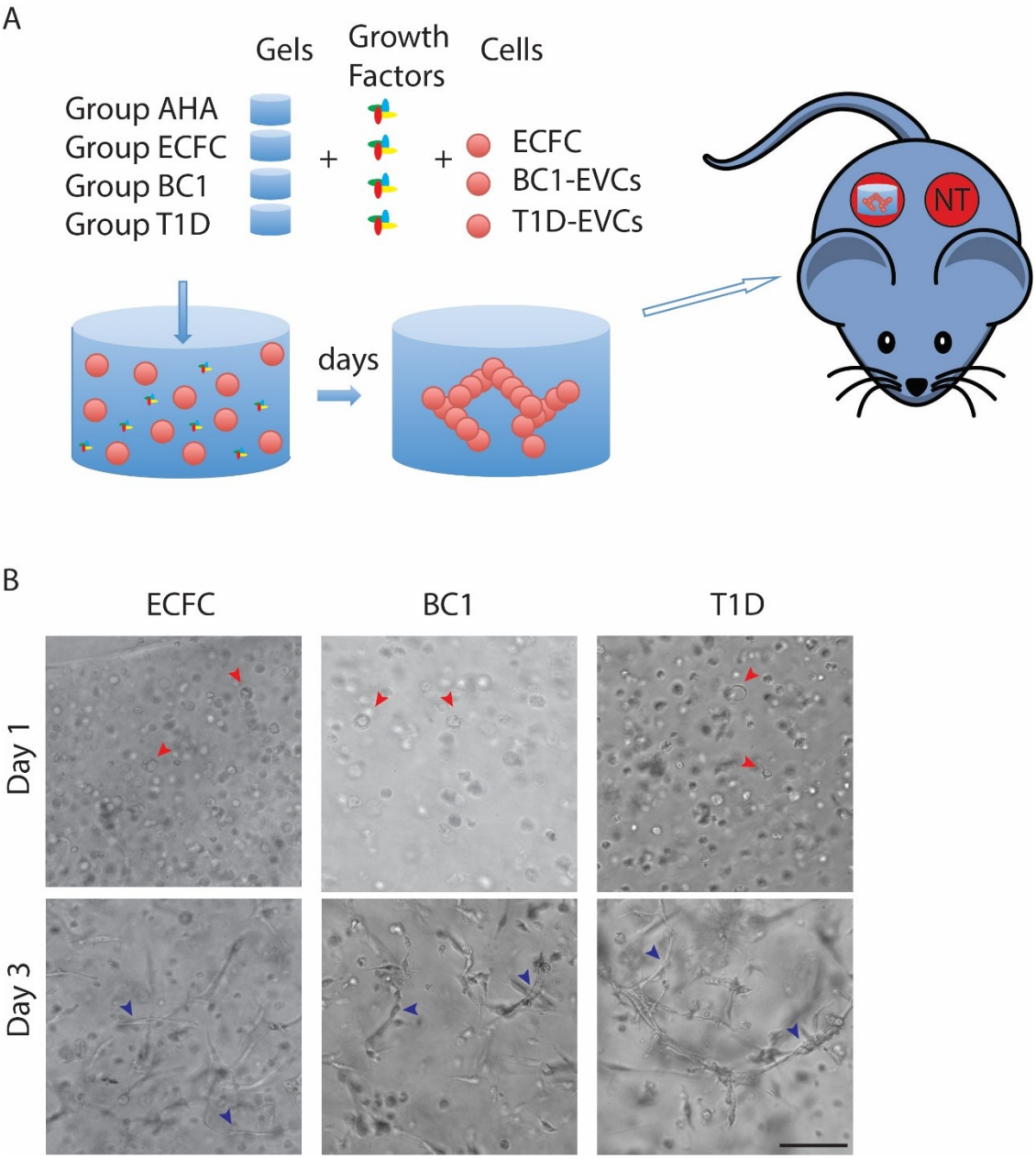

Figure 4-2. Experimental groups and in vitro engineered human vascular constructs.
(A) Treatment groups for DFU using acellular (AHA) and cellular (ECFC, EVC-BC1, EVC-T1D) vascularized constructs. NT=no treatment (B) in vitro cultures of the microvascular constructs at day 1 and day 3. Vacuoles are marked as red arrowheads and capillary structures are marked as blue arrowheads. Scale bar is 100 µm.

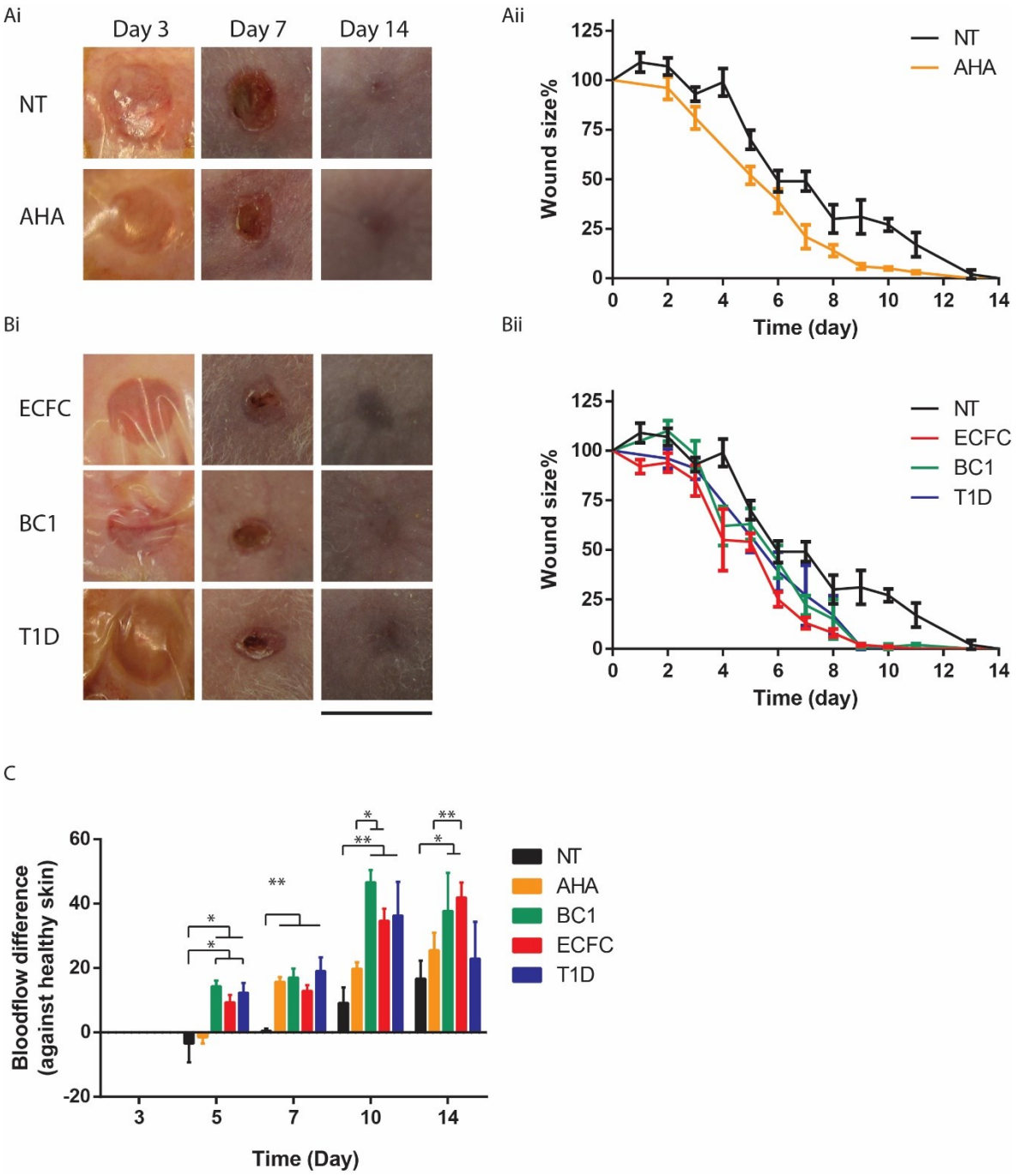

Figure 4-3. Macroscopic analysis for diabetic wound healing.
(A) Closure of wounds treated with acellular constructs and wounds receiving no-treatment: (i) planetary photos of wounds at day 3, 7 and 14; (ii) wound closure progression along the treatment period. (B) Closure of wounds treated with microvascular constructs and wounds receiving no-treatment: (i) planetary photos of the wounds at day 3, 7, and 14; (ii) wound closure progression along the treatment period. (C) Blood flow profile of different treatment groups at time intervals along the treatment period. Note that here we consolidated all NT controls together from all other control groups because significant differences were not observed between them. Scale bar is 1cm. n=12 for ECFC, EVC-BC1 and EVC-T1D n=6 for AHA and n=42 for NT.

4.3.4 **Wound Healing Rate Analysis**

Healing of tissue wounds has been extensively studied using mathematical modeling [167-170]. In our studies, the wound closure profiles closely matched theprofile of a logistic function. This allowed us to quantitatively model the wound healing using a mathematical equation to represent the time course of the healing and allowed us to study the underlying biological events. We chose a logistic growth curve to macroscopically model our wound healing profile, which not only provided an accuratefit, but also provided biophysical significance and predictive capability.

The equation below is written as for a non-linear regression fit, where *y* represents the progression of wound healing (in terms of percent skin closure), which corresponds to the open wound size *%* from (Figure 4-3**ai)** and (Figure 4-3**bi)**. t represents the time post implantation. The logistic growth equation used for modeling the wound healing is as followed.

$$y = \frac{100}{1 + e^{-\alpha(t-\beta)}}$$

The computed regression fit parameters are shown in Table 1. Goodness of fit of the regression model to our diabetic wound healing data is reported by the given R-squared value (Figure 4-4**A**). The parameter α stoichiometrically represents the intrinsic skin closure rate and the parameter β indicates the time to reach the maximum closure rate. We can compare different treatment groups by analyzing the parameters through a t-test (Table 4-1). Computing parameters α and β generates velocity (first derivative) and acceleration

(second derivative) profiles (Figure 4-4**B-C)** to visualize the closure rate profile and the healing acceleration profile. We found that all three cellular treatments groups (ECFC, EVC-BC1 and EVC-T1D) healed at a similar rate. In other words there were no statistically significant differences between the healing rates of the cellular treatment groups. All cellular treatments groups reached maximum peak closure rate significantly sooner when compared to the acellular and NT groups (Table 4-1). Wounds treated with ECFC had the earliest maximum closure rate when compared with EVC-BC1 and EVC-T1D treatments, however, there were no significant difference between wounds treated with EVC-BC1 or EVC-T1D in terms of both healing rate and the time to reach maximum rate. Wounds treated with acellular AHA constructs healed at a more accelerated manner (less time to reach maximum) and also greater in magnitude compared to the NT wounds (Figure 4-4**B-C)**.

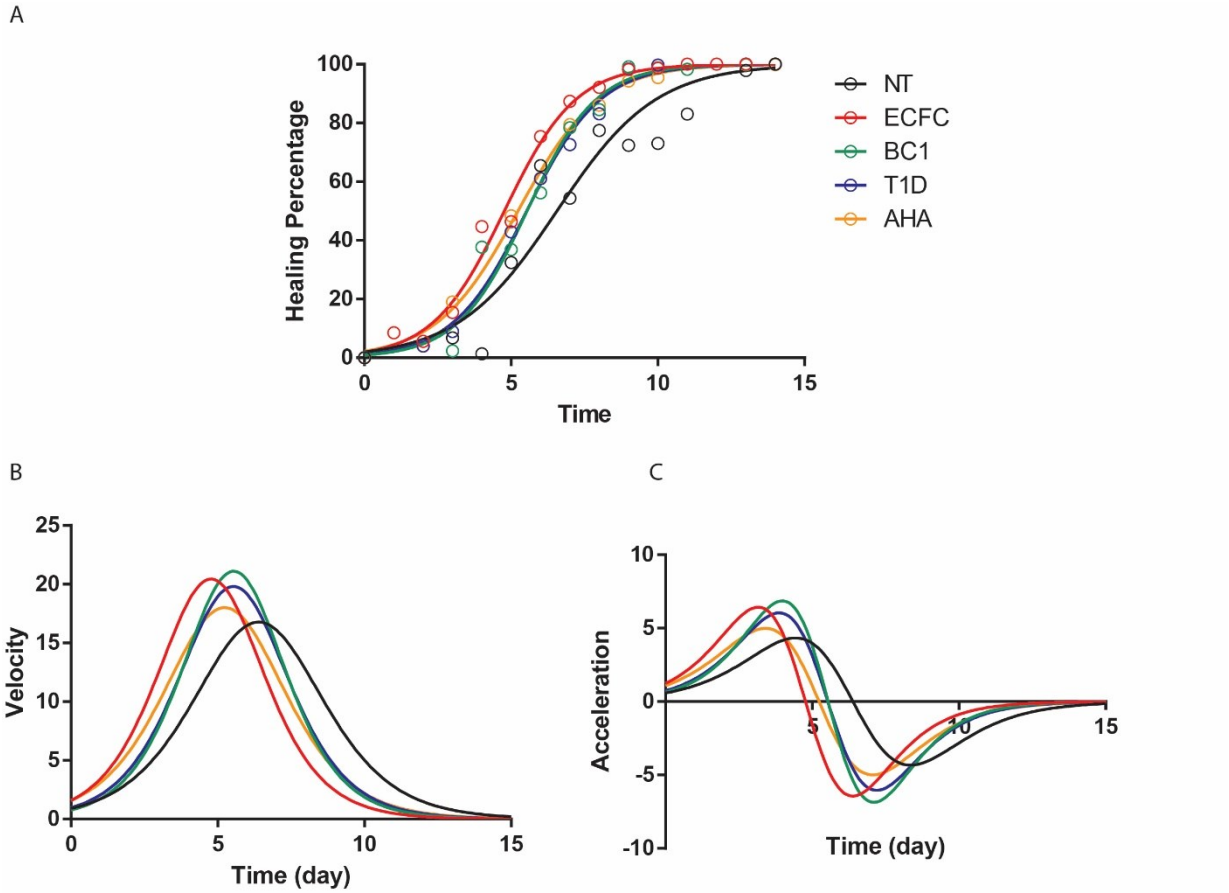

Figure 4-4. Would healing model profile, velocity and acceleration.
(A) Wound healing fitted model. Circles represent mean value of wounds healed at given time point from experimental results. Color lines are numeric value from the fitted model. (B) Velocity profile from first derivative of fitted model and (C) Acceleration profile from second derivative of the fitted model for assessment of healing of diabetic wound for each treatment group.

Table 4-1. Wound healing fitted curve parameters and regression fitness

	NT		ECFC		BC1		T1D		AHA	
	Value	SD	Value	SD	Value	SD	Value	SD	Value	SD
A	0.591^{ebta}	0.119	0.818^{na}	0.067	0.844^{na}	0.126	0.793^{na}	0.054	0.720^{ebtn}	0.037
-β	6.560^{ebta}	0.377	4.770^{btna}	0.113	5.541^{ena}	0.199	5.532^{ena}	0.094	5.233^{ebtn}	0.081
R^2	0.922		0.990		0.972		0.995		0.996	
	Significant difference when compared to NT(*n*) ECFC(*e*) BC1(*b*) T1D(*t*) AHA(*a*)									

4.4 *Discussion*

In this study, we first established an immunodeficent diabetic wound healing murine model for examining the therapeutic potential of our prevascularized constructs. We utilized STZ, a compound that has toxicity targeting the pancreatic β cells [94]. Inducing STZ in nude mice provided a platform to transplant human cell constructs and to test these constructs in an animal wound healing model. In establishing our model, we noted that the survival of nude mice following STZ treatments posed a greater challenge when compared to the wild type mouse, and literatures has shown the efficiency of induction is also varies from different source [171]. With a one-time high dose injection method, in our case, nearly 100% of mice develop diabetes within a week, however the high dose also leads to a high mortality rate 1 week after STZ injection and animals fail to survive past week 2. On the other hand, we found that using multiple low dose injections provided optimal diabetes

induction results, with low mortality rates and a relatively high rate of successful induction.

To study wound healing, many animal methods have been developed; one of the methods that has been extensively utilized to replicate human physiology is the splint model [95, 172, 173]. In the splint model, a circular splint, typically made of silicon, is attached with super glue and sutures on the uninjured skin around the wound to prevent wound contraction. This model addresses the contraction issues, which are a major difference between the human and rodent healing mechanisms. The splint wound was mostly used to test wound healing on the *db/db* mouse strain [174]. This specific strain has a baseline weight higher than many other mouse strains. This weight increase results in sluggish and slow movement of the animals, which is crucial for the splint to stay intact [173]. We tested the splint model in our STZ-induced nude mice and found that the splint lost its adherence after 5 days post operation due to the active nature of the nude mice. The usage of instant glue to better adhere the splint to the skin promoted scratching and further reduced the adherence of the splint after the glue lost its adherence. Consequently the splint was only left intact with sutures to the mouse skin. However, we found there was no significant difference between splinted vs un-splinted wounds (data not shown). A possible explanation is that the combination of betadine and tegaderm layered to seal the wound acted in a similar manner as the silicon splint. As a result, we simplified the procedure and treated the wounds without applying the splint, in so assuming the contraction rate remained the same magnitude throughout all experimental groups.

After establishing the diabetic wound healing model, we generated prevascularized constructs in AHA hydrogels with selected cell sources. We showed that all ECFCs and derived EVCs from hiPSC of BC1 and T1D undergo vacuolegenesis using our established

protocols [82, 89, 90], to form microvascular like structures. After implantation, we closely followed the wound healing process. Acellular treatment with hydrogel alone still enhanced the healing compared to NT. Vascularized constructs also enhanced healing. Among them, ECFC microvasculature enhanced closure the fastest compared to EVC-BC1 and EVC-T1D constructs. This may be attributed to the maturation stage of the cells; while ECFCs are progenitors derived from the cord blood, EVCs are derived from hiPSCs and are a less mature cell type. Examining the blood flow profiles, it is clear that the presence of implanted microvasculature facilitated faster blood perfusion, especially during the first week compared to acellular constructs and NT. From the histology sections, we found that non-degraded hydrogels remained in the wounds treated with acellular constructs, which may have hindered the blood perfusion toward the center of the wound. It is interesting to notice that wounds treated with ECFCs or EVC-BC1 constructs exhibit higher blood perfusion at all the time points. In wounds treated with EVC-T1D constructs, blood flow regresses after day 10. However, we were unable to follow the wound closure longer than 3 weeks to assess skin maturity in long term due to the poor health of the immunodeficient mice. The differences between ECFC and EVC-BC1 with EVC-T1D could be due to the genetic nature of the T1D. The hyperglycemia of the host could trigger a sequence of epigenetic events which cause vessel regression, which may damage the integrity of the vascular network.

Next, we used a non-linear logistic growth model to fit our diabetic wound healing profile. It allowed us to compare the healing progression of the wounds between treatment groups. We decided to use a supermacroscopic approach [168]. This approach focused on the mathematical description, in which the interactions are based on the recorded data at

the tissue level, where in our case was the size of the healed wound. We found that wounds treated with vascularized constructs healed at a faster rate, possibly because of increased blood flow. In the case of treatment with acellular constructs, wounds still healed faster than NT, where the contributing factor could be has lesser time to reach maximum closure rate. This could be attributed to the hydrogel providing a scaffold for cell migration towards the wound site, thereby enabling healing. This increased wound healing response may also have been due to the growth factors encapsulated in the hydrogels, which are known to activate wound healing pathways. It is worth noting that our approach poses limitations when compared to a microscopic approach [167] where the variables and relations were constructed at the cellular or molecular level. As a result, we do neglect the individual cellular mechanisms during wound healing. We can then only make indirect observations of relationships between the experimental data and our experimental groups. This analysis limits us to draw direct connections at a macroscopic level, rather than at acellular level. However, this supermacroscopic strategy is sufficient to provide quick and direct insight into the outcomes of our different treatments.

5 *Acellular hydrogels for regenerative burn wound healing: translation from a porcine model*

Healing following third-degree burn injuries is fraught with complications, often resulting in long-term physical and psychological sequelae. The use of currently available skin grafts and skin substitutes are often associated with complications and suboptimal outcomes. Synthetic treatment that can promote wound healing in a regenerative fashion would provide an off-the-shelf, non-immunogenic strategy to improve clinical care of severe burn wounds. Here, we demonstrate vulnerary efficacy of our dextran-based hydrogel in third-degree burn wounds in a large-animal model. This porcine model was optimized to allow examination of the hydrogel treatment for clinical translation and the mechanisms by which it promotes a regenerative response. Hydrogel treatment accelerated third-degree burn wound healing by rapid wound closure, improved reepithelialization, enhanced extracellular matrix remodeling, and greater nerve reinnervation, compared to the dressing treated group. These effects appear to be mediated through the ability of the hydrogel to facilitate a rapid but brief initial inflammatory response that coherently stimulates neovascularization within the granulation tissue during the first week of treatment, followed by an efficient vascular regression to promote a regenerative healing process. Our results demonstrate that the dextran-based hydrogels, without the use of additional cells or drugs, may significantly improve healing quality and reduce skin

grafting incidents and thus pave the way for clinical studies to improve the care of severe burn injury patients.

5.1 *Introduction*

Burns are a leading cause of accidental death that when survived, can result in serious disability and social impairment from disfigurement [175]. In 2013, approximately 450,000 burn injuries received medical treatment [176] and the estimated hospital care cost in high-income countries estimated to exceed $88,000 per burn patient [177]. In the United States, only ~4% of patients admitted to burn care centers die, and due to advances in critical care and medical management of these patients, survival has continued to improve with time [89]. Survival in the most severely burned patients is often accompanied with orthopedic, neurologic and metabolic complications and significant psychosocial challenges brought about by poor healing and excessive scar formation [178]. Therefore, the challenge remains to improve wound healing in the patients in order to reduce morbidity and mortality in those patients with the worst burns—those classified as third-degree burns and beyond. Third-degree burn wounds are characterized by the full-thickness damage of the skin, including both the epidermal and the dermal layer. Unlike superficial burn wounds that can heal on their own without advanced professional care, third-degree most often require surgical intervention and replacement of damaged skin with skin grafts or skin substitutes [179]. Biomaterials that are able to induce a regenerative response of healing would therefore promise significant improvement in clinical care and long-term outcomes of wound patients, particularly those sustaining burn injury.

Predicting which therapeutic interventions will elicit a regenerative response post-cutaneous wounding has remained challenging. Although murine models are irreplaceable for understanding mechanisms involved in normal and pathologic wound healing, mice, unlike humans, heal primarily by contraction. Additionally, there may be differences in the immune/inflammatory response to cutaneous injury, particularly that of burn injury [180], and the lack of significant naturally occurring pathologic scar formation in mice. Porcine wound healing is considered to be most similar to that of humans and as a translational model, pigs display the greatest concordance with human trials [181]. The Yorkshire pig is a well-established model that approximates the normal wound healing response in humans [182]. First, porcine skin most closely resembles human skin both anatomically and physiologically. Both have similar dermal-epidermal thickness ratio and dermal vascularization pattern [181, 183]. Biochemically, porcine and human skins have similar collagen matrix and keratinous proteins [175]. Studies have also shown an excellent agreement between pig and human with respect to wound healing responses from growth factors [181]. In addition, the size of the animal allows control and comparison of different treatment parameters in the same animal. Despite these benefits, technical difficulties limit the use of pig models for studies of third-degree burns. Indeed, unlike superficial burn wounds, which can easily be created using accessible tools and temperatures, there is limited literature on modeling severe burn injuries in a reproducible manner and on the criteria for assessing the healing kinetics, especially for the purpose of evaluating biomaterials.

Our laboratory has developed an acellular dextran-based hydrogel, dextran-allyl isocyanate-ethylamine, that is tailored to promote rapid neovascularization and has proven

to accelerate third-degree burn healing with complete skin regeneration in a murine model [85-87]. We have shown that compared to other treatments, the dextran-based hydrogel better promotes rapid neovascularization through its ability to facilitate infiltration and resolution of an early inflammatory response, leading to complete skin regeneration. This current translational study extends our understanding of the mechanisms of dextran-hydrogel induced healing in a porcine large-animal model and shows that dextran-based hydrogel alone, without the use of additional biologicals such as growth factors or cells, can safely promote a regenerative healing and thus paves the way for their use in clinical studies.

5.2 *Materials and Methods*

5.2.1 **Polymer Synthesis and hydrogel preparation**

The dextran hydrogel was synthesized and characterized as previously [85-87]. Briefly, allyl isocyanate (AI) was incorporated into dextran by dissolving pre-dried dextran (e.g. 2g) in anhydrous DMSO (20mL) at room temperature under nitrogen gas. Reaction catalyst DBTDL was added (0.210mL), and AI (0.240 mL) was added to the solution dropwise. After the reaction, the solution was precipitated in cold excess isopropanol and filtered. Next the remaining hydroxyl groups in Dex-AI were substituted with ethylamine groups. For this step, pre-dried Dex-AI (e.g. 2g) was first dissolved in DMSO (30ml) under nitrogen gas. Meanwhile, BEAHB (3.75g) was dissolved in DMSO (10ml) in a separate chamber. Catalyst TEA (11.2mL) was added to the Dex-AI DMSO solution, and the dissolved BEAHB in DMSO was added to the solution dropwise. After the reaction, TEA

salt was filtered and the resulting solution was precipitated in cold excess isopropanol and filtered. The resulting Dex-AE was then dialysized against distilled water for 3 days and lyophilized for additional 3 days. The purified polymer was stored in vacuum until further use. For characterization NMR of the polymer for degree of substitution for thiol group (AI) and aminated group (AE) was performed. For crosslinking, polyethylglycol diacrylate (PEGDA) was synthesized as previously established and dialysized against distilled water for 3 days and lyophilized for additional 3 days. The purified polymer was stored in 4°C until further use. For hydrogel preparation Dex-AE and PEGDA were dissolved at the weight ratio of 80:20 into phosphate-buffered saline containing 0.1% (w/w) Irgacure® 2959. The mixture was pipetted into a sterile mold made by polydimethylsiloxane and photocrosslinked (10mW/cm^2 of UV light for 10 minutes). Hydrogels were swelled against PBS for swelling ratio and crosslink density characterization. *In vitro* cell toxicity was carried using WST assay (Sigma) as well as pilot *in vivo* burn mice tests [87] were done to confirm AE hydrogel therapeutic properties.

5.2.2 **Animal use and surgical procedure**

Surgical procedures were approved by the Institutional Animal Care and Use Committee at Thomas D. Morris, Inc. prior to the experiments. All pigs were fasted for at least 12 hours prior to any surgical procedure. Anasthesia was induced by an intramuscular injection of Telazol cocktail reconstituted with ketamine and xylazine. Then, the pig was endotracheally intubated and ventilated mechanically to aid breathing and to provide up to 1.5% of isoflurane (depending on the painfulness of the procedure) to maintain anasthesia. In addition, blood pressure, heart rate, body temperature, and blood oxygen level was

monitored. Bair Hugger® was placed under the pig and set to 43°C to maintain a normal body temperature.

Two pigs were used to determine optimal wounding procedure and parameters for third degree burn. Temperature was set at 100 and 200 degree Celsius while maintaining contact pressure at 2kg/cm^2 and contact duration of 30 seconds. Biopsy was taken 24 and 48 hours after injury for histological analysis.

Three pigs were then used to investigate the therapeutic effect of dextran hydrogel on burn wounds. Following injury, the wounds were left for 48 hours for stabilization before the excision procedure. A total of 70 circular third-degree burn wounds (1.2 or 1.5cm in diameter) were created. Circular biopsy punches were used for partial or complete excision for full-thickness wound down to the necrotic adipose layer. Wounds were at least 3cm apart from one another to minimize hindered wound healing process due to proximity. After the excision procedure, wounds were cleaned with sterile gauze to temporarily stop bleeding. Half of the wounds were treated with dextran hydrogel and the other half were left untreated. Hydrogels were crosslinked in molds that matched the size of the excised wounds. Treated and untreated wounds were first sealed with Tegaderm® (3M). The peripheries of the wound site was applied with compound benzoin tincture (Medical Chemical, Corp) to enhance the Tegaderm® adherence to the skin. An additional layer of Vetrap® (3M) was applied to the torso and elastic body suit (VetMedCare) were worn over the body in order to minimize the disturbance of the healing wounds. To protect the newly forming epidermis from traumatization during bandage change, a non-adhesive Curity® dressing (Covidian) was placed under the Tegaderm® layer beginning at day 14. After wound closure, only an elastic body suit was worn over the wounds. For retreatment, re-

debridement was made and a new half the thickness hydrogel was placed on top for retreatment. Secondary excision was made on control group as well for the retreatment group. Dressings were changed three times a week until wound closure was complete. Before the dress change, the pig was put under anesthesia with an intramuscular injection of Telazol cocktail reconstituted with ketamine and xylazine. The pig did not receive isoflurane because the procedure was quick. Before reapplying dressings, the wound area was scrubbed with 4% chlorhexidine and ethanol. The area was wiped with dry gauze and new dressings were applied.

To evaluate healing, skin specimens were biopsied at each time point as complete horizontal cross-sections of approximately 5cm in thickness with a sterile blade. Analgesics were administered before wound creating and biopsy procedures, and transdermal fentanyl patch was applied for 9 days post-operation. Blood tests were performed regularly to monitor the pig's health throughout the study.

5.2.3 **Healing Evaluation**

During the study, the blood flow inside the wounds were monitored noninvasively using moorFLPI speckle contrast imager (Moor Instruments, Inc.). The measurements were normalized by the blood flow measurements of the healthy skin area adjacent to each wound. Photometric analysis was done along with blood flow measurement.

For immunohistochemical assay, collected skin specimens were first fixed with 10% formalin (Fisher Scientific, Inc.) for at least 48 hours. Following fixation, samples were dehydrated in graded ethanol (70% to 100%), embedded in paraffin, sectioned at 5μm or 25μm for nerve signal, and stained with either H&E, Masson trichrome, and Verhoeff-van

Gieson's stain or immunohistochemistry for CD31 (1:50 Abcam), cytokeratin 14 (1:50 Abcam), MAC387 (1:50 Abcam), SMA (1:100 Dako), Dapi (1:1000), PGP9.5 (1:500 AbD Serotec) and matching Alexaflour secondary (1:500 Lifetech). Histological images were taken with upright light microscope (Nikon Accuscope 3000) and Camera (Nikon DS-F12). Full specimens images were scanned and tiled together using automated motor controlled Nikon T1 and tiled together with corresponded software (Nikon Nis-Element). Fluorescent images were taken with confocal (Zeiss LSM780).

The area and number of vessels inside the wounds were quantified using ImageJ software (National Institutes of Health) with histology sample of each wound stained with CD31. The vessels were imaged at the edges, middle, and top portions of each wound, and the positively stained areas were selected using the software's threshold function. The selected areas were then quantified using "Analyze Particles" plugin of ImageJ. "Microvessels" with areas less than 78μm^2 were excluded to filter out noise.

Wound gap area was measure photometrically by tracing the opened wound edge using Image J. Histologically analysis for the maturation of the re-epithelialization is quantified by rete ridge formation density as previously described [99]. In brief, we first defined the entire wound length as the length between the two edges of the healthy dermis and epithelium. Then, re-epithelialization was calculated as the percentage of regenerated epithelium (K14 positive) of the entire wound. Percent reticulation is calculated as the percentage of the reticulated epithelium of the regenerated epithelium. The reticulated epithelium is defined as the epithelium from the first structural reticulation ridge to the last reticulation ridge within the wound. Rete density is calculated as the amount of reticulation ridges over the reticulated epithelium.

Collagen fiber deposition was quantified from Masson trichrome images by calculating the percentage of collagen fiber presented in the wound. Briefly, using ImageJ, we quantified the percentage of stained collagen fibers in the given area in each group. Elastin fibers were quantified from Verhoeff-van Gieson's stain across the dermis area adjacent to the epidermis similarly to the collagen.

Nerve innervation analysis was performed on a 25μm paraffin sections on gelatin coated slides. Samples were incubated in primary antibody overnight and 1 hour in secondary antibody. Slides were then analyzed in confocal using serial z-stack imaging. Final images were maximum intensity projected through z axis for the final images.

5.2.4 **Gene Expression**

Gene expression analysis was performed using two-step reverse transcription polymerase chain reaction (RT-PCR) on wound specimens in accordance with Applied Biosystems manufacturer instructions. To extract RNA, a small specimen was collected from each wound at different time points and snap-frozen in liquid nitrogen. The specimen was crushed with pestle and mortar, and the powdered sample was put in 1mL of Trizol reagent and stored in -80°C until further use. Wound healing and ECM RT-PCR array sets (Qiagen) were used to compare the expression profile inside the treated and non-treated wounds at different time points. For each primer, the comparative computerized method provided by the manufacturer was used to calculate the amplification differences between different samples.

5.2.5 **Statistical Analysis**

For wounding parameter determination two pigs were used. For wound healing analysis, total of three pigs with n>12 wounds for each condition with at least n=3 for each time point detailed throughout the manuscript. For quantification of blood vessels and reepithelialization whole wounds analyzed as detailed above. Real-time RT-PCR performed on triplicate samples (n=3) with triplicate readings. Statistic was calculated by the computerized method provided by the manufacturer to obtain p-value of the gene expression. For data presentation relative gene expression was graphed with relative fold change of the targeted group / dressing day 5. For all other assays, statistical analysis was performed using GraphPad Prism 6.01 (GraphPad Software Inc.) to perform t-tests, One Way ANOVA with Turkey's posttest, or Two Way ANOVA with Bonferroni's posttest where appropriate. Significance levels were set at *$p<0.05$, **$p<0.01$, ***$p<0.001$, and ****$p<0.0001$. Unless otherwise indicated, all graphical data are reported ±SD.

5.3 *Results*

5.3.1 **Dextran-based hydrogels for third-degree burn wounds in pigs**

To produce dextran-based hydrogels, dextran polymer was first modified with allyl isocyanate and ethylamine functional groups and cross-linked with polyethylglycol diacrylate [85-87]. The cross-linking density, controlled with low degree of substitution, was optimized to give high porosity and flexibility to the hydrogel in order to promote rapid inflammatory and angiogenic cell infiltration. Consistent with its synthetic and xeno-free composition, the dextran-based hydrogels are nonimmunogenic and thus can be used as an off-the-shelf therapy. Compared to other formulation and treatments, the dextran-based hydrogels accelerate wound healing in subcutaneous and burn wounds in murine studies, providing promising proof of principle evidence that dextran-based hydrogels promote a regenerative response post injury. However, compared to mouse skin (0.1-0.2mm), pig skin has a much thicker epidermal and dermal layers (3-4mm total) which, in addition to other anatomic features, is more similar to human skin. Therefore, the murine cutaneous anatomy protocol for creating third degree burn wounds in a mouse model was not sufficient in creating burn wounds at a third degree level.

In order to investigate the safety and efficacy of the dextran-based hydrogel in the porcine third-degree burn injury model, we designed a custom-made device that was inspired from a previous study [184]. This device which is comprised of three parts including metal heat source, and insulation and pressure units (Figure 5-1**Ai**), allows for reproducible delivery of the critical components known to influence extent of thermal injury, including temperature of the burning object, the duration of the contact with the

object [185] and to a lesser extent pressure [186]. The metal rod is being heated and used for generating the thermal injury. A digital thermometer probe placed within a predrilled hole is used to monitored metal rod's core temperature for consistent thermal injury source. The middle part is an insulating unit made of polytetrafluoroethylene for holding the device upright for the duration of the burn. The air trapped in the syringe unit provides a spring force when pressure is applied, which can be measured and kept constant for all wounds.

To create the wounds, the device was held at a 90° angle to the skin with a constant pressure of 2kg/cm^2 (Figure 5-1**Aii**). A standardized anatomic position (thoracic paravertebral zone) was chosen based on its relative protection against post-burn self-trauma associated with movement and recumbancy. As significant thermal insult is associated with progressive injury to deep tissues compared to superficial damages until 48 hours post-injury [187], the degree of burn damage was evaluated in wounds 24 hours or 48 hours after the burn [184, 188]. Healthy porcine skin tissue sections are provided in (Figure 5-2**)** for reference. To induce full thickness dermal injury, a heat source of 200°C, applied for 30 seconds was required (Figure 5-1**B**). In contrast, application of a heat source of 100°C for either 30 or 60 seconds (Figure 5-1**B**; data not shown for 60 seconds) was not sufficient to induce a third-degree burn injury. As anticipated, evidence of dermal injury progressed between 24 and 48 hours. Thus, use of 200°C for 30 seconds was chosen to generate third-degree burns in assessing the ability of the dextran-based hydrogel to improve healing of burn wounds. The significant damage induced by thermal injury in this model is evidenced by the reduction in blood flow, indicating more severe damage on blood vessels (Figure 5-1**C-D**). Immunohistochemistry for CD31 confirmed the lack of blood vessels throughout the injured dermis 48 hours after application of the 200°C for 30

seconds (Figure 5-1**E**). Given the previously defined ability of this biomaterial to induce angiogenesis, the optimized burn model provides a rigorous model of injury with severe, repeatable damage to blood flow to assess the ability of dextran-hydrogel to improve healing.

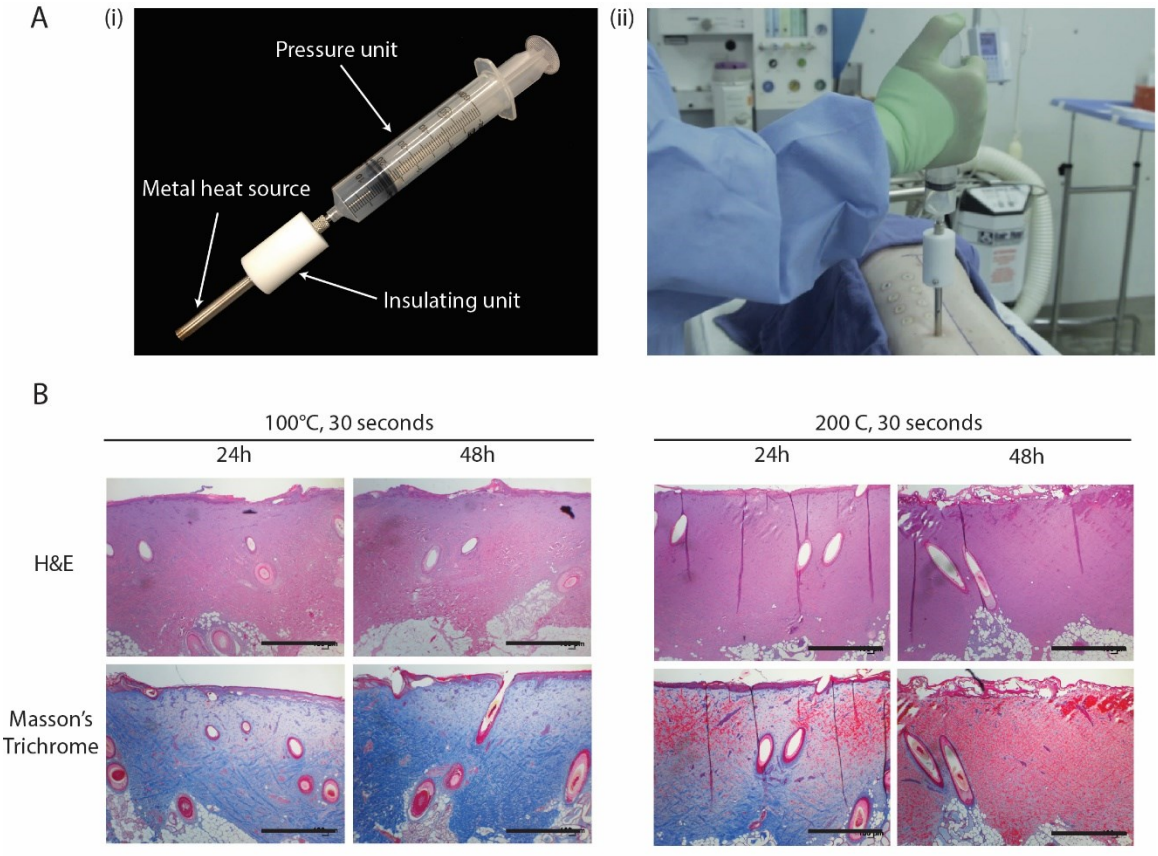

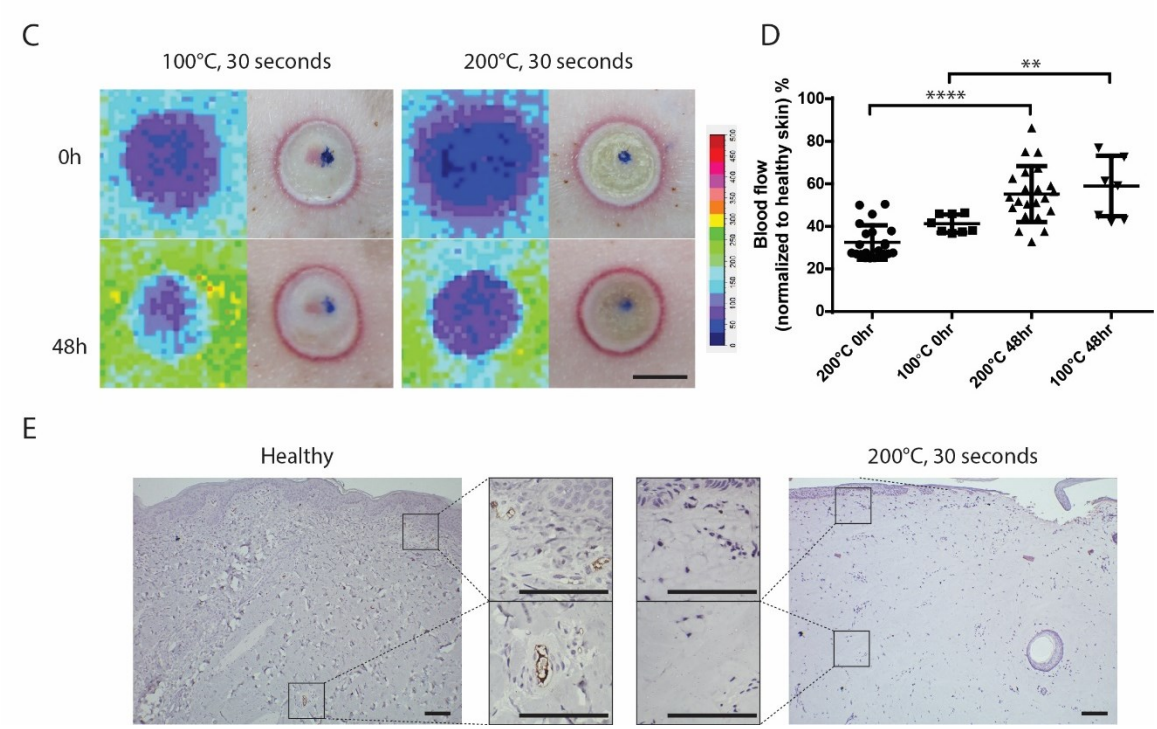

Figure 5-1. Induction of third degree burn injury in pigs.
(A) A custom-made burn device (i) is held upright on the pig's thoracic paravertebral zone (ii). (B) Representative images of H&E and mason trichrome histological stains of the wounds at different temperatures and burn durations. (C-D) Laser speckle contrast images (*left*) and quantification (*right*) of blood flow in healthy skin and burn wounds burn wound. N= 22 and N=8 for 200°C and 100°C respectively. (E) Immunohistochemistry for CD31 of the 200°C 30 seconds 48h show no vessels in the wounded area compared to healthy skin. Scale bars are 1mm in B, 1cm in C and 100µm in D. Significance levels were set at *p<0.05, **p<0.01, ***p<0.001, and ***p<0.0001

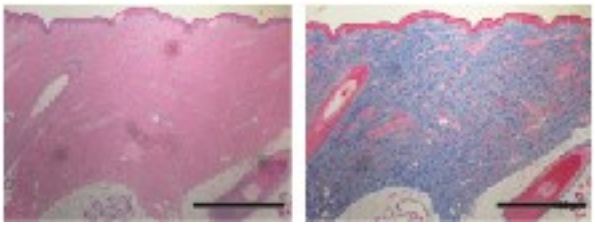

Figure 5-2. Healthy pig skin.
Representative images of H&E (left) and trichrome (right) histological stains of healthy skin at the thoracic paravertebral zone. Scale bars are 1mm.

5.3.2 **Vascular ingrowth, maturation, and regression in hydrogel-treated burn wounds**

Following excision of the necrotic tissue, hydrogels were applied as skin substitutes. Because complete excision of the avascular zone of coagulation has been shown to improve outcomes when biomaterials are used for burn wound treatment, we investigated whether it was necessary for maximal efficacy to resect beyond the original injury site (complete) or whether a more conservative resection (partial) would be sufficient. In the first protocol, we followed the approach used in our previously published murine burn model in which a 1.2 cm diameter biopsy punch was used to excise the burn wound made by a 1.2cm diameter stainless steel device [87] and excised the entire initial contact site of the thermal burn. Because peripheral injury extends radially beyond the contact area, this excision leaves a thin (~3mm) rim of damaged tissue. The excised areas were then treated with pre-crosslinked hydrogels shaped to fit the size of the wounds. For dressing, a layer of Tegaderm® was bandaged over the treated area to hold the hydrogels in place and prevent desiccation. In the second protocol, all the necrotic tissue was excised, including all grossly abnormal tissue which extended up to 3mm beyond the initial contact site.

Vascularization of the entire hydrogel (i.e. throughout the entire wound bed), as evidenced by immunohistochemical staining for CD31, was seen by day 5 only in wounds that had complete excision of the burn wound. In contrast, incomplete excision negatively impacted vascularization of the hydrogel during that time frame (Figure 5-3**A**). Hydrogel vascularization, quantified both as vessel density and the percentage of area covered by the vessels two weeks post-treatment, confirmed a more efficient vascularization followed by

vascular regression for the completely excised wounds, consistent with a superior healing process (Figure 5-3**B**), prompting selection of this model for use in all subsequent studies.

We next examined the ability of the hydrogel to promote vascularization and subsequent vessel regression within healing wounds compared to wounds treated with dressing alone following complete excision of burn injured tissue. In the first week after excision, mean vascular density in both groups were increased at both day 5 and 7 when compared to baseline. However, a more rapid vascular regression was noted in hydrogel treated wounds. Specifically, the hydrogel treated wounds exhibited significant decrease in vessel density by day 14, whereas the dressing-only treated group showed no significant change over the same time period (Figure 5-3**C**). Blood flow analysis on day 14 confirmed a significant reduction in blood flow in the hydrogel treated wounds compared to dressing-only treated wounds that was closer to that seen in uninjured skin (Figure 5-3**D**), supporting hydrogel-induced resolution of the initial vascular phase of wound repair.

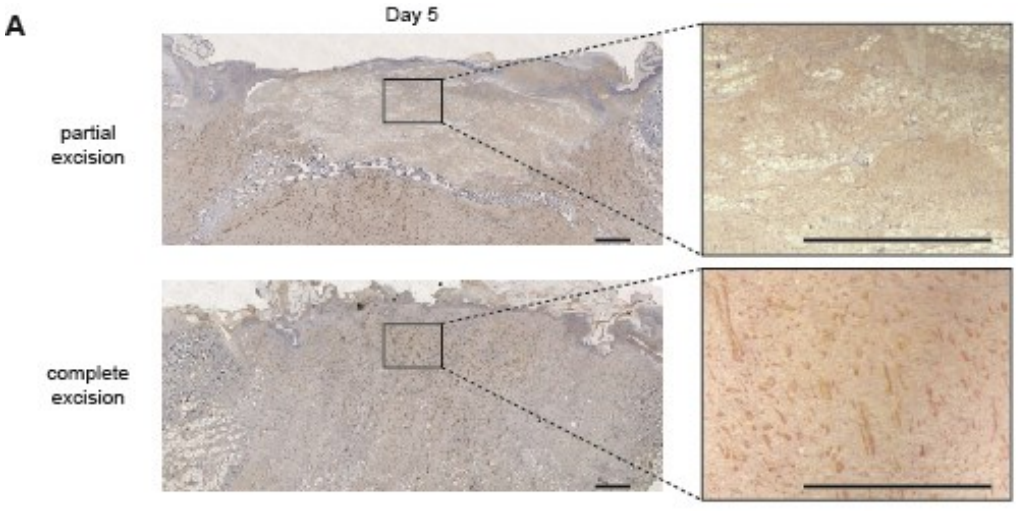

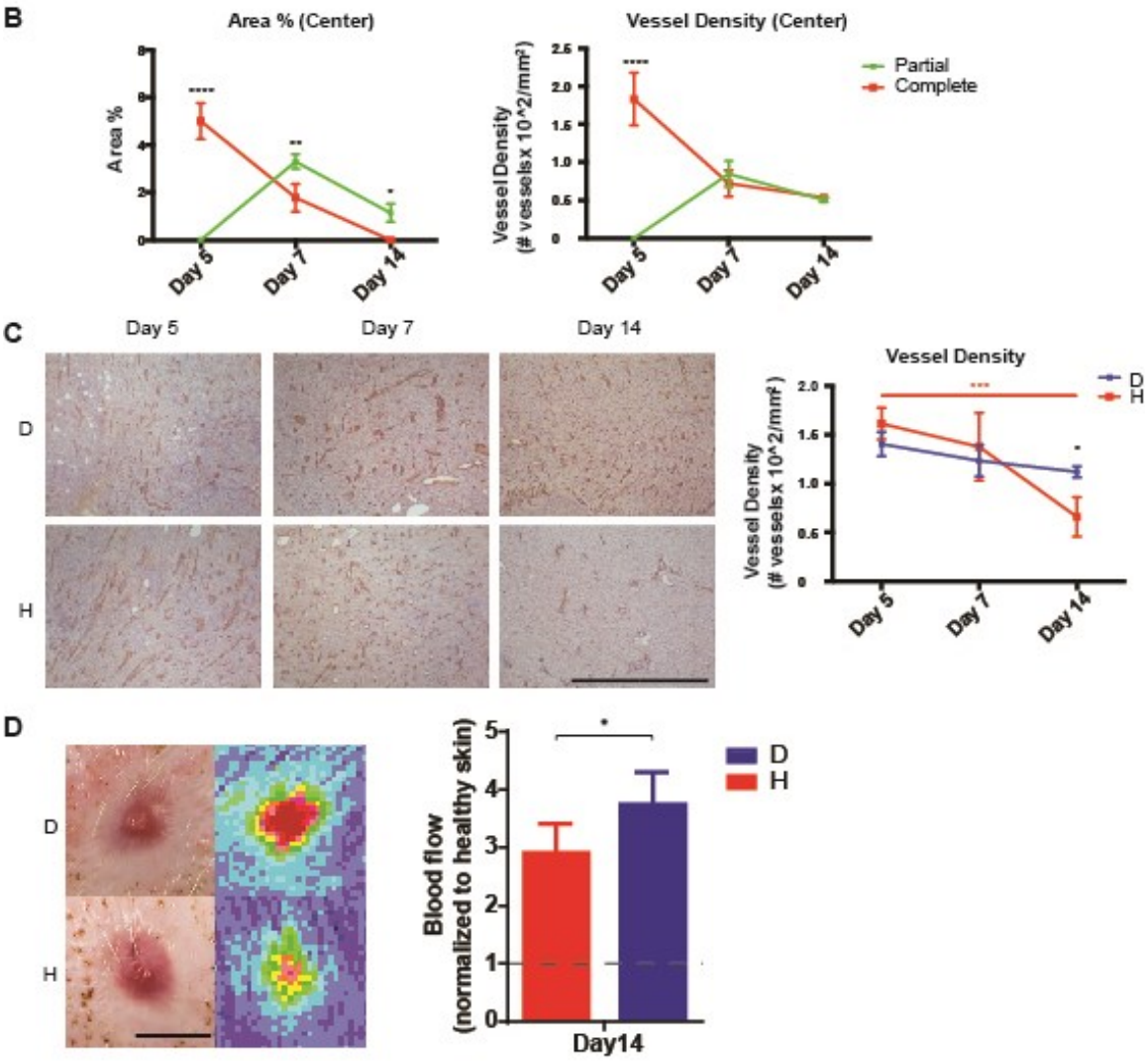

Figure 5-3. Wound excitement and kinetics of vascularization.
(A) Immunohistochemistry for CD31 of wound area depicting vascular ingrowth on day 5 for partially excised (method 1) and completely excised (method 2). High magnifications of the boxed areas are shown on the right. (B) Quantification of CD31 stains at of the wounds treated in both methods over two weeks N=3 per time point. (C) Immunohistochemistry for CD31 and quantification of vasculature over two week of the hydrogel-treated wounds and dressing-treated wounds over two weeks. N=3 per time point. (D) Laser speckle contrast images (right) and quantification (left) of blood flow in hydrogel-treated wounds and dressing-treated wounds on day 14. D= dressing-only treated wounds; H= hydrogel treated wounds. N=7. Scale bars are 1mm in A and C and 1cm in D. Significance levels were set at *p<0.05, **p<0.01, ***p<0.001, and ****p<0.0001. Red asterisks indicate significant change along time; Black asterisk indicate significant difference between the two treatments at a given time point.

5.3.3 **Wound closure and re-epithelialization**

A key feature of any healed wound is complete reepitheliazation. Compared to murine wounds, which heal primarily by contraction, the process of wound healing by reepithelialization in humans is better modeled in the pig. We have examined dressing versus hydrogel treatment. During the treatment period, dressings were changed three times a week until wound closure was complete. Occasionally, this dressing change on day 5 interrupted the integrity of the healing area, which prompted us to also examine the re-debridement on day 5 following by re-application of hydrogel or dressing-only. Gross examination of the wounds at day 14 revealed a delay in wound closure in the dressing only treated wounds compared to hydrogel treated wounds (Figure 5-4**Ai**). Examining gross wound closure, we found that all hydrogel treated wounds appeared closed while just 14% of dressing-only treated wounds and none of the dressing retreated wounds were closed (Figure 5-4**Aii**), resulting in wound gap in the dressing-only treated wounds and larger gap in the dressing retreated wounds (Figure 5-4**Aiii**). While all hydrogel treated wounds closed on day 14, all dressing-only treated wounds closed 7 days later on day 21 post treatment, shows a 33% delay in wound closure rate (data not shown). Identification of the neoepithelium on masson trichrome or K14 (keratinocyte marker) stained sections confirmed that dressing-only treated wounds had an epithelial gap, while hydrogel- treated wounds were completely re-epithelialized (Figure 5-4**B**). A similar trend was found with retreated wounds where dressing-only retreated wounds had a gap in the epithelial layer while hydrogel retreated wounds were closed with a thick and reticulated epithelial layer (Figure 5-4**C**). As it was noted the appearance of the neoepithelium of hydrogel treated wounds closer approximated uninjured epidermis, we next quantified the rete percentage

(i.e the percent of the reticulated epithelium in the regenerated epithelium) and the rete ridges [99]. We found that dressing-only treated wounds had a very low rete percentage and density, while hydrogel treated and retreated wounds exhibited high rete percentage and rete density. Consistent with a superior regenerative response, hydrogel treated wounds have rete density similar to healthy skin (Figure 5-4**Di-ii**). Finally, the hydrogel treated and hydrogel retreated wounds exhibited similar decrease in vessel density from day 7 to day 14, whereas the dressing and dressing re-treated group showed no significant change over the same time period (Figure 5-5). Based on these results, hydrogel treatment (without the retreating) procedure was used to continue our analyses of healing kinetic and remodeling.

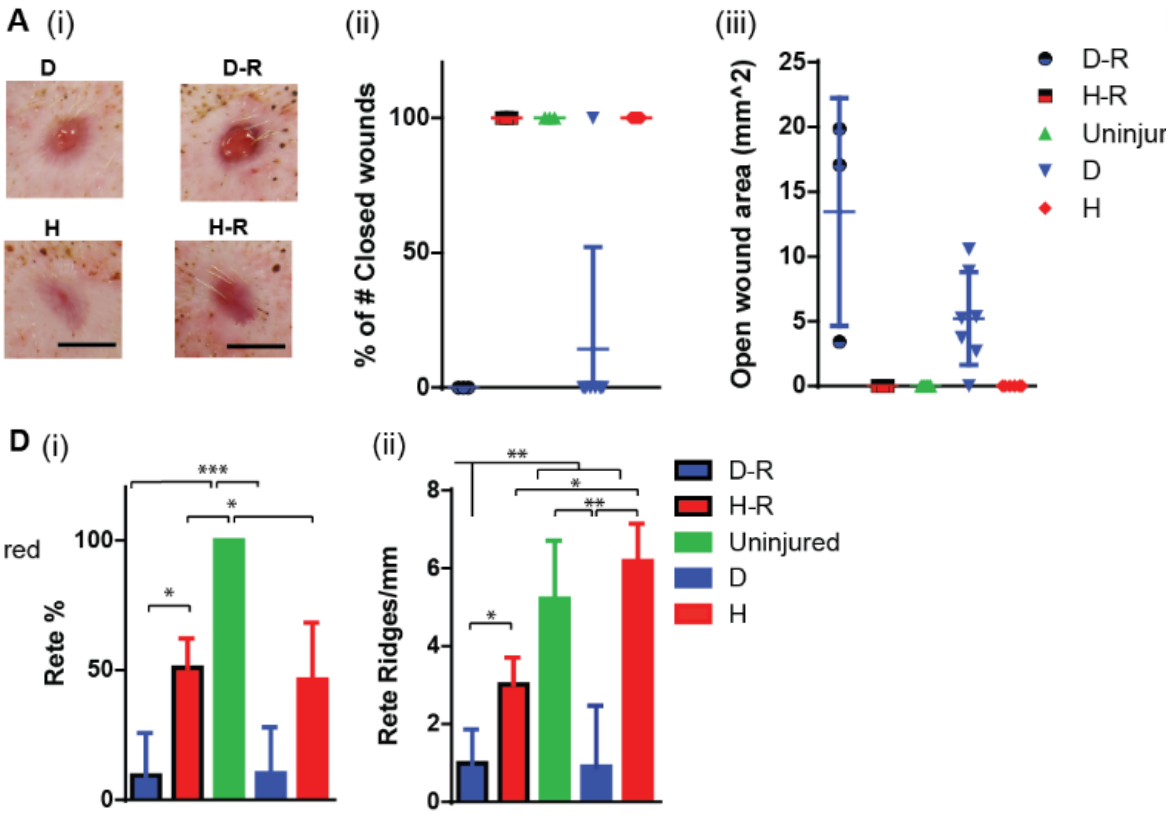

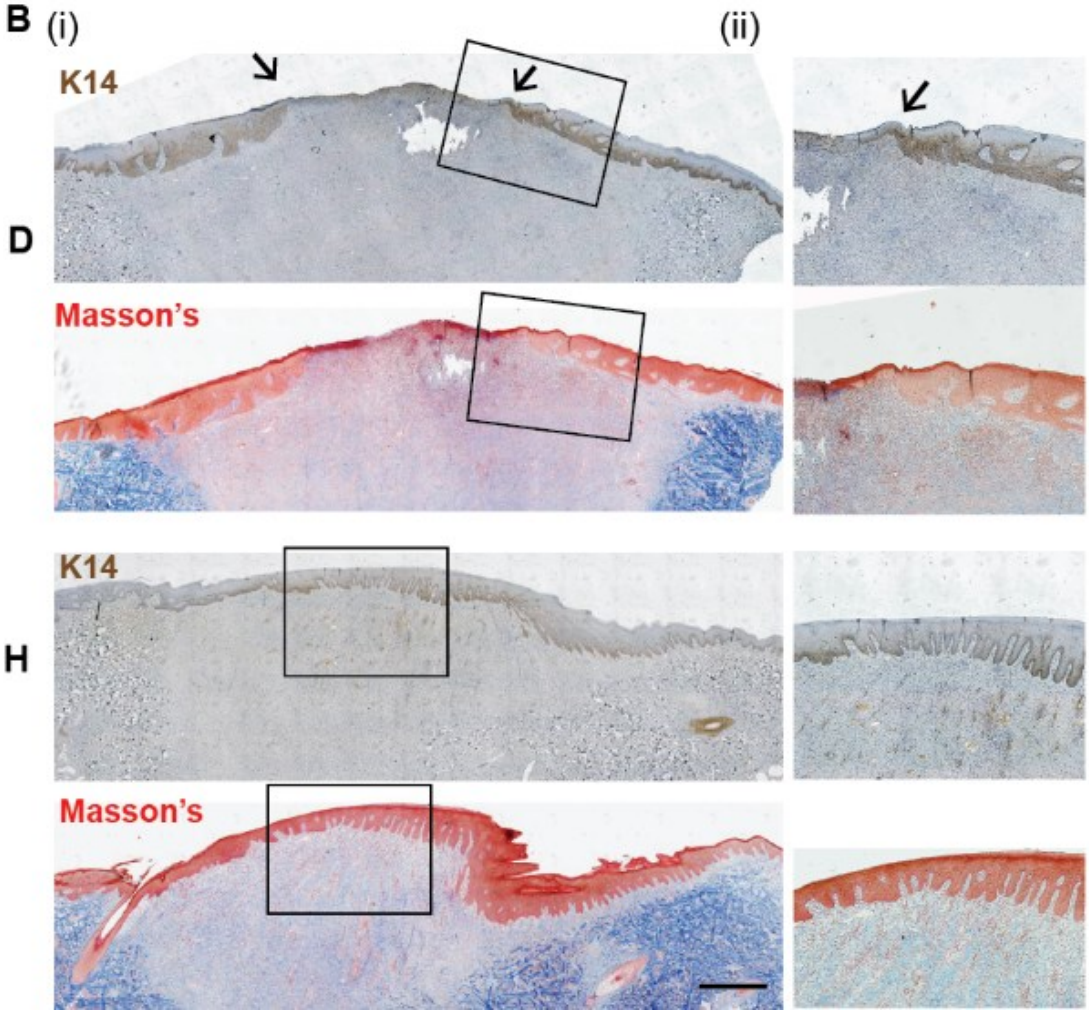
B
(i)
(ii)
K14
D
Masson's
K14
H
Masson's

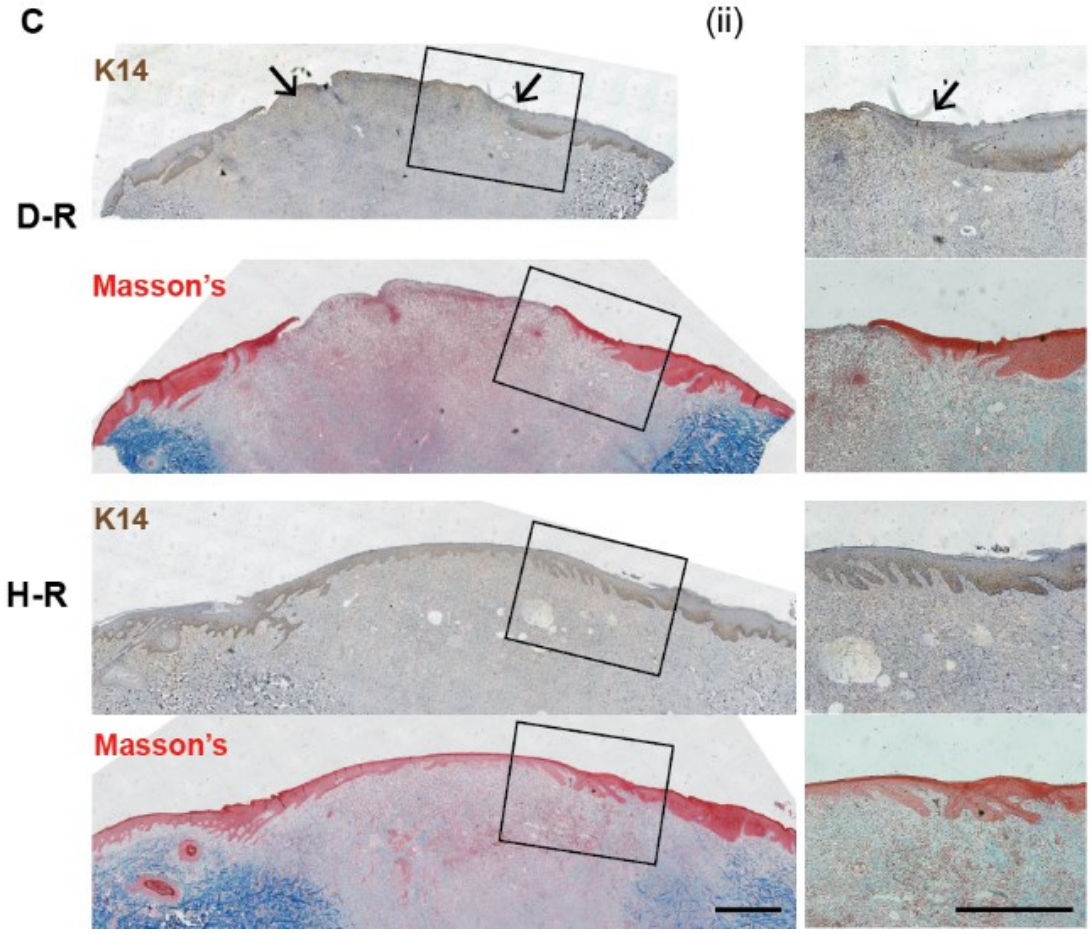

Figure 5-4. Wound closure and re-epithelialization.
(A) Wounds on day 14: (i) representative wound images; (ii) percentage closed wounds gap and (iii) open wound area. D= dressing-only treated wounds; H= hydrogel treated wounds; D-R= dressing retreated wounds; H-R= hydrogel retreated wounds. N=7 for D and H and N=3 for D-R and H-R. (B) Wounds on day 14: (i) representative wound images and (ii) immunohistochemistry for K14 (upper panel; arrows indicate open wound) and masson trichrome stain (lower panel). High magnifications of the boxed areas are shown on the right. D= dressing-only treated wounds; H= hydrogel treated wounds; (C) Wounds on day 14: (i) representative images and (ii) Immunohistochemistry with K14 (upper panel; arrows indicate open wound). High magnifications of the boxed areas are shown on the right. D-R= dressing retreated wounds; H-R= hydrogel retreated wounds. (D) Quantification of (i) rete percentage and (ii) rate density of day 14-treated wound. N=3. D= dressing-only treated wounds; H= hydrogel treated wounds; D-R= dressing retreated wounds; H-R= hydrogel retreated wounds. Scale bars are 1cm in Ai and Bi; 1mm in Aii, Bii and 0.5mm in high magnification inserts. Significance levels were set at *$p<0.05$, **$p<0.01$ and ***$p<0.001$.

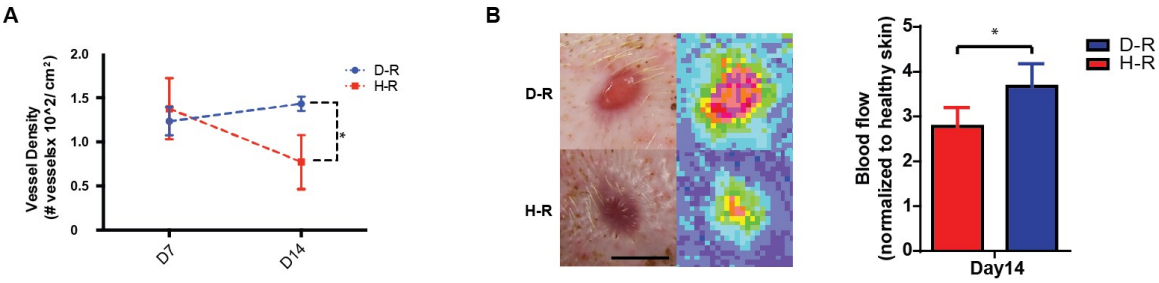

Figure 5-5. Blood vessels following re-treatment.
(A) Quantification of vasculature after re-treatment up to two weeks. (B) Laser speckle contrast images (right) and quantification (left) of blood flow in hydrogel-re-treated wounds and dressing-re-treated wounds on day 14. D-R= dressing only-re-treated wounds; H-R= hydrogel-re-treated wounds. N=3. Significance levels were set at *p<0.05, and **p<0.01.

5.3.4 **Healing kinetics**

To further analyze whether the dextran hydrogel treated wounds heal in a more efficient manner, gene array analysis on days 5,7, and 14 post treatment was performed. In general, we found that there was a higher expression of inflammatory mediators at day 5, suggestive of a stronger inflammatory response for dressing-only treated group, compared to hydrogel treated wounds and which regressed as time progress (Figure 5-6**A**). Notably, expression analysis suggests a persistence of inflammation may be driven by sustained expression of mediators such as chemokine (CCL2) and tumor necrosis factor (TNF) in the dressing treated wounds compared to hydrogel-treated wounds (Figure 5-6**B**). Immunostaining for macrophage marker (MAC387) revealed an abundance of macrophages throughout the granulation tissue at day 5 in the dressing-only treated wounds, which decreased in density on day 7. In contrast, although macrophages were present in dextran hydrogel treated wounds, significantly less macrophages were found in the granulation tissue in both time points (Figure 5-6**C**). In the meantime, hydrogel treatment induced expression of ECM and remodeling genes compared to control (dressing only treated) wounds beginning at day 7

with differences maintained through day 14, suggesting superior granulation tissue formation (replacement of the hydrogel with native matrix and fibroblasts) and more efficient remodeling of this matrix in hydrogel-treated wounds (Figure 5-6**D**). Overall, these results suggest that hydrogels, in comparison to treatment with dressing only, can promote a controlled healing response that is characteristic of a regenerative response including efficient resolution of inflammation, promotion of an ECM rich granulation tissue with accelerated vascular regression and a superior rate of reepithelialization and quality of neoepithelium formed (shown in Figure 5-4).

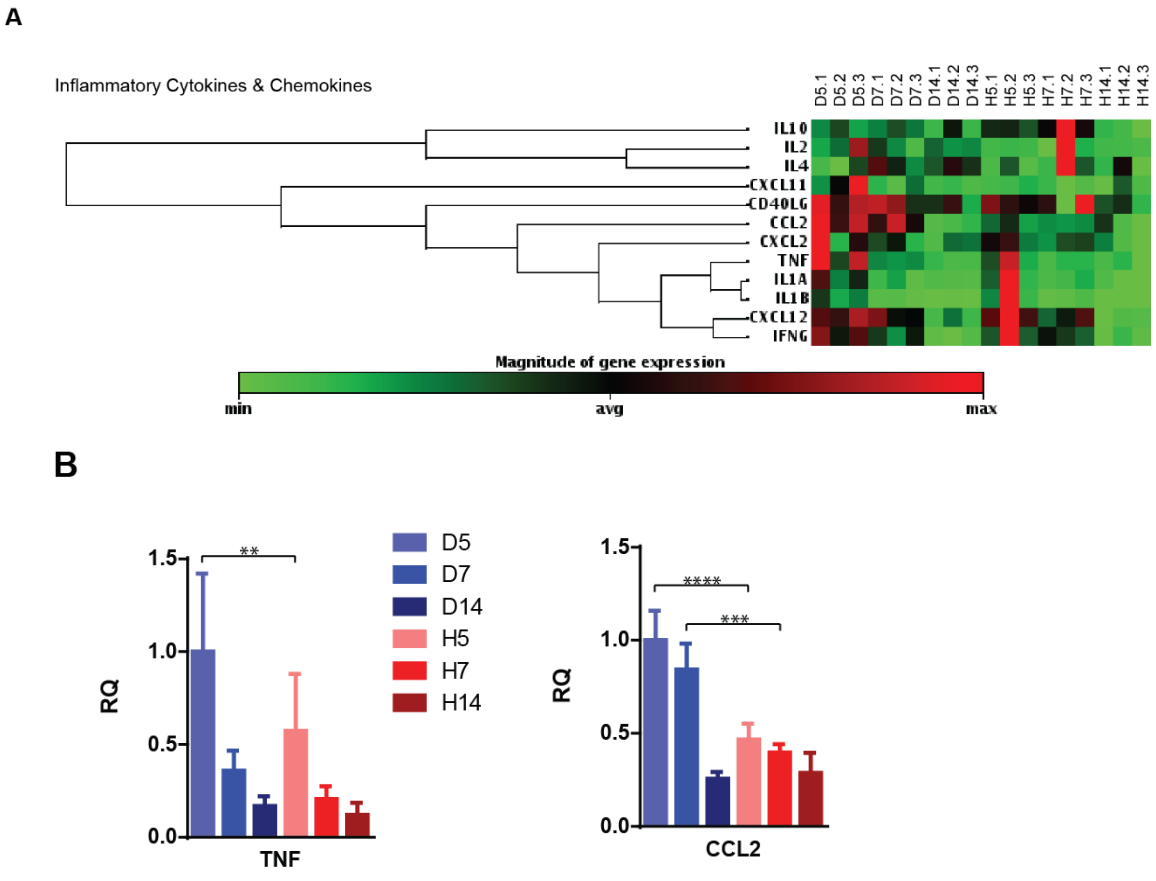

C

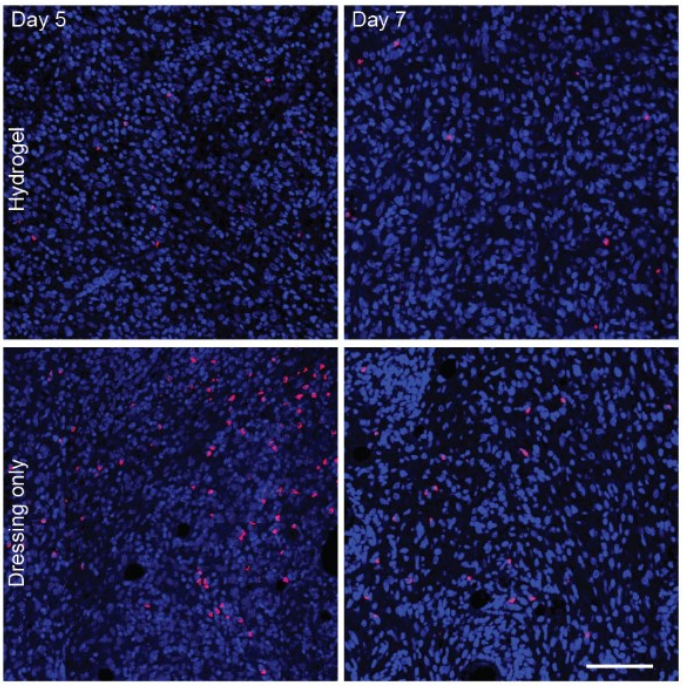
Day 5
Day 7
Hydrogel
Dressing only

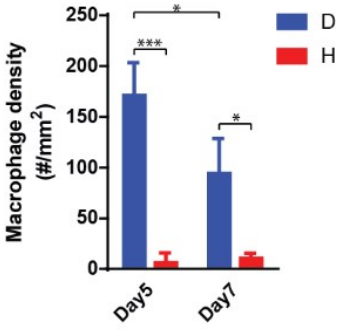
Macrophage density (#/mm2)
250
200
150
100
50
0
*
***
*
D
H
Day5
Day7

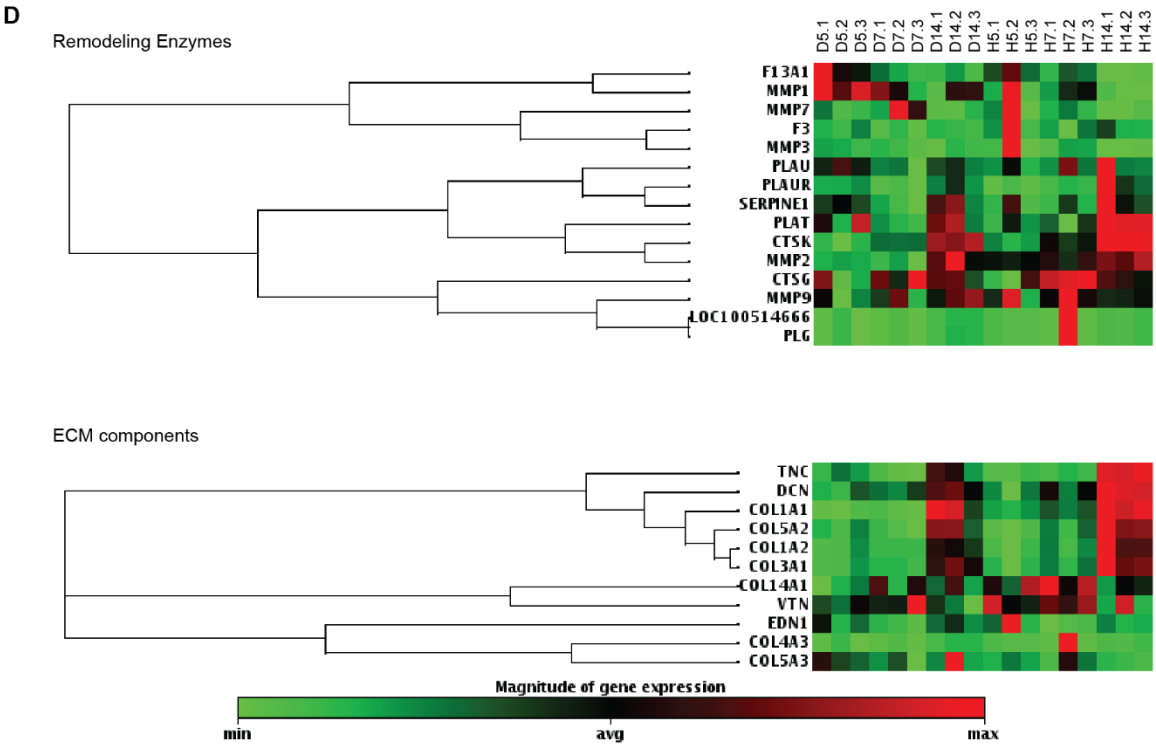

Figure 5-6. Healing kinetics.
(A) Wound healing gene array analysis for inflammatory mediators on day 5,7 and 14. (B) Relative gene expression of TNF and CCL2 of the treatments on day 5,7 and 14. (C) (left panel) Representative images of immunefluorescence stain for macrophage (red; nuclei in blue) and (right panel) quantification of macrophage density in the wound area on days 5 and 7. (D) Wound healing gene array analysis for ECM associated genes on day 5,7 and 14. D= dressing-only treated wounds; H= hydrogel treated wounds. Significance levels were set at *p<0.05, **p<0.01, ***p<0.001, and ****p<0.0001.

5.3.5 **Wound Remodeling and Re-innervation**

So far, we have shown that treatment with the dextran hydrogel enabled the re-epithelialization and wound closure by day 14 accompanied by rapid inflammatory response, angiogenesis and vessel regression. Underneath the reepithelialized wound, further dermal remodeling is needed to achieve complete healing. To further examine the effect of hydrogel treatment on this process, we analyzed dermal ECM protein composition at day 40 post treatment. We found that mature collagen fibers could be observed throughout the neodermis of hydrogel treated wounds, while dressing treated wounds had mature collagen fibers primarily at the periphery of the wounds as evidenced by Masson trichrome staining (Figure 5-7**A** and Figure 5-7**Bi**). Moreover, we found that elastic fibers were present in the periphery of hydrogel-treated wounds but were significantly reduced in dressing treated wounds (Figure 5-7**Ci-ii**), suggesting that hydrogel treated wounds were at a more advanced stage of remodeling compared to dressing treated wounds at the same time.

In addition to significantly increased deposition of collagen and elastin fibers in hydrogel treated wounds compared to controls, gene analysis revealed significant upregulation of KAL1 and Laminin alpha 2 mRNA expression (Figure 5-8**A**). These two genes are associated with neuron guidance [189-191] indicating a potential greater peripheral neuron infiltration. To assess whether dextran hydrogel promote re-innervation of healing burn wounds, the presence of peripheral nerve ingrowth was assessed by immunoflourecence for the neuronal marker protein gene product 9.5. This data shows that while both wound types have nerve fibers present at the edges of the wounds,

peripheral nerve ingrowth to the central portion of the wounds was observed only in the hydrogel-treated wounds but not in the dressing-treated wounds (Figure 5-8**B**).

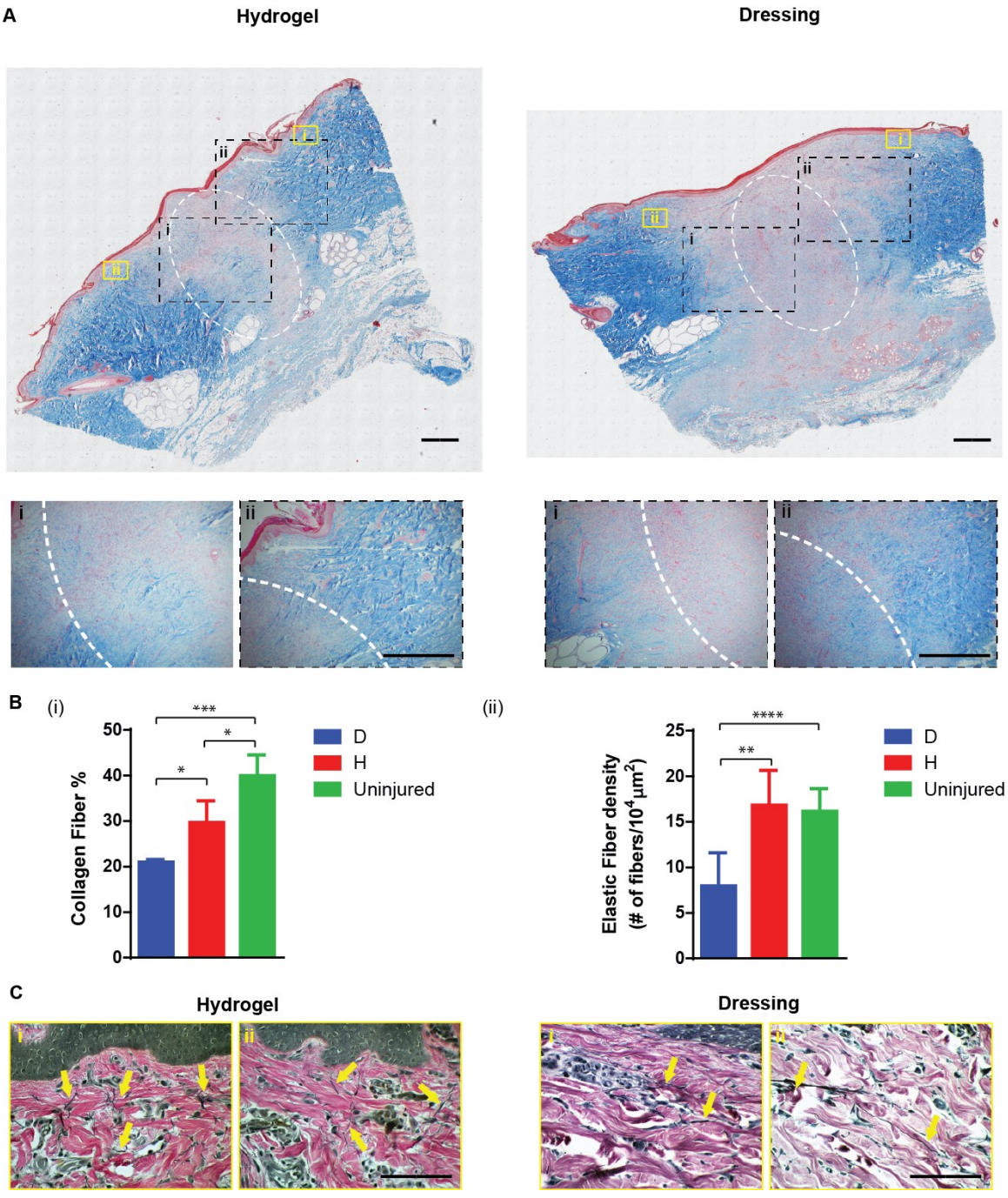

Figure 5-7. Remodeling of third-degree burns.
(A) Representative images of Masson Trichome histological stains of d40 hydrogel treated wounds or dressing-only treated wounds. High magnifications of the boxed areas shown below. (B) (i) Quantification of collagen fiber % in the wounded area (indicated in the white dotted circle in A). (ii) Quantification of elastin fiber density in the dermis area adjacent to the epidermis. N=4 (C) Representative images of Verhoeff–Van Gieson histological stains of d40 hydrogel treated wounds or dressing-only treated wounds. High magnifications of the color-coded boxed areas near the epidermis in A are shown. Yellow boxes are at the wound edge and green boxes are at the middle of the wound. Yellow arrows indicate mature elastin fibers. Significance levels were set at *p<0.05, **p<0.01 and ***p<0.001. Scale bars are 1mm in A and 100μm in C.

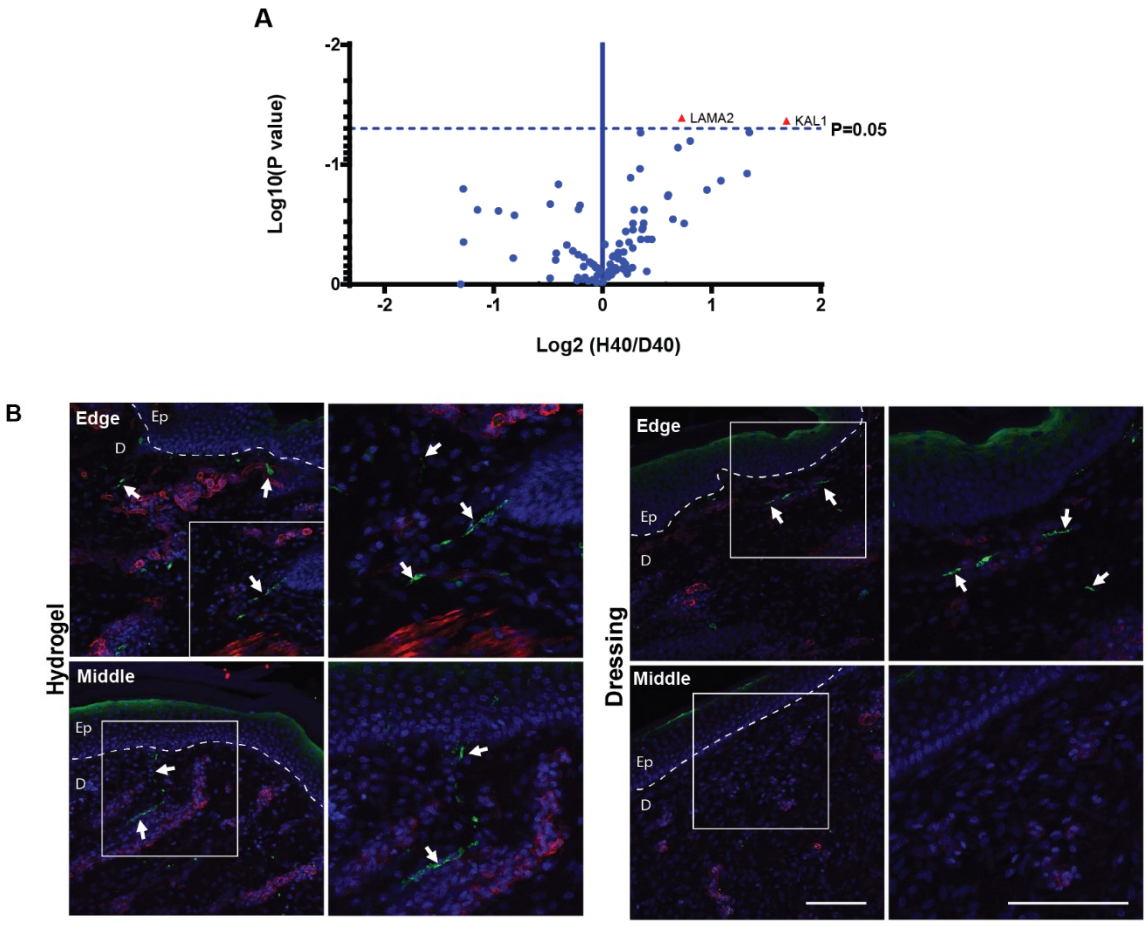

Figure 5-8. Reinnervation of third-degree burns.
(A) Gene array analysis for wound remodeling associated genes of tissue from hydrogel treated wounds versus dressing-only re-treated wounds. (B) Immunoflorescent staining for neuronal fibers (indicated by white arrows) at the edge of the wounds and in the middle of dressing -treated (upper panel) and hydrogel-treated (lower panel) treated wounds. Neurons (PGP9.5) in green, blood vessels (SMA) in red, nuclei (Dapi) in blue). Scale bars are 100μm.

5.4 *Discussion*

Full- or split-thickness skin grafting is the current gold standard for wound closure following severe burn wound injury, but not only do these grafts have a limited availability, they can also leave thick scars and distorted contractures. Given these suboptimal functional, aesthetic and financial outcomes, significant research efforts have focused on developing cell-based skin substitutes, but there are many hurdles for these biological products to attain approval before reaching clinical use. A few synthetic substitutes have made their ways to the market, but most provide only a temporary barrier until autografts are available for permanent closure [192]. To the best of our knowledge, there is no synthetic product currently indicated for treating third-degree burns.

In the current study, we have tested our initial findings which revealed proregenerative properties of dextran-based hydrogel in a murine burn wound model by examining the vulnerary capacity of these hydrogels as a treatment for third-degree burns in pigs towards their potential use in clinical studies. The dextran-based hydrogels have been shown to accelerate wound healing in subcutaneous and burn wounds in murine studies [87] suggesting that they promote a regenerative response post injury. However, the murine cutaneous wound healing model has several known limitations as a translational wound healing model, particularly for burn wound therapies.

We began by establishing a reproducible protocol for creating third-degree burn wounds in adult pigs. In murine studies, a 100°C heat source is sufficient for creating a full-thickness burn wounds, and others have also used this temperature in adult pigs as well to create first- and second- degree burn wounds [187, 188]. However, for third-degree

burns in adult pigs, we found that 200°C provides the sufficient heat for the wounds to progress into a full-thickness dermal damage within 48 hours. This progression of burn injury after the initial heat damage is also seen in human burn patients [193].

We then moved on to optimize the dextran hydrogel treatment procedure by examining the kinetics of the vasculature inside the wounds.. Angiogenesis followed by vessel regression plays a crucial role in wound healing progress [194, 195], but compared to excisional wounds, sever burn wounds exhibit impaired and slower neovascularization, potentially due to delayed mobilization of circulating angiogenic cells [196, 197]. Therefore, we theorized that treatment methods that can facilitate rapid angiogenic response followed by fast vascular regression would be great candidates for wound healing therapies. In order to simulate the clinical settings where the necrotic tissues are either debrided completely or partially, we treated the wounds with the hydrogels after either completely or partially excising the burned skin and tested which method provides better healing results. In terms of treating the wounds with the dextran hydrogels, we found that completely excising the necrotic skin accelerated the infiltration of blood vessels into the treated areas and more profound regression of the neovessels over time, indicating better healing kinetics.

Comparing this treatment method to the dressing-only treated wounds, wound closure was accelerated in dextran-based hydrogel treated wounds, and the healing occurred in a regenerative fashion, characterized by a rapid angiogenic response followed by vascular regression. Furthermore, rapid re-epithelialization and high quality of epithelium formed were present in the dextran-based hydrogel treated wounds compared to control wounds. Even when the healing process was interfered with debridement, additional topical

treatment with the hydrogel allowed fast re-epithelialization, demonstrating the robustness of the hydrogel treatment and its potential in the clinics. The rapid wound closure in the dextran treated burns may be due to combination of factors including the moist environment provided by the hydrogels, which leads to a more efficient re-epithelialization and faster stromal cell migration [198], excellent mechanical properties along with charged functional groups of the dextran hydrogel [85], and the high angiogenic capability of the dextran hydrogel [85-87] result in an overall quicker and better epidermis reconstruction.

The rapid onset and regression of the inflammatory response plays a crucial role in coordinating the process of wound healing [149]. Examining inflammatory signals over time in both hydrogel and dressing-only treated groups, we found higher expression of proinflammatory mediators on day 5 in the dressing treated wounds compared to the hydrogel treated wounds suggesting persistent inflammatory response. While the necessity of inflammatory response in wound healing is debated [199, 200], in the context of biomaterial-induced healing, appropriate timings and durations of acute and chronic inflammatory responses would be needed for better healing results [201]. Gene array analysis on days 5, 7, and 14 revealed lesser inflammatory response in the hydrogel treated group than in the dressing-only treated group. Immunohistochemistry showed high density of macrophages in the dressing treated wounds on day 5, which regressed by day 7. In contrast, only few macrophages in the dextran hydrogel treated wounds could be observed during these time points. Since inflammatory cells, especially macrophages, secrete essential cytokines and growth factors necessary for angiogenesis and stromal cell migration [202], the elevated neovascularization followed by early vascular regression in the hydrogel treated group strongly suggests earlier onset of the inflammatory response.

During wound remodeling stage, the granulation tissue is being remodeled in order to reconstruct the loose regenerated dermis and strengthen the repaired tissue [149]. The severity of scarring depends on the amount and the organization of the secreted ECM during this phase. Therefore, an ideal skin substitute would induce high ECM deposition and organized crosslinking of ECM fibers in order to minimize scarring. Gene array analysis indicated that hydrogel treatment induced the expression of ECM and remodeling genes on days 7 and 14. Indeed, after 40 days of treatment, hydrogel treated healing wounds showed higher density of collagen compared to the dressing-only group, and the structure of the newly deposited collagen observed in the hydrogel treated wounds showed higher organization. In addition, elastin fibers, which is usually poorly restored in scars [203], were deposited in higher density in hydrogel treated wounds. Together with collagen, the regeneration of elastin provides favorable fiber frameworks for the later phase of wound healing [202].

Since the skin is also a highly sensitive organ, after a deep burn injury, cutaneous nerves regenerates from the wound bed with the new nerve fiber migration, or collateral sprouting from the adjacent skin [191]. In fact, burn victims often suffer permanent sensory deficits from abnormal sensation to chronic pain [204-206]. In addition, these deficits are more pronounced following skin graft [207]. As a result, neuron regeneration poses a major challenges in order to improved patients' quality of life by restoring its sensory perceptions of the regenerated skin. We found that dextran hydrogel treatment promoted nerve ingrowth into the regenerated skin with the nerve fibers presents close to the center of the wound on day 40. In contrast, we were unable to locate nerve fiber in the dressing treated wounds. Combining our findings, the hydrogel treatment not only induced ECM

remolding, but also improved the re-innervation of the repaired wound. However, further examination of the nerve fiber will be need to identify which type and maturity of nerve fibers as well as the mechanism of the recruitment. While we examined our samples, we found that these nerve fibers often time co-localized with the blood vessels. We thus speculate that perhaps the enhanced neovascularization during hydrogel treatment as well as more rapid re-epithelialization consequently contributed greater neural ingrowths during the healing progress.

5.5 *Conclusion*

Consistent with our previous murine study, we observed regenerative wound healing induced by the hydrogels in adult pigs. Although there are many similarities between pig and human skins, clinical testing with burn patients is still necessary as some of the physiological differences between the species may affect the healing timeline and also the quality of the healed skin. For example, pig skin is much less prone to infection and contamination compared to human skin [175]. As the wounds infected by the external environment may slow down the healing process and result in serious scar formation, thorough debridement of necrotic tissue is essential to optimal hydrogel response when translating the therapy in a clinical setting. In addition, to reduce infection occurrence, the dextran hydrogels can be embedded with antimicrobial agents, similarly to our previous work with cytokines encapsulation [86].

Our translational study establishes a robust protocol for injury and hydrogel treatment of third-degree burns in a porcine large-animal model and thus paves the way for their use in clinical studies. Encouragingly, treating the burned, full-thickness wound with our dextran-based hydrogel allows functional regeneration of the tissue through fast neovascularization and epithelial wound closure. In addition, the dextran hydrogel promotes more efficient dermis reconstruction and enhanced re-innervation. The absence of drugs or cells may allow our therapy to avoid numerous regulatory hurdles and speed up its translation into the clinics [208, 209]. Overall, our findings support the dextran-based hydrogels as an ideal candidate of next generation of low-cost, off-the-shelf and readily available treatment of a range of dermal injuries, which translates to enhance wound care for patients when skin autograft is neither available nor desirable.

6 *Thesis conclusions and future work*

6.1 *Conclusions*

Angiogenesis is essential during wound healing and also plays critical roles in various diseases. Using biomaterials as an accelular scaffold to study vascular restoration or use it as a scaffold to induce vascular network *in vitro* towards vascularized constructs has provided an alternative approach for wound repair and tissue regeneration. We utilized two types of bioactive hydrogel systems. Dextran is functionalized with amine groups and further crosslinked using UV irradiation with PEGDA for vascular restoration. Hyaluronic hydrogel modified with biding adhesive domain RGD and MMP cleavable sites, are designed to induce vascular network formation *in vitro* from encapsulated human vascular cells. At the same time, the tunability of our hydrogel system provide a valuable tools and allow us to adapt three dimensional (3D) tissue culture models that recapitulate aspects of the tumorogenic *in vivo* microenvironment to study cancer progression *in vitro*.

For example, both hypoxia and matrix stiffness were shown to promote tumor growth. In **Chapter3**, using the HA hydrogel systems and mathematical modeling we found that hypoxic activation of HT1080 cells encapsulated in the 3D HA hydrogel enables better cell survival through autophagy and supports greater EC sprouting with lesser extent in matrix stiffness effects on the cancer cells. Potential uses for this system includes comparing the responses of different cancer cell lines at different stages of tumorigenesis

to external stresses such as inflammatory cytokines, and selectively impeding cancerous processes.

We have also previously engineered this modular HA hydrogel culture system to engineer a functional microvascular network from EPCs, EVCs derived from the hiPSCs that are comprised of VEcad+ and PDGFRβ+ cells (ie endothelial cell and pericytes, respectively.) In **Chapter4**, we first developed an immunodeficient rodent DFU models. We further successfully engineered vascularized constructs by using various vascular cell sources within the HA hydrogel which can be used for transplantation treatment. We show that all vascularized constructs enhances faster wound closures compared to none treated wounds or wounds treated with HA alone. We have demonstrated a potential therapeutic strategy using stem cell derived vascularized scaffold to treat diabetic foot ulcers.

Lastly, we investigated another deep tissue injury model. Burns, a dermal wound affecting millions, often heals as fibrous scar tissue. We have utilized acellular bioactive polysaccharide hydrogels with tunable properties suitable for promoting vascularization and healing in treating full thickness dermal wounds. Dextran polymer is modified with functional ethylamine groups (AE) designed to promote interactions with surrounding host tissue. Burn wounds treated with dextran hydrogels have showed enhanced re-epithelialization, hair follicle recruitment and neovasculargenesis during the healing process in rodent model. In **Chapter5**, we extended our dextran hydrogel treatment in a porcine model for full thickness burn injury. Our translational study establishes a robust protocol for injury and hydrogel treatment of third-degree burns in a porcine large-animal model and at the same time treating the burned, full-thickness wound with dextran-based hydrogel allows functional regeneration of the tissue through fast neovascularization and

epithelial wound closure. In addition, the dextran hydrogel also promotes more efficient dermis reconstruction and enhanced re-innervation.

6.2 *Suggestions for future works*

The work presented in this thesis demonstrates our ability to utilized bioactive hydrogel scaffolds to study microenvironmental effects on vascular diseases and at the same time, engineering vascularized constructs to treat deep tissue injuries. However, further improvement of our systems could allow us to better study the ECs involvement in tumorigenesis as well as engineered a more matured functional vascularized constructs for therapeutic treatment.

For instance, we demonstrated tumor cell angiogenic potential using 2D assay. However, co-cultures of ECs and tumor cells in 3D could provide insights on how these wound interact with each other during tumorigenesis which could provide a robust *in vitro* platform for drug screening. Also, further modification of the polymer would allow us to investigate larger range of elastic modulus and we could scan through a library of cancer cell lines or the same tumorigenic cell source with different metastatic potential investigate the cellular behaviors to gain more insights on potentials therapeutic strategy.

From the regenerative medicine perspective, fostering from the biology advancements, co-cultured of mature cell line such as vascular smooth muscle cell with sequential growth factors release strategy may improve our *in vitro* vascularized constructs. However, one of the drawback of our current systems is that we lack reporter signal for our multipolar stem cell derived EVCs. Developing a reporter signaling strategy could allow us to gain more direct access the interaction between these cell types during

vasculargenesis and further modulate the sequence of events in real time when encapsulated in the constructs *in vitro* in 3D or *in vivo*.

At last, we could also incorporate inflammatory cells such as macrophages since during the course of wound healing, inflammation is followed by onset of angiogenesis and the regression of the inflammatory signals maturation of the recruited blood vessels. It's now accepted that macrophages are bi polar where one promote inflammation and the other signals maturation and stabilization of the blood vessels. By understand how these cells coplay with each other *in vitro* will benefit us to develop a more efficient angiogenesis therapy.

Bibliography

1. Luong, E. and S. Gerecht, *Stem cells and scaffolds for vascularizing engineered tissue constructs.* Adv Biochem Eng Biotechnol, 2009. **114**: p. 129-72.
2. Weinberg, C.B. and E. Bell, *A blood vessel model constructed from collagen and cultured vascular cells.* Science, 1986. **231**(4736): p. 397-400.
3. Mano, J.F., et al., *Natural origin biodegradable systems in tissue engineering and regenerative medicine: present status and some moving trends.* J R Soc Interface, 2007. **4**(17): p. 999-1030.
4. Boesel, L.F.R., R L *Injectable biodegradable systems.*, in *Biodegradable systems in tissue engineering and regenerative medicine*, R.L.R.J.S. Roma´n, Editor. 2004, CRC Press. p. 13-28.
5. Wallace, D.G. and J. Rosenblatt, *Collagen gel systems for sustained delivery and tissue engineering.* Adv Drug Deliv Rev, 2003. **55**(12): p. 1631-49.
6. Taguchi, T., et al., *Encapsulation of chondrocytes in injectable alkali-treated collagen gels prepared using poly(ethylene glycol)-based 4-armed star polymer.* Biomaterials, 2005. **26**(11): p. 1247-52.
7. Marston, W.A., et al., *Initial report of the use of an injectable porcine collagen-derived matrix to stimulate healing of diabetic foot wounds in humans.* Wound Repair Regen, 2005. **13**(3): p. 243-7.
8. Ishibashi, K. and T. Matsuda, *Reconstruction of a hybrid vascular graft hierarchically layered with three cell types.* Asaio J, 1994. **40**(3): p. M284-90.
9. Matsuda, T. and H. Miwa, *A hybrid vascular model biomimicking the hierarchic structure of arterial wall: neointimal stability and neoarterial regeneration process under arterial circulation.* J Thorac Cardiovasc Surg, 1995. **110**(4 Pt 1): p. 988-97.
10. Park, Y.D., N. Tirelli, and J.A. Hubbell, *Photopolymerized hyaluronic acid-based hydrogels and interpenetrating networks.* Biomaterials, 2003. **24**(6): p. 893-900.
11. Burdick, J.A., et al., *Controlled degradation and mechanical behavior of photopolymerized hyaluronic acid networks.* Biomacromolecules, 2005. **6**(1): p. 386-91.
12. Arrigoni, C., et al., *The effect of sodium ascorbate on the mechanical properties of hyaluronan-based vascular constructs.* Biomaterials, 2006. **27**(4): p. 623-30.
13. Slevin, M., S. Kumar, and J. Gaffney, *Angiogenic oligosaccharides of hyaluronan induce multiple signaling pathways affecting vascular endothelial cell mitogenic and wound healing responses.* J Biol Chem, 2002. **277**(43): p. 41046-59.
14. Solchaga, L.A., et al., *Hyaluronan-based polymers in the treatment of osteochondral defects.* J Orthop Res, 2000. **18**(5): p. 773-80.
15. Sahni, A. and C.W. Francis, *Vascular endothelial growth factor binds to fibrinogen and fibrin and stimulates endothelial cell proliferation.* Blood, 2000. **96**(12): p. 3772-8.
16. Hubbell, J.A., *Materials as morphogenetic guides in tissue engineering.* Current Opinion in Biotechnology, 2003. **14**(5): p. 551-558.

17. Fasol, R., Schumacher, B., Schlaudraff, K., Hauesnstein, K.H., and Seitelberger, R., *Experimental use of a modified fibrin glue to induce site-directed angiogenesis from the aorta to the heart.* J Thorac Cardiovasc Surg, 1994. **107**: p. 1432-39.
18. Percival, E.M., R. H., *Methods in plant biochemistry. Carbohydrates*, in *Algal polysaccharides*, P.M. Rey, Editor. 1990, Academic Press. p. 523-547.
19. Gerecht-Nir, S., et al., *Three-dimensional porous alginate scaffolds provide a conducive environment for generation of well-vascularized embryoid bodies from human embryonic stem cells.* Biotechnology and Bioengineering, 2004. **88**(3): p. 313-320.
20. Bouhadir, K.H., et al., *Degradation of partially oxidized alginate and its potential application for tissue engineering.* Biotechnology Progress, 2001. **17**(5): p. 945-950.
21. Awad, H.A., et al., *Chondrogenic differentiation of adipose-derived adult stem cells in agarose, alginate, and gelatin scaffolds.* Biomaterials, 2004. **25**(16): p. 3211-22.
22. Kurita, K., *Controlled functionalization of the polysaccharide chitin.* Progress in Polymer Science, 2001. **26**(9): p. 1921-1971.
23. Erbacher, P., et al., *Chitosan-based vector/DNA complexes for gene delivery: Biophysical characteristics and transfection ability.* Pharmaceutical Research, 1998. **15**(9): p. 1332-1339.
24. Nettles, D.L., S.H. Elder, and J.A. Gilbert, *Potential use of chitosan as a cell scaffold material for cartilage tissue engineering.* Tissue Engineering, 2002. **8**(6): p. 1009-1016.
25. Sun, G., et al., *Functional groups affect physical and biological properties of dextran-based hydrogels.* J Biomed Mater Res A, 2009.
26. Massia, S.P. and J. Stark, *Immobilized RGD peptides on surface-grafted dextran promote biospecific cell attachment.* J Biomed Mater Res, 2001. **56**(3): p. 390-9.
27. Berglund, J.D. and Z.S. Galis, *Designer blood vessels and therapeutic revascularization.* Br J Pharmacol, 2003. **140**(4): p. 627-36.
28. Soucy, P.A. and L.H. Romer, *Endothelial cell adhesion, signaling, and morphogenesis in fibroblast-derived matrix.* Matrix Biol, 2009. **28**(5): p. 273-83.
29. Vlodavsky, I., et al., *Extracellular matrix-resident basic fibroblast growth factor: implication for the control of angiogenesis.* J Cell Biochem, 1991. **45**(2): p. 167-76.
30. Schonherr, E. and H.J. Hausser, *Extracellular matrix and cytokines: a functional unit.* Dev Immunol, 2000. **7**(2-4): p. 89-101.
31. Jay, S.M. and W.M. Saltzman, *Shining light on a new class of hydrogels.* Nat Biotechnol, 2009. **27**(6): p. 543-4.
32. Seal, B.L., T.C. Otero, and A. Panitch, *Polymeric biomaterials for tissue and organ regeneration.* Materials Science & Engineering R-Reports, 2001. **34**(4-5): p. 147-230.
33. Mooney, D.T., et al., *Stabilized polyglycolic acid fibre based tubes for tissue engineering.* Biomaterials, 1996. **17**(2): p. 115-124.
34. Vert, M., S.M. Li, and H. Garreau, *Attempts to Map the Structure and Degradation Characteristics of Aliphatic Polyesters Derived from Lactic and*

Glycolic Acids. Journal of Biomaterials Science-Polymer Edition, 1994. **6**(7): p. 639-649.
35. Kulkarni, R.K., et al., *Biodegradable poly(lactic acid) polymers.* J Biomed Mater Res, 1971. **5**(3): p. 169-81.
36. Levenberg, S., et al., *Differentiation of human embryonic stem cells on three-dimensional polymer scaffolds.* Proc Natl Acad Sci U S A, 2003. **100**(22): p. 12741-6.
37. Zisch, A.H., M.P. Lutolf, and J.A. Hubbell, *Biopolymeric delivery matrices for angiogenic growth factors.* Cardiovasc Pathol, 2003. **12**(6): p. 295-310.
38. Sawhney, A.S., C.P. Pathak, and J.A. Hubbell, *Bioerodible Hydrogels Based on Photopolymerized Poly(Ethylene Glycol)-Co-Poly(Alpha-Hydroxy Acid) Diacrylate Macromers.* Macromolecules, 1993. **26**(4): p. 581-587.
39. Zalipsky, S., *Functionalized Poly(Ethylene Glycol) for Preparation of Biologically Relevant Conjugates.* Bioconjugate Chemistry, 1995. **6**(2): p. 150-165.
40. Elisseeff, J., et al., *Transdermal photopolymerization for minimally invasive implantation.* Proceedings of the National Academy of Sciences of the United States of America, 1999. **96**(6): p. 3104-3107.
41. Moon, J.J., et al., *Biomimetic hydrogels with pro-angiogenic properties.* Biomaterials, 2010. **31**(14): p. 3840-7.
42. Humphries, M.J., et al., *Identification of an Alternatively Spliced Site in Human-Plasma Fibronectin That Mediates Cell Type-Specific Adhesion.* Journal of Cell Biology, 1986. **103**(6): p. 2637-2647.
43. Shin, H., S. Jo, and A.G. Mikos, *Biomimetic materials for tissue engineering.* Biomaterials, 2003. **24**(24): p. 4353-64.
44. Rezania, A., et al., *Bioactivation of metal oxide surfaces. 1. Surface characterization and cell response.* Langmuir, 1999. **15**(20): p. 6931-6939.
45. Wacker, B.K., et al., *Endothelial cell migration on RGD-peptide-containing PEG hydrogels in the presence of sphingosine 1-phosphate.* Biophys J, 2008. **94**(1): p. 273-85.
46. Mann, B.K., R.H. Schmedlen, and J.L. West, *Tethered-TGF-beta increases extracellular matrix production of vascular smooth muscle cells.* Biomaterials, 2001. **22**(5): p. 439-44.
47. Hubbell, J.A., et al., *Endothelial cell-selective materials for tissue engineering in the vascular graft via a new receptor.* Biotechnology (N Y), 1991. **9**(6): p. 568-72.
48. Schense, J.C., et al., *Enzymatic incorporation of bioactive peptides into fibrin matrices enhances neurite extension.* Nature Biotechnology, 2000. **18**(4): p. 415-419.
49. Ranieri, J.P., et al., *Neuronal Cell Attachment to Fluorinated Ethylene-Propylene Films with Covalently Immobilized Laminin Oligopeptides Yigsr and Ikvav .2.* Journal of Biomedical Materials Research, 1995. **29**(6): p. 779-785.
50. Kam, L., et al., *Selective adhesion of astrocytes to surfaces modified with immobilized peptides.* Biomaterials, 2002. **23**(2): p. 511-5.

51. Panitch, A., et al., *Design and biosynthesis of elastin-like artificial extracellular matrix proteins containing periodically spaced fibronectin CS5 domains.* Macromolecules, 1999. **32**(5): p. 1701-1703.
52. Dee, K.C., T.T. Andersen, and R. Bizios, *Design and function of novel osteoblast-adhesive peptides for chemical modification of biomaterials.* J Biomed Mater Res, 1998. **40**(3): p. 371-7.
53. West, J.L. and J.A. Hubbell, *Polymeric biomaterials with degradation sites for proteases involved in cell migration.* Macromolecules, 1999. **32**(1): p. 241-244.
54. Elbert, D.L. and J.A. Hubbell, *Conjugate addition reactions combined with free-radical cross-linking for the design of materials for tissue engineering.* Biomacromolecules, 2001. **2**(2): p. 430-41.
55. Hern, D.L. and J.A. Hubbell, *Incorporation of adhesion peptides into nonadhesive hydrogels useful for tissue resurfacing.* Journal of Biomedical Materials Research, 1998. **39**(2): p. 266-276.
56. Rowley, J.A., G. Madlambayan, and D.J. Mooney, *Alginate hydrogels as synthetic extracellular matrix materials.* Biomaterials, 1999. **20**(1): p. 45-53.
57. Marler, J.J., et al., *Soft-tissue augmentation with injectable alginate and syngeneic fibroblasts.* Plastic and Reconstructive Surgery, 2000. **105**(6): p. 2049-2058.
58. Engler, A.J., et al., *Microtissue elasticity: Measurements by atomic force microscopy and its influence on cell differentiation.* Cell Mechanics, 2007. **83**: p. 521-+.
59. Niklason, L.E., et al., *Functional arteries grown in vitro.* Science, 1999. **284**(5413): p. 489-93.
60. Smith, D.H., J.A. Wolf, and D.F. Meaney, *A new strategy to produce sustained growth of central nervous system axons: continuous mechanical tension.* Tissue Engineering, 2001. **7**(2): p. 131-9.
61. Kloxin, A.M., et al., *Photodegradable hydrogels for dynamic tuning of physical and chemical properties.* Science, 2009. **324**(5923): p. 59-63.
62. Critser, P.J., et al., *Collagen matrix physical properties modulate endothelial colony forming cell-derived vessels in vivo.* Microvasc Res. **80**(1): p. 23-30.
63. Tabata, Y., *Biomaterial technology for tissue engineering applications.* J R Soc Interface, 2009. **6 Suppl 3**: p. S311-24.
64. Slack, J.M., *Stem cells in epithelial tissues.* Science, 2000. **287**(5457): p. 1431-3.
65. Asahara, T., et al., *Isolation of putative progenitor endothelial cells for angiogenesis.* Science, 1997. **275**(5302): p. 964-967.
66. Dimmeler, S. and M. Vasa-Nicotera, *Aging of progenitor cells: limitation for regenerative capacity?* J Am Coll Cardiol, 2003. **42**(12): p. 2081-2.
67. Yamanaka, S., *Strategies and new developments in the generation of patient-specific pluripotent stem cells.* Cell Stem Cell, 2007. **1**(1): p. 39-49.
68. Yu, J., et al., *Human induced pluripotent stem cells free of vector and transgene sequences.* Science, 2009. **324**(5928): p. 797-801.
69. Nelson, T.J., et al., *Repair of acute myocardial infarction by human stemness factors induced pluripotent stem cells.* Circulation, 2009. **120**(5): p. 408-16.
70. Taura, D., et al., *Induction and isolation of vascular cells from human induced pluripotent stem cells--brief report.* Arterioscler Thromb Vasc Biol, 2009. **29**(7): p. 1100-3.

71. Sachlos, E. and J.T. Czernuszka, *Making tissue engineering scaffolds work. Review: the application of solid freeform fabrication technology to the production of tissue engineering scaffolds.* Eur Cell Mater, 2003. **5**: p. 29-39; discussion 39-40.
72. Botchwey, E.A., et al., *Tissue engineered bone: measurement of nutrient transport in three-dimensional matrices.* J Biomed Mater Res A, 2003. **67**(1): p. 357-67.
73. Ferreira, L.S., et al., *Bioactive hydrogel scaffolds for controllable vascular differentiation of human embryonic stem cells.* Biomaterials, 2007. **28**(17): p. 2706-17.
74. Gerecht, S., et al., *Hyaluronic acid hydrogel for controlled self-renewal and differentiation of human embryonic stem cells.* Proc Natl Acad Sci U S A, 2007. **104**(27): p. 11298-303.
75. Gerecht-Nir, S., et al., *Three-dimensional porous alginate scaffolds provide a conducive environment for generation of well-vascularized embryoid bodies from human embryonic stem cells.* Biotechnol Bioeng, 2004. **88**(3): p. 313-20.
76. Levenberg, S., et al., *Endothelial cells derived from human embryonic stem cells.* Proc Natl Acad Sci U S A, 2002. **99**(7): p. 4391-6.
77. Au, P., et al., *Differential in vivo potential of endothelial progenitor cells from human umbilical cord blood and adult peripheral blood to form functional long-lasting vessels.* Blood, 2007.
78. van Weel, V., et al., *Vascular growth in ischemic limbs: a review of mechanisms and possible therapeutic stimulation.* Ann Vasc Surg, 2008. **22**(4): p. 582-97.
79. Peattie, R.A., et al., *Stimulation of in vivo angiogenesis by cytokine-loaded hyaluronic acid hydrogel implants.* Biomaterials, 2004. **25**(14): p. 2789-98.
80. Ehrbar, M., et al., *Endothelial cell proliferation and progenitor maturation by fibrin-bound VEGF variants with differential susceptibilities to local cellular activity.* J Control Release, 2005. **101**(1-3): p. 93-109.
81. Koch, S., et al., *Enhancing angiogenesis in collagen matrices by covalent incorporation of VEGF.* Journal of Materials Science-Materials in Medicine, 2006. **17**(8): p. 735-741.
82. Hanjaya-Putra, D., et al., *Controlled activation of morphogenesis to generate a functional human microvasculature in a synthetic matrix.* Blood, 2011. **118**(3): p. 804-15.
83. Khetan, S. and J. Burdick, *Cellular encapsulation in 3D hydrogels for tissue engineering.* J Vis Exp, 2009(32).
84. Khetan, S., C. Chung, and J.A. Burdick, *Tuning hydrogel properties for applications in tissue engineering.* Conf Proc IEEE Eng Med Biol Soc, 2009. **2009**: p. 2094-6.
85. Sun, G., et al., *Functional groups affect physical and biological properties of dextran-based hydrogels.* J Biomed Mater Res A, 2010. **93**(3): p. 1080-90.
86. Sun, G., et al., *Functional neovascularization of biodegradable dextran hydrogels with multiple angiogenic growth factors.* Biomaterials, 2011. **32**(1): p. 95-106.
87. Sun, G., et al., *Dextran hydrogel scaffolds enhance angiogenic responses and promote complete skin regeneration during burn wound healing.* Proc Natl Acad Sci U S A, 2011. **108**(52): p. 20976-81.

88. Hanjaya-Putra, D., et al., *Spatial control of cell-mediated degradation to regulate vasculogenesis and angiogenesis in hyaluronan hydrogels.* Biomaterials, 2012. **33**(26): p. 6123-31.
89. Kusuma, S., et al., *Self-organized vascular networks from human pluripotent stem cells in a synthetic matrix.* Proc Natl Acad Sci U S A, 2013. **110**(31): p. 12601-6.
90. Chan, X., et al., *Generation and network assembly of endothelial cells and pericytes from diabetic patient-derived induced pluripotent stem cells*.
91. Hanjaya-Putra, D., et al., *Integration and regression of implanted engineered human vascular networks during deep wound healing.* Stem Cells Transl Med, 2013. **2**(4): p. 297-306.
92. Brosius, F.C., 3rd, et al., *Mouse models of diabetic nephropathy.* J Am Soc Nephrol, 2009. **20**(12): p. 2503-12.
93. Alpers, C.E. and K.L. Hudkins, *Mouse models of diabetic nephropathy.* Curr Opin Nephrol Hypertens, 2011. **20**(3): p. 278-84.
94. Breyer, M.D., et al., *Mouse models of diabetic nephropathy.* J Am Soc Nephrol, 2005. **16**(1): p. 27-45.
95. Dunn, L., et al., *Murine model of wound healing.* J Vis Exp, 2013(75): p. e50265.
96. Duscher, D., et al., *Transdermal deferoxamine prevents pressure-induced diabetic ulcers.* Proc Natl Acad Sci U S A, 2014.
97. Martinez-Santamaria, L., et al., *The regenerative potential of fibroblasts in a new diabetes-induced delayed humanised wound healing model.* Exp Dermatol, 2013. **22**(3): p. 195-201.
98. Wu, K.K. and Y. Huan, *Streptozotocin-induced diabetic models in mice and rats.* Curr Protoc Pharmacol, 2008. **Chapter 5**: p. Unit 5 47.
99. Kiwanuka, E., et al., *Comparison of healing parameters in porcine full-thickness wounds transplanted with skin micrografts, split-thickness skin grafts, and cultured keratinocytes.* Journal of the American College of Surgeons, 2011. **213**(6): p. 728-735.
100. Gurski, L.A., et al., *Hyaluronic acid-based hydrogels as 3D matrices for in vitro evaluation of chemotherapeutic drugs using poorly adherent prostate cancer cells (vol 30, pg 6076, 2009).* Biomaterials, 2010. **31**(14): p. 4248-4248.
101. Szot, C.S., et al., *3D in vitro bioengineered tumors based on collagen I hydrogels.* Biomaterials, 2011. **32**(31): p. 7905-12.
102. Yamada, K.M. and E. Cukierman, *Modeling tissue morphogenesis and cancer in 3D.* Cell, 2007. **130**(4): p. 601-610.
103. Nyga, A., U. Cheema, and M. Loizidou, *3D tumour models: novel in vitro approaches to cancer studies.* J Cell Commun Signal, 2011. **5**(3): p. 239-48.
104. Hielscher, A.C. and S. Gerecht, *Engineering approaches for investigating tumor angiogenesis: exploiting the role of the extracellular matrix.* Cancer Res, 2012. **72**(23): p. 6089-96.
105. Discher, D.E., P. Janmey, and Y.-l. Wang, *Tissue Cells Feel and Respond to the Stiffness of Their Substrate.* Science, 2005. **310**(5751): p. 1139-1143.
106. Engler, A.J., et al., *Matrix elasticity directs stem cell lineage specification.* Cell, 2006. **126**(4): p. 677-89.
107. Ghosh, K., et al., *Cell adaptation to a physiologically relevant ECM mimic with different viscoelastic properties.* Biomaterials, 2007. **28**(4): p. 671-679.

108. Verbridge, S.S., E.M. Chandler, and C. Fischbach, *Tissue-engineered three-dimensional tumor models to study tumor angiogenesis.* Tissue Eng Part A, 2010. **16**(7): p. 2147-52.
109. Fischbach, C., et al., *Engineering tumors with 3D scaffolds.* Nat Methods, 2007. **4**(10): p. 855-60.
110. Gill, B.J., et al., *A synthetic matrix with independently tunable biochemistry and mechanical properties to study epithelial morphogenesis and EMT in a lung adenocarcinoma model.* Cancer Res, 2012. **72**(22): p. 6013-23.
111. Pathak, A. and S. Kumar, *Independent regulation of tumor cell migration by matrix stiffness and confinement.* Proc Natl Acad Sci U S A, 2012. **109**(26): p. 10334-9.
112. Schrader, J., et al., *Matrix stiffness modulates proliferation, chemotherapeutic response, and dormancy in hepatocellular carcinoma cells.* Hepatology, 2011. **53**(4): p. 1192-205.
113. Hanjaya-Putra, D., et al., *Vascular endothelial growth factor and substrate mechanics regulate in vitro tubulogenesis of endothelial progenitor cells.* J Cell Mol Med, 2010. **14**(10): p. 2436-47.
114. Sieminski, A.L., R.P. Hebbel, and K.J. Gooch, *The relative magnitudes of endothelial force generation and matrix stiffness modulate capillary morphogenesis in vitro.* Exp Cell Res, 2004. **297**(2): p. 574-84.
115. Gordan, J.D. and M.C. Simon, *Hypoxia-inducible factors: central regulators of the tumor phenotype.* Curr Opin Genet Dev, 2007. **17**(1): p. 71-7.
116. Wang, G.L. and G.L. Semenza, *Purification and characterization of hypoxia-inducible factor 1.* J Biol Chem, 1995. **270**(3): p. 1230-7.
117. Heddleston, J.M., et al., *Hypoxia inducible factors in cancer stem cells.* Br J Cancer, 2010. **102**(5): p. 789-95.
118. Manalo, D.J., et al., *Transcriptional regulation of vascular endothelial cell responses to hypoxia by HIF-1.* Blood, 2005. **105**(2): p. 659-69.
119. Ramirez-Bergeron, D.L. and M.C. Simon, *Hypoxia-inducible factor and the development of stem cells of the cardiovascular system.* Stem Cells, 2001. **19**(4): p. 279-86.
120. Maltepe, E. and M.C. Simon, *Oxygen, genes, and development: an analysis of the role of hypoxic gene regulation during murine vascular development.* J Mol Med, 1998. **76**(6): p. 391-401.
121. Fong, G.H., *Regulation of angiogenesis by oxygen sensing mechanisms.* J Mol Med, 2009. **87**(6): p. 549-60.
122. Yamakawa, M., et al., *Hypoxia-inducible factor-1 mediates activation of cultured vascular endothelial cells by inducing multiple angiogenic factors.* Circ Res, 2003. **93**(7): p. 664-73.
123. Simon, M.C. and B. Keith, *The role of oxygen availability in embryonic development and stem cell function.* Nat Rev Mol Cell Biol, 2008. **9**(4): p. 285-96.
124. Jopling, C., et al., *Hypoxia induces myocardial regeneration in zebrafish.* Circulation, 2012. **126**(25): p. 3017-27.
125. Khetan, S., J.S. Katz, and J.A. Burdick, *Sequential crosslinking to control cellular spreading in 3-dimensional hydrogels.* Soft Matter, 2009. **5**(8): p. 1601-1606.

126. Abaci, H.E., et al., *Unforeseen decreases in dissolved oxygen levels affect tube formation kinetics in collagen gels.* Am J Physiol Cell Physiol, 2011. **301**(2): p. C431-40.
127. Abaci, H.E., et al., *Unforeseen decreases in dissolved oxygen levels affect tube formation kinetics in collagen gels.* American Journal of Physiology-Cell Physiology, 2011. **301**(2): p. C431-C440.
128. Bayless, K.J., H.I. Kwak, and S.C. Su, *Investigating endothelial invasion and sprouting behavior in three-dimensional collagen matrices.* Nature Protocols, 2009. **4**(12): p. 1888-1898.
129. Dickinson, L.E., et al., *Functional surfaces for high-resolution analysis of cancer cell interactions on exogenous hyaluronic acid.* Biomaterials, 2010. **31**(20): p. 5472-5478.
130. Bancroft, L.W., et al., *Soft tissue tumors of the lower extremities.* Radiol Clin North Am, 2002. **40**(5): p. 991-1011.
131. Al-Mehdi, A.B., et al., *Intravascular origin of metastasis from the proliferation of endothelium-attached tumor cells: a new model for metastasis.* Nat Med, 2000. **6**(1): p. 100-2.
132. Krouskop, T.A., et al., *Elastic moduli of breast and prostate tissues under compression.* Ultrason Imaging, 1998. **20**(4): p. 260-74.
133. Abaci, H.E., et al., *Adaptation to oxygen deprivation in cultures of human pluripotent stem cells, endothelial progenitor cells, and umbilical vein endothelial cells.* Am J Physiol Cell Physiol, 2010. **298**(6): p. C1527-37.
134. Abaci, H.E., et al., *Adaptation to oxygen deprivation in cultures of human pluripotent stem cells, endothelial progenitor cells, and umbilical vein endothelial cells.* Am J Physiol Cell Physiol. **298**(6): p. C1527-37.
135. Abaci, H.E., et al., *Unforeseen decreases in dissolved oxygen levels affect tube formation kinetics in collagen gels.* Am J Physiol Cell Physiol. **301**(2): p. C431-40.
136. Joyce, J.A. and J.W. Pollard, *Microenvironmental regulation of metastasis.* Nat Rev Cancer, 2009. **9**(4): p. 239-52.
137. Chambers, A.F., A.C. Groom, and I.C. MacDonald, *Dissemination and growth of cancer cells in metastatic sites.* Nature Reviews Cancer, 2002. **2**(8): p. 563-572.
138. Holmgren, L., M.S. O'Reilly, and J. Folkman, *Dormancy of micrometastases: balanced proliferation and apoptosis in the presence of angiogenesis suppression.* Nat Med, 1995. **1**(2): p. 149-53.
139. Zhang, H., et al., *Mitochondrial autophagy is an HIF-1-dependent adaptive metabolic response to hypoxia.* J Biol Chem, 2008. **283**(16): p. 10892-903.
140. Davis, G.E., W. Kon, and A.N. Stratman, *Mechanisms controlling human endothelial lumen formation and tube assembly in three-dimensional extracellular matrices.* Birth Defects Research Part C - Embryo Today: Reviews, 2007. **81**(4): p. 270-285.
141. Bayless, K.J., H.-I. Kwak, and S.-C. Su, *Investigating endothelial invasion and sprouting behavior in three-dimensional collagen matrices.* Nat. Protocols, 2009. **4**(12): p. 1888-1898.

142. Hanjaya-Putra, D., Wong, K., Hirotsu, K., Khetan, S., Burdick, J.A., Gerecht, S., *Spatial control of cell-mediated degradation to regulate vasculogenesis and angiogenesis in synthetic hydrogels.* Submitted, 2012.
143. Yee, D., et al., *Hyaluronic Acid hydrogels support cord-like structures from endothelial colony-forming cells.* Tissue Eng Part A, 2011. **17**(9-10): p. 1351-61.
144. Hanjaya-Putra, D., et al., *Vascular endothelial growth factor and substrate mechanics regulate in vitro tubulogenesis of endothelial progenitor cells.* J Cell Mol Med, 2009.
145. Hanjaya-Putra, D., et al., *Vascular endothelial growth factor and substrate mechanics regulate in vitro tubulogenesis of endothelial progenitor cells.* Journal of Cellular and Molecular Medicine, 2010. **14**(10): p. 2436-47.
146. Bayless, K.J., R. Salazar, and G.E. Davis, *RGD-dependent vacuolation and lumen formation observed during endothelial cell morphogenesis in three-dimensional fibrin matrices involves the alpha(v)beta(3) and alpha(5)beta(1) integrins.* Am J Pathol, 2000. **156**(5): p. 1673-83.
147. Nagahashi, M., et al., *Sphingosine-1-phosphate produced by sphingosine kinase 1 promotes breast cancer progression by stimulating angiogenesis and lymphangiogenesis.* Cancer Res, 2012. **72**(3): p. 726-35.
148. Shen, Y.I., et al., *Hyaluronic acid hydrogel stiffness and oxygen tension affect cancer cell fate and endothelial sprouting.* Biomater Sci, 2014. **2**(5): p. 655-665.
149. Gurtner, G.C., et al., *Wound repair and regeneration.* Nature, 2008. **453**(7193): p. 314-21.
150. Bannon, P., et al., *Diabetes induces stable intrinsic changes to myeloid cells that contribute to chronic inflammation during wound healing in mice.* Dis Model Mech, 2013. **6**(6): p. 1434-47.
151. Andrews, K.L., M.T. Houdek, and L.J. Kiemele, *Wound management of chronic diabetic foot ulcers: From the basics to regenerative medicine.* Prosthet Orthot Int, 2015. **39**(1): p. 29-39.
152. Falanga, V., *Wound healing and its impairment in the diabetic foot.* Lancet, 2005. **366**(9498): p. 1736-43.
153. Chao, C.Y. and G.L. Cheing, *Microvascular dysfunction in diabetic foot disease and ulceration.* Diabetes Metab Res Rev, 2009. **25**(7): p. 604-14.
154. Callaghan, B.C., et al., *Diabetic neuropathy: clinical manifestations and current treatments.* Lancet Neurol, 2012. **11**(6): p. 521-34.
155. American Diabetes, A., *Economic costs of diabetes in the U.S. in 2012.* Diabetes Care, 2013. **36**(4): p. 1033-46.
156. Ferreira, L.S., et al., *Vascular progenitor cells isolated from human embryonic stem cells give rise to endothelial and smooth muscle like cells and form vascular networks in vivo.* Circ Res, 2007. **101**(3): p. 286-94.
157. Levenberg, S., et al., *Engineering vascularized skeletal muscle tissue.* Nat Biotechnol, 2005. **23**(7): p. 879-84.
158. Wang, Z.Z., et al., *Endothelial cells derived from human embryonic stem cells form durable blood vessels in vivo.* Nature Biotechnology, 2007. **25**(3): p. 317-318.

159. Melero-Martin, J.M., et al., *Engineering robust and functional vascular networks in vivo with human adult and cord blood-derived progenitor cells.* Circulation Research, 2008. **103**(2): p. 194-202.
160. Critser, P.J., et al., *Collagen matrix physical properties modulate endothelial colony forming cell-derived vessels in vivo.* Microvascular Research, 2010. **80**(1): p. 23-30.
161. Kang, K.-T., P. Allen, and J. Bischoff, *Bioengineered human vascular networks transplanted into secondary mice reconnect with the host vasculature and re-establish perfusion.* Blood, 2011. **118**(25): p. 6718-6721.
162. Au, P., et al., *Bone marrow derived mesenchymal stem cells facilitate engineering of long-lasting functional vasculature.* Blood, 2008. **111**(9): p. 4551-4558.
163. Marrotte, E.J., et al., *Manganese superoxide dismutase expression in endothelial progenitor cells accelerates wound healing in diabetic mice.* J Clin Invest, 2010. **120**(12): p. 4207-19.
164. Tellechea, A., et al., *Increased skin inflammation and blood vessel density in human and experimental diabetes.* Int J Low Extrem Wounds, 2013. **12**(1): p. 4-11.
165. Cho, H., et al., *Regulation of endothelial cell activation and angiogenesis by injectable peptide nanofibers.* Acta Biomater, 2012. **8**(1): p. 154-64.
166. Hurley, J.R., et al., *Nanofiber Microenvironment Effectively Restores Angiogenic Potential of Diabetic Endothelial Cells.* Adv Wound Care (New Rochelle), 2014. **3**(11): p. 717-728.
167. Sherratt, J.A. and J.D. Murray, *Models of epidermal wound healing.* Proc Biol Sci, 1990. **241**(1300): p. 29-36.
168. Tabatabai, M.A., W.M. Eby, and K.P. Singh, *Hyperbolastic modeling of wound healing.* Mathematical and Computer Modelling, 2011. **53**(5-6): p. 755-768.
169. Cukjati, D., et al., *Modelling of chronic wound healing dynamics.* Med Biol Eng Comput, 2000. **38**(3): p. 339-47.
170. Fusi, L., *Macroscopic models for fibroproliferative disorders: A review.* Mathematical and Computer Modelling, 2009. **50**(9–10): p. 1474-1494.
171. Graham, M.L., et al., *The Streptozotocin-Induced Diabetic Nude Mouse Model: Differences between Animals from Different Sources.* Comparative Medicine, 2011. **61**(4): p. 356-360.
172. Galiano, R.D., et al., *Quantitative and reproducible murine model of excisional wound healing.* Wound Repair Regen, 2004. **12**(4): p. 485-92.
173. Wang, X., et al., *The mouse excisional wound splinting model, including applications for stem cell transplantation.* Nat Protoc, 2013. **8**(2): p. 302-9.
174. Fang, R.C., et al., *Limitations of the db/db mouse in translational wound healing research: Is the NONcNZO10 polygenic mouse model superior?* Wound Repair Regen, 2010. **18**(6): p. 605-13.
175. Singer, A.J. and S.A. McClain, *A Porcine Burn Model*, in *Wound Healing: Methods and Protocols*. 2003. p. 107-119.
176. *National Burn Repository Annual Report 2014*. 2014: American Burn Association.
177. Hop, M.J., et al., *Costs of burn care: A systematic review.* Wound Repair Regen, 2014. **22**(4): p. 436-50.

178. Stoddard, F.J., Jr., C.M. Ryan, and J.C. Schneider, *Physical and Psychiatric Recovery from Burns.* Surg Clin North Am, 2014. **94**(4): p. 863-878.
179. Sheridan, R.L., *Burns : a practical approach to immediate treatment and long-term care*. 2012, Manson Publishing: London :.
180. Seok, J., et al., *Genomic responses in mouse models poorly mimic human inflammatory diseases.* Proc Natl Acad Sci U S A, 2013. **110**(9): p. 3507-12.
181. Sullivan, T.P., et al., *The pig as a model for human wound healing.* Wound repair and regeneration, 2001. **9**(2): p. 66-76.
182. Zhu, K.Q., et al., *Review of the female Duroc/Yorkshire pig model of human fibroproliferative scarring.* Wound Repair Regen, 2007. **15 Suppl 1**: p. S32-9.
183. Middelkoop, E., et al., *Porcine wound models for skin substitution and burn treatment.* Biomaterials, 2004. **25**(9): p. 1559-1567.
184. Branski, L.K., et al., *A porcine model of full-thickness burn, excision and skin autografting.* Burns, 2008. **34**(8): p. 1119-27.
185. Falabella, A., *Wound Healing*, R. Kirsner, Editor. 2013, Taylor and Francis: Hoboken :.
186. Robson, M.C., *Physiological Responses to Burning Injury.* JAMA, 1983. **249**(23): p. 3252-3252.
187. Papp, A., et al., *The progression of burn depth in experimental burns: a histological and methodological study.* Burns, 2004. **30**(7): p. 684-690.
188. Gaines, C., et al., *Development of a porcine deep partial thickness burn model.* Burns, 2013. **39**(2): p. 311-9.
189. Tengara, S., et al., *Keratinocyte-derived anosmin-1, an extracellular glycoprotein encoded by the X-linked Kallmann syndrome gene, is involved in modulation of epidermal nerve density in atopic dermatitis.* J Dermatol Sci, 2010. **58**(1): p. 64-71.
190. Blais, M., M. Grenier, and F. Berthod, *Improvement of nerve regeneration in tissue-engineered skin enriched with schwann cells.* J Invest Dermatol, 2009. **129**(12): p. 2895-900.
191. Blais, M., et al., *Concise review: tissue-engineered skin and nerve regeneration in burn treatment.* Stem Cells Transl Med, 2013. **2**(7): p. 545-51.
192. Supp, D.M., *Skin substitutes for burn wound healing: current and future approaches.* 2011.
193. Nanney, L.B., B.A. Wenczak, and J.B. Lynch, *Progressive burn injury documented with vimentin immunostaining.* Journal of Burn Care & Research, 1996. **17**(3): p. 191-198.
194. DiPietro, L.A., *Angiogenesis and scar formation in healing wounds.* Current opinion in rheumatology, 2013. **25**(1): p. 87-91.
195. Hanjaya-Putra, D., et al., *Integration and Regression of Implanted Engineered Human Vascular Networks During Deep Wound Healing.* Stem cells translational medicine, 2013. **2**(4): p. 297-306.
196. Zhang, X., et al., *Association of increasing burn severity in mice with delayed mobilization of circulating angiogenic cells.* Archives of Surgery, 2010. **145**(3): p. 259-266.
197. Guo, R., et al., *Comparison studies of the in vivo treatment of full‐thickness excisional wounds and burns by an artificial bilayer dermal equivalent and J‐1*

acellular dermal matrix. Wound Repair and Regeneration, 2014. **22**(3): p. 390-398.
198. Boateng, J.S., et al., *Wound healing dressings and drug delivery systems: a review.* Journal of pharmaceutical sciences, 2008. **97**(8): p. 2892-2923.
199. Ashcroft, G.S., et al., *Mice lacking Smad3 show accelerated wound healing and an impaired local inflammatory response.* Nat Cell Biol, 1999. **1**(5): p. 260-6.
200. Martin, P., et al., *Wound healing in the PU.1 null mouse--tissue repair is not dependent on inflammatory cells.* Curr Biol, 2003. **13**(13): p. 1122-8.
201. Koh, T.J. and L.A. DiPietro, *Inflammation and wound healing: the role of the macrophage.* Expert Rev Mol Med, 2011. **13**: p. e23.
202. Eming, S.A., T. Krieg, and J.M. Davidson, *Inflammation in wound repair: molecular and cellular mechanisms.* J Invest Dermatol, 2007. **127**(3): p. 514-25.
203. Lamme, E.N., et al., *Extracellular matrix characterization during healing of full-thickness wounds treated with a collagen/elastin dermal substitute shows improved skin regeneration in pigs.* Journal of Histochemistry & Cytochemistry, 1996. **44**(11): p. 1311-1322.
204. Malenfant, A., et al., *Prevalence and characteristics of chronic sensory problems in burn patients.* Pain, 1996. **67**(2-3): p. 493-500.
205. Ward, R.S., et al., *Sensory loss over grafted areas in patients with burns.* J Burn Care Rehabil, 1989. **10**(6): p. 536-8.
206. Ward, R.S. and R.P. Tuckett, *Quantitative threshold changes in cutaneous sensation of patients with burns.* J Burn Care Rehabil, 1991. **12**(6): p. 569-75.
207. Nedelec, B., et al., *Sensory perception and neuroanatomical structures in normal and grafted skin of burn survivors.* Burns, 2005. **31**(7): p. 817-30.
208. Burdick, J.A., et al., *Acellular biomaterials: an evolving alternative to cell-based therapies.* Science translational medicine, 2013. **5**(176): p. 176ps4-176ps4.
209. Pashuck, E.T. and M.M. Stevens, *Designing regenerative biomaterial therapies for the clinic.* Science translational medicine, 2012. **4**(160): p. 160sr4-160sr4.

CURRICULUM VITAE

Yu-I (Tom) Shen

Education

Spring, 2015 Ph.D. in Chemical and Biomolecular Engineering
Johns Hopkins University, Baltimore, MD

May, 2008 Bachelor of Engineering in Chemical and Biomolecular Engineering
Molecular and Cellular Bioengineering
Johns Hopkins University, Baltimore, MD

Predoctoral , Johns Hopkins University, P.I. - Dr. Sharon Gerecht

Utilize synthetic bioactive hydrogel scaffold to study vascular disease and therapeutic angiogenesis on skin injuries treatment

2010 – 2015

- Develop bioactive hyaluronic acid hydrogel for stem cell/vasculature delivery construct to treat diabetic ulcer disease.
- Analyze dextran hydrogel in procine skin wound healing model.
- Engineer vascularized construct in hydrogel *in vitro.*
- Model oxygen stress and vascular recruiting potential from cancer cell *in vitro*.

Graduate researcher (MSc. discontinued) , Johns Hopkins University, P.I. - Dr. Sharon Gerecht

2008-2009

- Synthesized bioactive dextran hydrogel for tissue engineering purpose.
- Encapsulated growth factor in microparticles for control release for drug delivery purpose.
- Established *in vivo* protocols and standard procedure for the laboratory.

Summer research assistant, National Yang Ming University, Taiwan

- Analyzed retinal iron toxicity in clinical and experimental studies.
- Formulate therapeutic mechanisms of neuroprotectant against retinal ischaemia/experimental glaucoma

Publications

1. **Shen, Y.I** et al, Engineered human vascularized hyaluronic acid hydrogels to treat diabetic food ulcer wounds. *in preparation*
2. **Shen, Y.I**, HH.G. Song, A. Papa, J. Burke, S. Volk, S. Gerecht Acellular hydrogels for regnerative burn wound healing: translation from a porcine model, J of Investigative Dermatology. *in revision*
3. Stahl, P.J., T.R. Chan, **Y.I. Shen**, G. Sun, S. Gerecht, and S.M. Yu, Capillary Network-Like Organization of Endothelial Cells in PEGDA Scaffolds Encoded

with Angiogenic Signals Triple Helical Hybridization. Adv Funct Mater, 2014. **24**(21): p. 3213-3225.

4. Abaci, H.E., **Y.I. Shen**, S. Tan, and S. Gerecht, Recapitulating physiological and pathological shear stress and oxygen to model vasculature in health and disease. Sci Rep, 2014. **4**: p. 4951.
5. **Shen, Y.I**., H.E. Abaci, Y. Krupsi, L.C. Weng, J.A. Burdick, and S. Gerecht, Hyaluronic acid hydrogel stiffness and oxygen tension affect cancer cell fate and endothelial sprouting. Biomater Sci, 2014. **2**(5): p. 655-665.
6. Kusuma, S., **Y.I. Shen**, D. Hanjaya-Putra, P. Mali, L. Cheng, and S. Gerecht, *Self-organized vascular networks from human pluripotent stem cells in a synthetic matrix.* Proc Natl Acad Sci U S A, 2013. **110**(31): p. 12601-6.
7. Hanjaya-Putra, D., **Y.I. Shen**, A. Wilson, K. Fox-Talbot, S. Khetan, J.A. Burdick, C. Steenbergen, and S. Gerecht, *Integration and regression of implanted engineered human vascular networks during deep wound healing.* Stem Cells Transl Med, 2013. **2**(4): p. 297-306.
8. Hanjaya-Putra, D., V. Bose, **Y.I. Shen**, J. Yee, S. Khetan, K. Fox-Talbot, C. Steenbergen, J.A. Burdick, and S. Gerecht, *Controlled activation of morphogenesis to generate a functional human microvasculature in a synthetic matrix.* Blood, 2011. **118**(3): p. 804-15.
9. Sun, G., X. Zhang, **Y.I. Shen**, R. Sebastian, L.E. Dickinson, K. Fox-Talbot, M. Reinblatt, C. Steenbergen, J.W. Harmon, and S. Gerecht, *Dextran hydrogel scaffolds enhance angiogenic responses and promote complete skin regeneration during burn wound healing.* Proc Natl Acad Sci U S A, 2011. **108**(52): p. 20976-81.
10. Sun, G., **Y.I. Shen**, S. Kusuma, K. Fox-Talbot, C.J. Steenbergen, and S. Gerecht, *Functional neovascularization of biodegradable dextran hydrogels with multiple angiogenic growth factors.* Biomaterials, 2011. **32**(1): p. 95-106.
11. Cuddy, A.C*., **Y.-I. Shen***, and S. Gerecht, *Engineering Bioactive Scaffolds 8 for Stem Cell Vascular Therapy.* Stem Cells: From Mechanisms to Technologies, 2011.
12. Sun, G., **Y.I. Shen**, C.C. Ho, S. Kusuma, and S. Gerecht, *Functional groups affect physical and biological properties of dextran-based hydrogels.* J Biomed Mater Res A, 2010. **93**(3): p. 1080-90.

Patents

Gerecht, S., Y.-I. Shen, C.C. Ho, and G. Sun, *Biocompatible polysaccharide-based hydrogels*. 2009, US Patent App. 13/140,324.

Gerecht, S., G. Sun, and Y.-I. Shen, Functional vascularization with biocompatible polysaccharide-based hydrogels. 2011, US Patent App. 13/807,502.

National conference Presentations

1. “Acrylated hyaluronic acid hydrogels to study cancer angiogenesis”
   AICHE San Francisco2013
2. “Engineering bioactive hydrogels for treating full thickness dermal wounds”
   AICHE San Francisco2013
3. “Engineering functional vascular networks ysing hydrogel and vascular stem cells to augment diabetic wound healing”
   MSCRF Baltimore 2013.
4. “Engineering bioactive hydrogel for vascularization”
   AICHE Salt Lake City 2010.
5. “Dextran-based biodegradable hydrogel scaffolds for controllable studies of vasculogenesis”
   Substituted presenter at the ACS 238th National Meeting, DC 2009.
6. “Functional groups affect physical and biological characteristic of dextran-based hydrogels”
   Poster Presentation at AICHE, Philadelphia 2008